

Fluorinated Barnase-Barstar Complexes

Inaugural-Dissertation

to obtain the academic degree

Doctor rerum naturalium (Dr. rer. nat.)

submitted to the Department of Biology, Chemistry, Pharmacy
of Freie Universität Berlin

by

Alexander Langhans, M.Sc.

from Berlin, Germany

July 2023

The research presented in this thesis was performed under the guidance of Prof. Dr. Beate Kokschi from October 2018 until July 2023, at the Institute of Chemistry and Biochemistry in the Department of Biology, Chemistry, and Pharmacy of Freie Universität Berlin.

1st reviewer: Prof. Dr. Beate Kokschi

2nd reviewer: Dr. Christian Roth

Date of defense: 13.10.2023

Statutory declaration

I hereby declare that I wrote my dissertation with the title “Fluorinated Barnase-Barstar Complexes” independently and have not used any sources or resources other than those specified by me. Intellectual property of other authors has been marked accordingly. I also declare that I have not applied for an examination procedure at any other institution and that I have not submitted the dissertation in this or any other form to any other faculty as a dissertation.

Berlin, July 2023

Alexander Langhans

Acknowledgements

First of all, I would like to thank Prof. Dr. Beate Kokschi for giving me the opportunity to write my doctoral thesis in such an interesting field of research. I would also like to thank her for the trust and support she gave me in implementing my own ideas. Finally, I would like to thank her for always pushing me out of my comfort zone.

I would also like to thank Dr. Ana Vila-Verde for motivating and fruitful discussions as well as her encouraging words during our IMPRS meetings.

I would like to thank Dr. Christian Roth not only for agreeing to write the second review for this thesis, but also for his active support in its preparation and for providing the needed recombinant enzymes. Furthermore, I would like to thank him for granting me access to his facilities in his group at the Max-Planck-Institute of Colloids and Interfaces.

Michael Krummhaar I want to thank for his support in operating the devices in the Roth Group, fruitful discussions sprouting countless ideas that led to the success of my work, and his work in providing me necessary recombinant inhibitor variants.

I want to thank Dr. Johann Moschner, who supported me in word and deed since the beginning of my bachelor thesis, and who never tired of doing so even in the beginning of my PhD career.

Dr. Allison Berger I want to thank for always having an open ear for any kind of questions, and for always finding an answer to even the most absurd questions. I am also grateful for her active support in the preparation of this thesis through careful proofreading.

My Students Marc Safferthal, Sina Schmidt and Mayar Elbendary I want to thank for their participation in my research project, also letting me know when my ideas did not make too much sense. Thank you for letting me work with you and more importantly grow with you as a scientist.

I want to thank all current and former members of the Kocsch group for fruitful discussions and a pleasant working atmosphere. Especially I want to thank Zeinab Mahfouz and Jonas Proksch for quality office time.

Thomas Hohmann and Suvrat Chowdhary I want to thank for providing fluorinated amino acids used in this thesis.

For financial support, I thank the Deutsche Forschungsgemeinschaft (DFG) under the International Max-Planck Research School (IMPRS) on Multiscale Bio-Systems and under the collaborative research center 1349 "Fluorine Specific Interactions".

Furthermore, I would like to thank the CoreFacility BioSupraMol for the immense number of samples measured. Especially I want to thank Dr. Andreas Springer for his support in finding solutions to complex analysis issues.

Thank you to all of my friends for your emotional support and allowing me to escape reality during our gaming sessions when necessary.

Lastly, I want to express my gratitude towards my parents for their continuous, all-embracing support since the very beginning of my life, which ultimately enabled me to complete this thesis.

Oral Presentations

(1) *“Fluorinated Barnase-Barstar complexes”*, Spring-Workshop of International Max-Planck Research School (IMPRS) on Multiscale Bio-Systems, Golm (Potsdam), Germany
25.04.2019

(2) *“Fluorinated Barnase-Barstar complexes”*, Spring-Workshop of International Max-Planck Research School (IMPRS) on Multiscale Bio-Systems, Golm (Potsdam), Germany
04.05.2020

(3) *“Fluorinated Barnase-Barstar complexes”*, Autumn-Workshop of International Max-Planck Research School (IMPRS) on Multiscale Bio-Systems, Golm (Potsdam), Germany
08.10.2020

Poster Presentations

(1) *“Fluorinated Barnase-Barstar complexes”*, 36th European and 12th International Peptide Symposium (EPS 2022), Sitges, Spain, 28.08-02.09.2022

(2) *“Fluorinated Barnase-Barstar complexes”*, 20th European Symposium on Fluorine Chemistry, Berlin (ESFC 2022), Germany, 14.08-19.09.2022

(3) *“Fluorinated Barnase-Barstar complexes”*, Autumn-Workshop of International Max-Planck Research School (IMPRS) on Multiscale Bio-Systems, Golm (Potsdam), Germany
06.10.2021

(4) *“Fluorinated Barnase-Barstar complexes”*, Autumn-Workshop of International Max-Planck Research School (IMPRS) on Multiscale Bio-Systems, Golm (Potsdam), Germany
10.09.2019

(5) *“Fluorinated Barnase-Barstar complexes”*, 14th German Peptide Symposium (GPS 2019), Cologne, Germany, 18.03-21.03.2019

Abstract

Proteins play a critical role in all living organisms and are responsible for the regulation of various biological processes. Their properties and functions result directly from their primary sequence, which is dictated by the DNA that encodes them. Mutations of the primary sequence can alter properties such as stability or activity. This can be used in chemical protein synthesis with canonical as well as non-canonical building blocks to rationally design or modify peptides and proteins to specifically change their properties. In this thesis, the influence of fluorinated amino acids in particular on the activity of an enzyme and the interaction between it and its natural inhibitor barstar was investigated. For this purpose, different fluorinated variants of aminobutyric acid were incorporated at site Lys27 of the enzyme sequence.

The first major hurdle of this project was the development of suitable synthesis methods to produce barnase, which consists of 110 amino acids. In order to minimize the consumption of the fluorinated amino acids, which are only accessible to a limited extent, during protein synthesis, special cycles were used. However, it was found that due to the position of the amino acid to be incorporated in the synthesis sequence, a reduction in equivalents used reduced achieved yields. The purified proteins were then subjected to various methods of structure elucidation to ensure purity and native folding. All barnase variants were analyzed for their enzymatic activity, as well as interaction with the natural inhibitor barstar. It was found that although all variants showed activity, non-natural variants showed significantly reduced activity compared to natural barnase. Nevertheless, calculated values for $k_{\text{cat}}/k_{\text{M}}$ were in line with literature reported values for all variants.

In future research, inhibitory efficiency and affinity of the different complexes can be investigated by means of fluorescence based inhibitory assays and ITC measurements. Furthermore, the herein presented results can be used as a basis for the characterization of precise complex structures.

Zusammenfassung

Proteine spielen eine zentrale Rolle in allen lebenden Organismen und sind für die Regulierung verschiedener biologischer Prozesse verantwortlich. Ihre Eigenschaften sowie Funktionen ergeben sich direkt aus ihrer Primärsequenz welche in der DNA verankert ist. Durch Mutationen der Primärsequenz können Eigenschaften wie bspw. Stabilität oder Aktivität verändert werden. Dies kann man sich in der chemischen Proteinsynthese zu nutzen machen, um Peptide oder Proteine rational zu designen oder zu modifizieren um ihre Eigenschaften gezielt zu verändern.

In der vorliegenden Arbeit wurde der Einfluss von fluorierten Aminosäuren auf Aktivität sowie Interaktion zum natürlichen Inhibitor Barstar, des natürlichen Enzyms Barnase untersucht. Hierzu wurden verschiedene fluorierte Varianten der Aminobuttersäure punktspezifisch in die Sequenz des Enzyms eingebaut.

Die erste große Hürde dieses Projekts war die Erarbeitung geeigneter Synthesemethoden zur Herstellung der aus 110 Aminosäuren bestehenden Ribonuklease. Um den Verbrauch der nur begrenzt zugänglichen fluorierten Aminosäuren bei der Proteinsynthese zu minimieren, wurden spezielle Synthesesyklen verwendet. Allerdings konnte hierbei bereits festgestellt werden, dass auf Grund der Position der einzubauenden Aminosäure in der Synthesesequenz, eine Reduzierung der Äquivalente den Syntheserfolg progressiv verschlechterte. Die aufgereinigten Proteine wurden anschließend verschiedenen Methoden der Strukturaufklärung unterzogen, um Reinheit sowie native Faltung zu gewährleisten. Alle nicht natürlichen Barnasevarianten wurden auf enzymatische Aktivität, sowie Interaktion zum natürlichen Inhibitor Barstar untersucht. Hier konnte festgestellt werden, dass zwar alle Varianten Aktivität zeigten, diese im Vergleich zur natürlichen Barnase jedoch signifikant eingeschränkt war. Dennoch waren die berechneten Werte für die katalytische Effizienz k_{cat}/k_M für alle untersuchten Barnasevarianten vergleichbar mit den in der Literatur beschriebenen Daten. In weiterführenden Untersuchungen können die hier präsentierten Proteine im Hinblick auf Enzymhemmung sowie Bindungsaffinität mittels fluoreszenzbasierter Assays und ITC-Messungen betrachtet werden. Weiterhin können die erarbeiteten Ergebnisse als Grundlage für eine präzise Charakterisierung der Kristallstruktur der Komplexe herangezogen werden.

Table of Content

1. Proteins – A cornerstone of life	7
1.1 Model System Barnase-Barstar	15
1.1.1 Barnase	15
1.1.2 Barstar	18
1.1.3 Barnase-Barstar Complex	19
2 Fluorine - élément extraordinaire	21
2.1 Fluorine, a tool for rational design of small and macromolecules	24
2.2 Fluorinated amino acids – a tool for rational protein design	28
2.2.1 Fluorinated amino acids – a tool to rational protein design	28
2.2.2 Fluorinated amino acids in SPPS	31
2.2.3 Fluorine’s impact on peptide engineering	31
2.2.4 Fluorine’s impact on protein engineering	34
3 Aim	45
4 Results and Discussion	46
4.1 Barnase as system to investigate fluorine’s impact on protein-protein interaction	46
4.2 Access to fluorinated derivatives of aminobutyric acid	46
4.2.1 Microwave-assisted SPPS	47
4.2.2 Establishing a MW-assisted SPPS approach to barnase	49
4.2.3 Results after optimization and adapting for unnatural amino acids	57
4.2.4 Purification of Barnase – from HPLC to SEC	60
4.3 NCL vs. full-length synthesis	71
4.4 Structural investigations – CD Spectroscopy	79
4.5 Activity assays	81
5 Summary and Outlook	88
6 Materials and Methods	91
6.1 Mass spectrometry	92
6.2 NMR-Spectroscopy	92
6.3 Manual Coupling protocol for resin loading	93
6.4 Determination of resin loading	93
6.5 Microwave assisted Solid Phase Peptide Synthesis	94
6.5.1 Microwave Methods and Coupling Cycles	94
6.5.2 Synthesis preparation – Reagents – CarboMax™ Approach	96
6.6 Analytics	98
6.6.1 <i>General procedure for test-cleavages</i>	98
6.6.2 <i>General procedure for full cleavage</i>	98
6.7 Purification and Analysis	99
6.7.1 Chromaster HPLC system	99
6.7.2 LaChrom Elite HPLC system	99
6.7.3 Primaid HPLC system	100

6.7.4 Preparative HPLC LaPrepΣ	101
6.8 Purification of Barnase variants – Dialysis and Size Exclusion Chromatography (SEC)	102
6.9 Lyophilization	102
6.10 Determination of protein concentration	102
6.11 Hydrazide-based native chemical ligation	103
6.11.1 <i>General procedure to the synthesis of MPAA thioester</i>	103
6.11.2 <i>General procedure to native chemical ligation</i>	104
6.12 CD Spectroscopy	104
6.13 RNase activity Assay	105
6.14 Synthesized Barnase variants and fragments	106
6.14.1 <i>Synthesis of wild-type barnase</i>	107
6.14.2 <i>Synthesis of BarAbu27</i>	108
6.14.3 <i>Synthesis of BarTfeGly27</i>	109
6.14.4 <i>Synthesis of BarDfeGly27</i>	110
6.14.5 <i>Synthesis of BarMfeGly27</i>	111
6.14.6 <i>Synthesis of BarPfpGly27</i>	112
6.14.7 <i>Synthesis of BarDfpGly27</i>	113
6.14.8 <i>Synthesis of Bar1-36-NHNH₂</i>	114
6.14.9 <i>Synthesis of Bar³⁷Cys-¹¹⁰Arg</i>	115
6.15 Native Chemical Ligation Approach to barnase	116
6.15.1 <i>Synthesis of Bar¹Ala-³⁶Val-SR.</i>	116
6.15.2 <i>Synthesis of BarA37C variant by native chemical ligation</i>	117
7 References	118

List of abbreviations

¹⁸ F-FDG	¹⁸ F-fluorodeoxyglucose
2-Aha	2-aminoheptanoic acid
AA	amino acid
Abu	aminobutyric acid
Aib	aminoisobutyric acid
BDE	bond dissociation energy
BfR	Bundesinstitut für Risikobewertung
Boc	<i>tert</i> -butyloxycarbonyl
BPTI	bovine pancreatic trypsin inhibitor
CD	circular dichroism
Da	dalton
DAD	diode array detector
DBU	1,8-diazabicyclo[5.4.0]undec-7-en
DCM	dichloromethane
DfeGly	difluoroethyl glycine
DfpGly	difluoropropyl glycine
DIC	diisopropylcarbodiimide
DIPEA	diisopropylethyl amine
Dmb	2,4-dimethoxybenzyl
DNA	desoxyribonucleic acid
DSC	differential scanning calorimetry
DTT	dithiothreitol
EDT	ethanedithiol
EN	electronegativity
ESI	electron spray ionisation
EtOH	ethanol
eq.	equivalents
FA	fluoroacetate
fAA	fluorinated amino acid

FAM	6-carboxyfluorescein
F-Leu	fluoroleucine
Fmoc	9-fluorenylmethoxycarbonyl
GCN4	general control nondepressible 4
GnHCl	guanidinium hydrochloride
h	hour
HATU	1-[bis(dimethylamino)methylene]-1 <i>H</i> -1,2,3-triazolo[4,5- <i>b</i>]pyridinium-3-oxide hexafluorophosphate
HCl	hydrochloric acid
HDMS	high definition mass spectrometry
HOBt	1-hydroxy-benzotriazole
HPLC	high performance liquid chromatography
HR-MS	high resolution mass spectrometry
<i>i</i> PrOH	isopropanol
ITC	isothermal calorimetry
KAHA	α -ketoacid-Hydroxylamine
KI	potassium iodide
LL	low loading
<i>m/z</i>	<i>mass per charge</i>
Mbm	<i>p</i> -methoxybenzyloxymethyl
MeCN	acetonitrile
MeOH	methanol
MeSNa	sodium methanethiolate
MfeGly	monofluoroethyl glycine
MfLeu	monofluoroleucine
min	minutes
MPAA	4-mercaptophenylacetic acid
MPI	Max-Planck-Institute
MS	mass spectrometry
MW	microwave
NCL	native chemical ligation

Ni	nickel
Nle	norleucine
NMP	<i>N</i> -methyl-2-morpholine
NMR	nuclear magnetic resonance
NTL9	nac transcription factor-like 9
Nvl	norvaline
OBno	O-5- <i>n</i> -butyl-5-nonyl
OEpe	O-3-ethyl-pent-3-yl
OMpe	O-3-methyl-pent-3-yl
Osu	O-succinimide
PDA	photodiode array
PDB	protein data bank
PFAS	per- and polyfluoroalkyl substances
PFOA	perfluorooctanoic acid
PFOS	Perfluorooctanesulfonic acid
PfpGly	pentafluoropropyl glycine
Q-ToF	quadrupole time-of-flight
RNA	ribonucleic acid
RNase	ribonuclease
RP	reverse phase
RT	room temperature
SEA	<i>bis</i> (2-sulfanylethyl)amido
SEC	size exclusion chromatography
SPPS	solid phase peptide synthesis
STL	serine/threonine ligation
^t Bu	<i>tert</i> -butyl
TCEP	tris-(2-carboxyethyl)phosphine
TFA	trifluoroacetic acid
TfeGly	trifluoroethyl glycine
Tfile	trifluoroisoleucine
Tfleu	trifluoroleucine

TfVal	trifluorovaline
TIS	triisopropylsilane
Trt	trityl
UPLC	ultra performance liquid chromatography
UV	ultra violet
VA-044	2,2'-azobis[2-(2-imidazolin-2-yl)propan]dihydrochlorid
Vis	visible
WT	wild-type
α -TfmAla	α -trifluoromethyl alanine

Abbreviations of the 20 canonical amino acids are consistent with the one- or three-letter code recommended by the IUPAC-IUB Joint Commission on Biochemical Nomenclature (Eur. J. Biochem. 1984, 138, 9-37)

Abbreviations for fluorinated L amino acids used in this thesis are given below with corresponding IUPAC description.

TfeGly	Trifluoroethyl glycine
(S)-2-amino-4,4,4-trifluorobutanoic acid	
DfeGly	Difluoroethyl glycine
(S)-2-amino-4,4-difluorobutanoic acid	
MfeGly	Monofluoroethyl glycine
(S)-2-amino-4-monofluorobutanoic acid	
DfpGly	Difluoropropyl glycine
(S)-2-amino-4,4-difluoropentanoic acid	
PfpGly	Pentafluoropropyl glycine
(S)-2-amino-4,4,5,5,5-pentafluoropentanoic acid	

1. Proteins – A cornerstone of life

Peptides and proteins are one major subgroup of biomolecules created by nature, aside from DNA and RNA, carbohydrates, and lipids. These amino acid (AA) polymers carry out a multitude of important tasks in every living organism, e.g., DNA replication, transcription, translation, and repair; signal transduction; metabolic processes; and transport of small molecules like oxygen. The AA building blocks themselves can be sorted into three major groups: hydrophobic, charged, and polar.^{1, 2} (**Figure 1**)

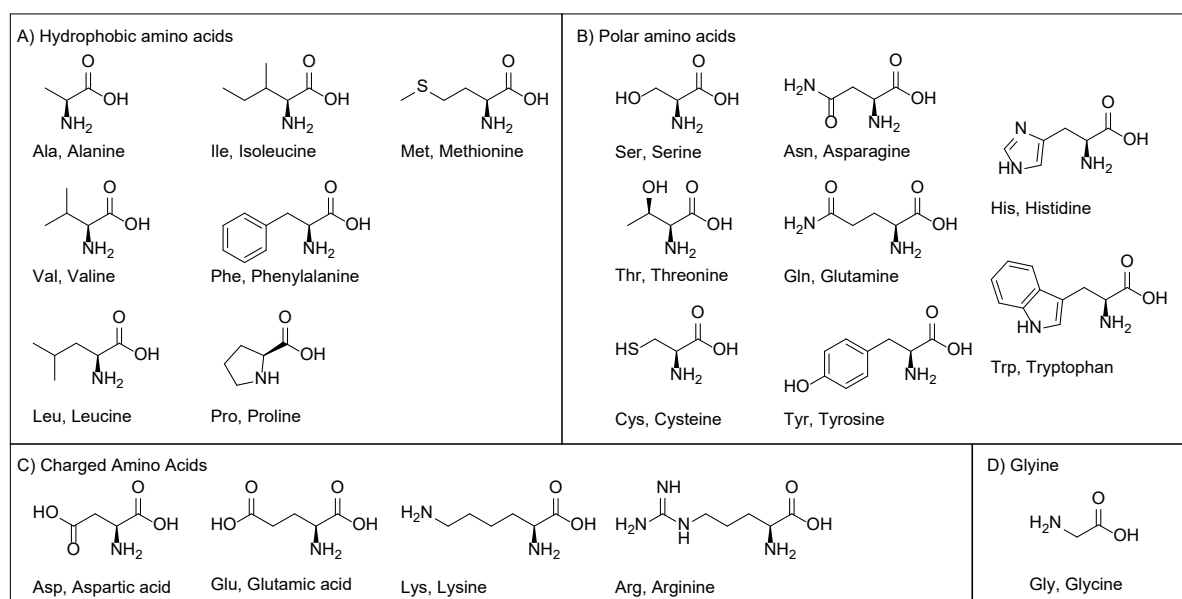


Figure 1: AAs grouped according to their side chains into A) hydrophobic residues, B) polar residues, C) charged residues, D) Glycine, which is the simplest AA and does not possess a side chain other than protons. Adapted from C. Brandon & J. Tooze.¹

Building sequences by combining these different aa's side chain functionalities leads to a staggering variety of structures and functions. The primary structure is determined in nature by a cell's biosynthetic machinery according to the genetic code; in artificial proteins, however, the primary structure can be designed by the chemist. The organization of side chain functionalities in turn determines the intra- and intermolecular interactions of the hydrophobic, polar and ionic groups, which lead to specific secondary, tertiary and quaternary structures. It is important to note that each AA residue occupies conformational space in a distinct way.^{1, 2} Due to the rather rigid conformation of the peptide backbone, every AA has only two degrees of freedom. These are the dihedral

angles N-C_α (phi Φ) and C'-C_α (psi Ψ), which are directly restricted by the side chain in question.³ (**Figure 2**) Thus, phi and psi can be used to generate an AA's intrinsic secondary structure propensity,⁴ a value helpful in predicting the frequency with which an AA will be present in a given specific structural motif.⁵

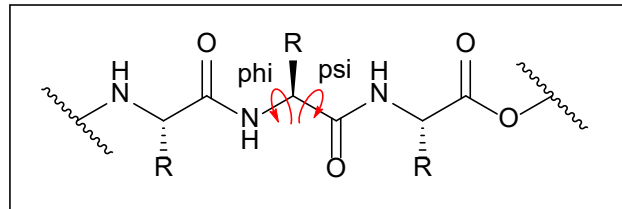


Figure 2: Representation of dihedral angles phi (Φ) and psi (Ψ), restricting possible conformation.

The most abundant secondary structure motif in nature is the α -helix,⁶ followed by the β -strand.⁷

α -Helix

The α -helix was first described by Linus Pauling in the 1950s.⁸ It is generally a right handed, wound secondary structure motif of an AA chain, which is stabilized via main chain hydrogen bonds that run parallel to the helix axis. This leads to a specific hydrogen bonding pattern with interactions between positions denoted i and $i+4$. This pattern leads to a characteristic winding of 3.6 AA residues per turn.⁹ (**Figure 3**) This structure corresponds to dihedral angles of -60° and -50° for Φ and Ψ , respectively.¹⁰

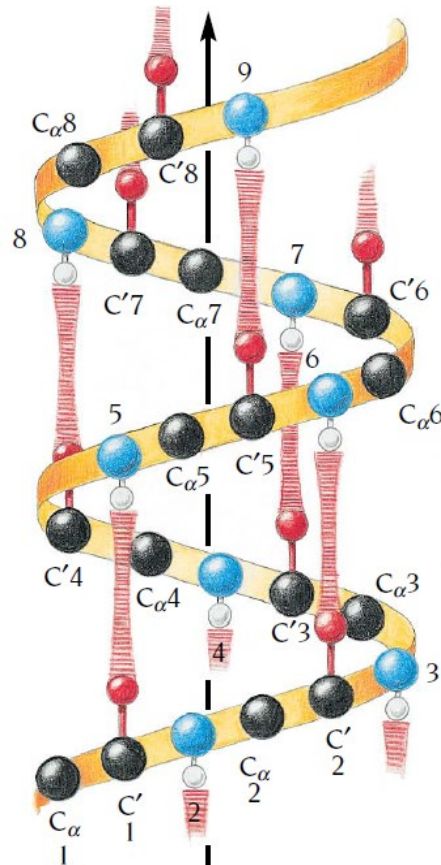


Figure 3: Cartoon of an α -helix highlighting the parallel hydrogen bonds along the helix axis, between backbone carbonyls and amides. Reprinted with permission from C. Branden & J. Tooze¹.

Aside from the classical α -helical motif, several variations are possible: the 3_{10} helix has three AA residues per turn, and the π -helix has 4.4.⁶

β -Sheet

The second most commonly observed structural motif is the β -sheet, proposed by Pauling and Corey in 1951.¹¹ The first monomeric structure, in the form of a β -hairpin, was, however, described in 1993.¹² β -Sheets comprise multiple β -strands, short 5-10 residue chains, which align either parallel or anti-parallel to one another. This structure is also stabilized by main chain hydrogen bonds.¹³ (**Figure 4**) The dihedral angles Φ and ψ are -120° and $+115^\circ$ for parallel and -140° and $+135^\circ$, respectively, for anti-parallel sheets.¹⁰

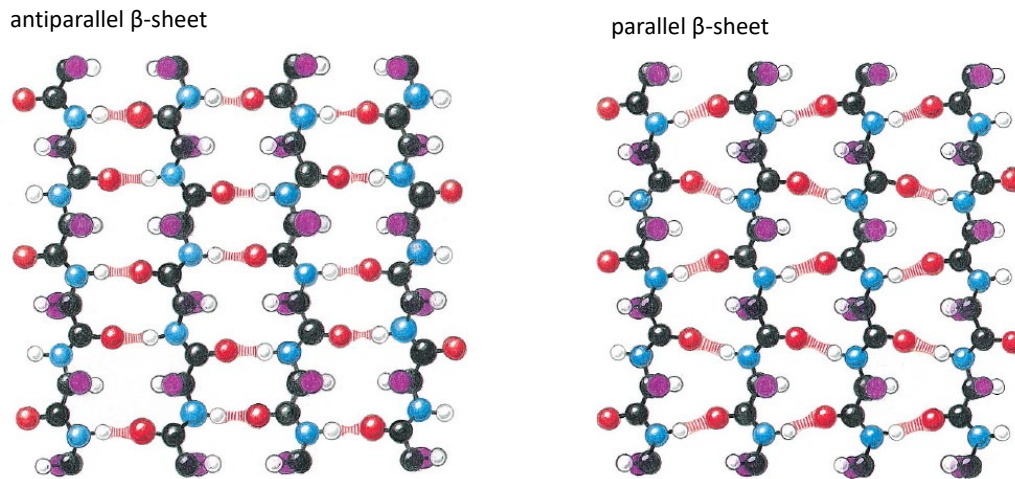


Figure 4: Cartoon of an antiparallel β -sheet (left) and parallel β -sheet (right), highlighting the hydrogen bonds between the individual β -strands of backbone carbonyls and amides. Reprinted (adapted) with permission from C. Branden & J. Tooze.¹

Following a hierarchical pattern, the next level of structure in proteins is the formation of multiple secondary structure motifs during protein folding, resulting in the overall tertiary structure. As stated in the Anfinsen Dogma, every protein possesses a native fold under physiological conditions, having optimal thermodynamic stability.¹⁴ In 1961 he further postulated that the information required to reach this most stable state is contained within the protein's primary sequence.¹⁵ This, however, was challenged by the Levinthal Paradox, which discussed the fast folding of proteins into the native structure despite the astronomical number of possible conformations.¹⁶ The assumption that folding could be achieved by randomly sampling conformations shows that protein folding would be impossible on any feasible time scale. Hence, a semi-directed pathway (now known to be facilitated by chaperones), explained by a so-called folding funnel, suggesting meta-stable folding intermediates, was proposed.^{17,18} With decreasing energy, fewer folding intermediates become possible. The native fold corresponds to the structure showing the lowest free energy state, and thus is the most stable. **(Figure 5)**

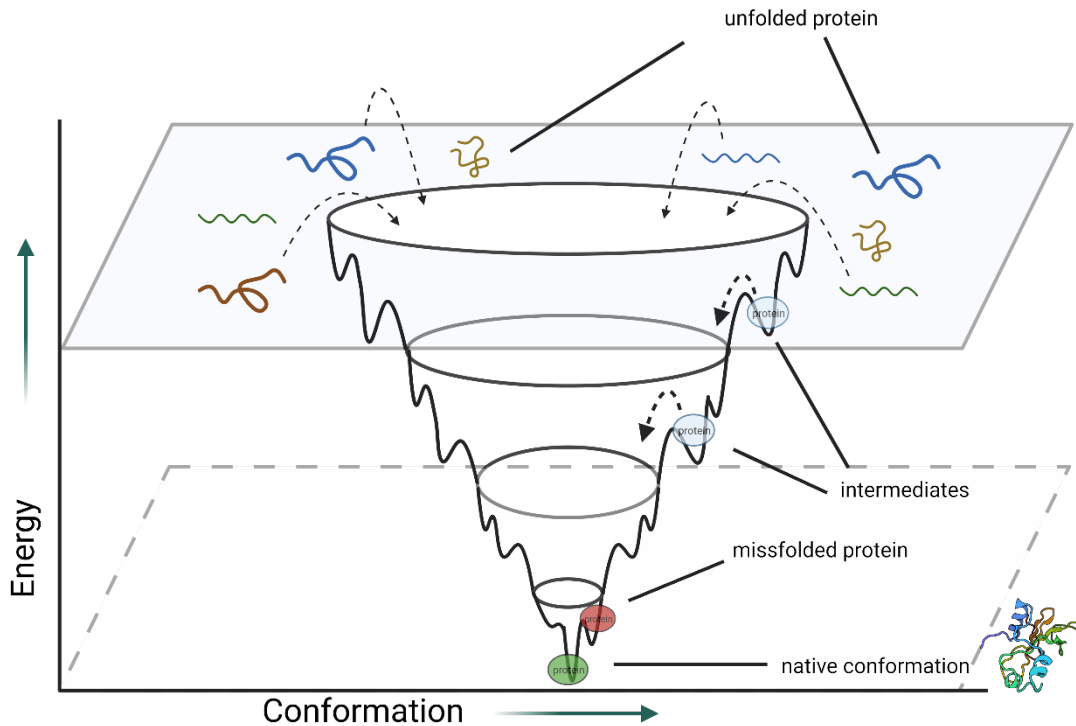


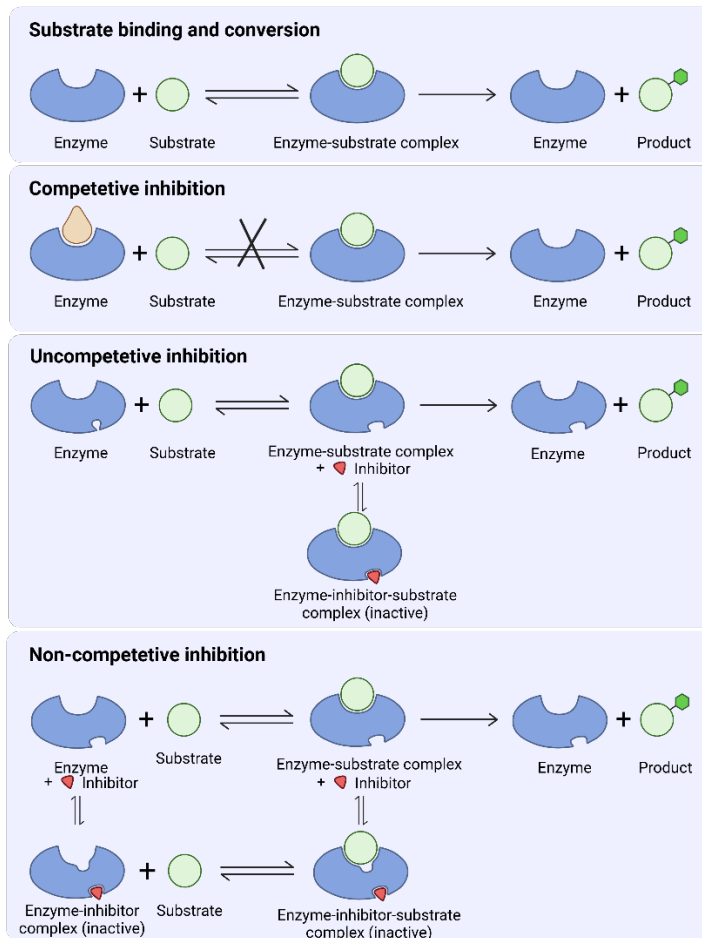
Figure 5: Depiction of a folding funnel. Adapted from A. Mogk et al.¹⁹ Created with BioRender.com.

One of the main driving forces considered in protein folding is the hydrophobic effect.^{20, 21} During the folding process the hydrophobic core is built up first, burying hydrophobic side chains and excluding water, resulting in an overall entropy gain.^{14, 22} However, many proteins need tools to reach their native fold, such as cofactors, coenzymes,²³ or chaperones.²⁴

Four main structural classes have been described: all- α , like α -globin, the α -unit of hemoglobin²⁵; all- β , like green fluorescent protein (GFP)²⁶; $\alpha + \beta$, including ferredoxin-like proteins²⁷; and α/β , of which BPTI and barnase are well-described representatives.²⁸⁻³⁰ Further more detailed information on protein structure and structural similarities between different proteins can be found in the Structural Classification of Proteins Database (SCOP).^{31, 32}

The final level of the protein folding hierarchy is the quaternary structure, a complex of multiple tertiary structures, e.g., hemoglobin, which is a tetramer composed of two α -subunits and two β -subunits.³³ Consequently, both the primary structure as well as the native folded tertiary structure affect a protein's inherent function.³⁴ As stated above, proteins perform many important tasks in nature. One class of proteins that is

particularly relevant for this thesis are enzymes, which are nature's catalysts. Enzymes are further divided into seven subgroups: EC1 oxidoreductases, EC2 transferases, EC3 hydrolases, EC4 lyases, EC5 isomerases, EC6 ligases, and EC7 translocases.³⁵ Discussing all of them individually is, however, beyond the scope of this thesis. The subgroup to be considered in the context of this thesis is EC3 hydrolases, as it contains ribonucleases, of which barnase is one. Ribonucleases are enzymes capable of hydrolytically cleaving the phosphodiester bond between polyribonucleotides. To ensure the proper deployment of enzymes in living organisms, that is, to avoid undesired tissue damage associated with enzyme activity in the wrong place at the wrong time, another protein subgroup exists in nature: inhibitors. These interact with their cognate enzymes via hydrophobic, ionic, or polar interactions, deactivating them reversibly, or via covalent bonding, deactivating them irreversibly.^{36, 37} For reversible inhibitors, relevant for this thesis, different modes of inhibition are known: competitive, uncompetitive and non-competitive. **(Figure 6)** Examples of reversible inhibitors, namely barstar and BPTI, will be discussed in this thesis in **sections 1.1** and **2.2.4**.



The inhibitor **mimicks** the substrate. Both the inhibitor and substrate **compete for the active site** of the enzyme. The relative concentration and their affinity to the enzyme determines the degree of competitive inhibition.

The inhibitor **binds to the allosteric site of the enzyme-substrate complex**, but not to the free enzyme. The inhibitor is not structurally similar to the substrate and does not compete for the active site.

The inhibitor binds to the enzyme or enzyme-substrate complex at an **allosteric site**. Catalysis is prevented due to a change in the enzyme conformation.

Figure 6: Standard mechanism for the formation of Enzyme-substrate complexes (top), inhibition by the three variants of reversible inhibitors. Created with BioRender.com.

Competitive inhibition

Here the enzyme's substrate as well as the inhibitor compete for active site access. The inhibitor mimics the substrate, thus the substrate cannot bind to the active site and the enzyme's activity is inhibited, preventing any reaction. Increased concentrations of substrate can, however, outcompete the inhibitor. Inhibition is a matter of binding affinities. The process can be observed via reduced velocity. **(Figure 7)**

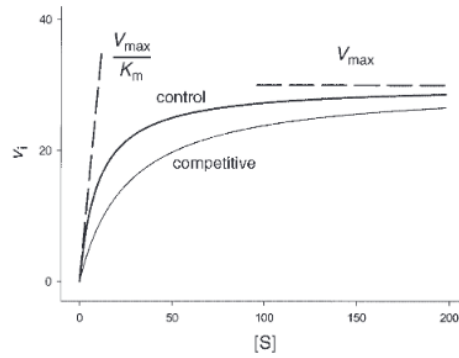


Figure 7: Effect of competitive inhibitor on reaction velocity when plotted as initial velocity vs. substrate concentration. Reprinted with permission from R.S. Ochs.³⁸ Copyright © 2000, American Chemical Society.

Uncompetitive inhibition

This type of inhibition is characterized by binding of the inhibitor to the enzyme-substrate complex, or simply the substrate, rather than to the enzyme itself. This can happen due to either a conformational change after substrate binding, revealing a binding site for the inhibitor, or binding of the inhibitor directly to the substrate. In this case of inhibition, increasing the substrate concentration does not overcome the inhibitory effect.

Non-competitive inhibition

In this case, also referred to as allosteric inhibition, the inhibitor binds to the enzyme, but not at the active site, generating an inactive complex.

1.1 Model System Barnase-Barstar

The enzyme-inhibitor complex barnase-barstar has been very well described experimentally, including mutation studies, as have the isolated components. Thus, this system lends itself to further investigation of the type described in the aim of this thesis, namely the impact of site-specific fluorination on protein folding and protein-protein interaction. Furthermore, being inherently catalytically competent, barnase also offers an interesting opportunity to investigate fluorine's influence on enzyme activity.

1.1.1 Barnase

Barnase is a small single-chain protein of 110 AAs (12,382 Da) belonging to the family of microbial ribonucleases.³⁹⁻⁴¹ It is the extracellular ribonuclease of *Bacillus amyliquefaciens*, which was in the past considered a subspecies of *Bacillus subtilis*; however, in 1987 it was instated as its own species.⁴² Hence, barnase was first described by Nishimura and Nomura in 1958 as an enzyme of *Bacillus subtilis*.⁴³ The crystal structure of barnase was first reported by Mauguen et al. in 1982.³⁹ As mentioned above, barnase belongs to the class of α/β proteins. It is built up from three α -helices and one five-stranded antiparallel β -sheet, secondary structure elements which are connected via multiple loops and turns (**Figure 8**).

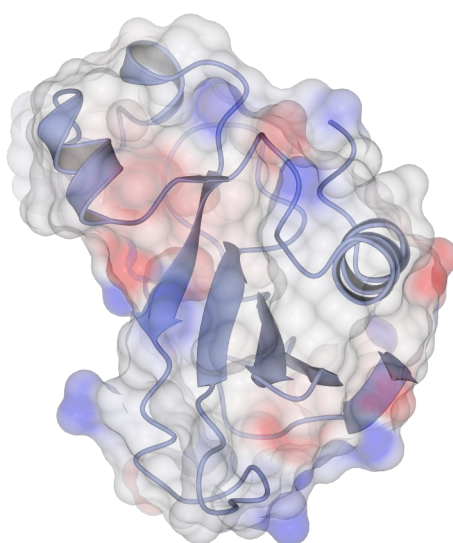


Figure 8: Crystal structure of barnase. Created in CCP4MG, PDB code 1BRS.

Table1 summarizes all secondary structure motifs as found from N to C terminus.

Table 1: Secondary structure motifs ordered N->C.²⁹

Section	Secondary structure motif	Comment
residues 6-18	first helix	
residues 19-25	first loop	21-24 create a type 1 turn
residues 26-34	second helix	
residues 35-40	second loop	
residues 41-46	third helix	
residues 46-49	type 2 turn	
residues 50-55	first β -strand	
residues 56-69	third loop	
residues 70-76	second β -strand	
residues 77-84	fourth loop	
residues 85-91	third β -strand	
residues 91-94	type 1 turn	
residues 94-99	fourth β -strand	
residues 100-105	fifth loop	
residues 106-108	fifth β -strand	

Studying the structure, Nishimura and Nomura also noticed that the sequence of barnase does not contain cysteines,⁴³ which led to the assumption that the enzyme could be an intriguing target to investigate protein folding. Research pursued on this revealed a reversible folding mechanism which can be triggered by heat or denaturing agents, such as urea or guanidine hydrochloride (GnHCl).⁴⁴ Furthermore, barnase folds into its native conformation merely by hydrophobic interactions, not requiring cofactors or coenzymes, within seconds.^{45,46}

Being a ribonuclease, barnase is able to cleave oligonucleotides. Its active site lies on the β -strand across from α -helix 1 and is located in a groove flanked by loop 2, helix 2, and loop 3.⁴⁷ It was assumed that barnase, belonging to the family of microbial ribonucleases, shows a mechanism of action similar to RNaseA. Mossakowska et al. in 1989 confirmed this assumption; however, barnase features a glutamic acid (Glu-73)

instead of a second histidine. Nevertheless, the reaction mechanism is similar, transforming a 3'-5' internucleotide phosphodiester into a 2'-3' intranucleotide cyclic phosphate (**Figure 9**).⁴⁸ His102 acts as proton donor, Glu73 is the respective acceptor. Further AAs relevant during the hydrolysis are Lys27, Glu60, Arg83 and Arg87.

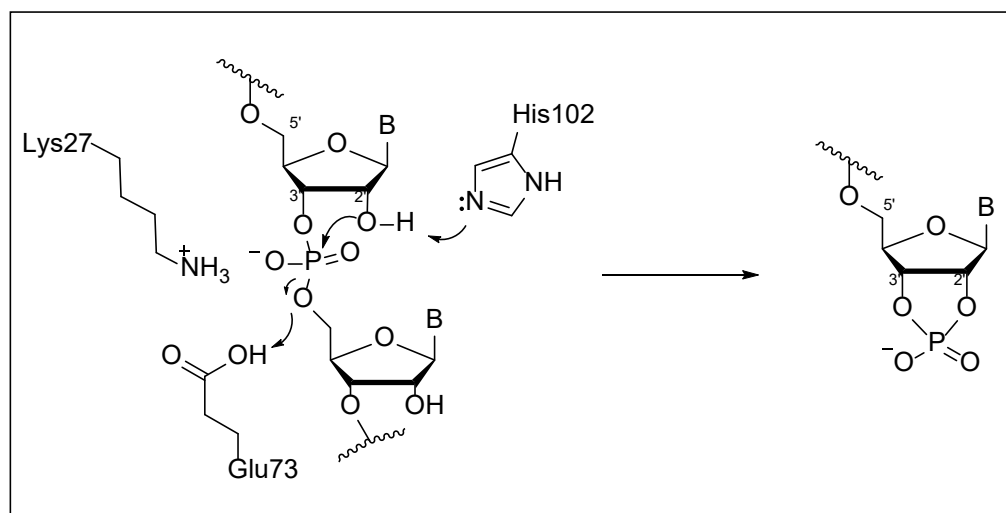


Figure 9: Mechanism of RNA hydrolysis catalyzed by His102 and Glu73 of barnase. Lys27 of barnase stabilizing phosphate. 3'-5' intermolecular phosphodiester is converted into an intramolecular 3'-2' phosphodiester.

Mutating His102 to Ala removed barnase activity entirely, showing its relevance in catalysis. Mutations to Lys27, which is the AA of key relevance for this thesis, also showed a reduction in enzyme activity,⁴⁹ demonstrating its relevance for catalysis. However, this change was only reflected in k_{cat} , retaining K_M (binding affinity), pointing towards Lys27 playing a role in stabilizing the transition state. This residue interacts with the nucleotide substrate's phosphate group⁵⁰ and is thus important for lowering the energy of the transition state, thus stabilizing it, as has been shown by single mutation of Lys27 to Ala.⁴⁸ Barnase's activity is specific towards nucleotides of the form GpN, showing further selectivity favoring GpA > GpG > GpC ~ GpU.⁵¹ Since this activity causes inherent cytotoxicity towards the bacteria itself, barnase is coexpressed with its cognate inhibitor barstar. Upon leaving the cell the inhibitor is cleaved to reveal barnase's activity.⁵² The purpose of this extracellular activity was, however, debated in literature. It was assumed to be of nutritional relevance⁴⁶ but could also act as a kind of defense mechanism.⁵³

1.1.2 Barstar

Barstar is the native inhibitor to barnase. It is an even smaller protein of 89 AAs, showing similar α/β secondary structure motifs. These motifs comprise three parallel β -strands, four helices, and three loops as follows:

Table 2: Secondary structure motifs ordered N->C.⁵⁴

Section	Secondary structure motif
residues 1-7	first β -strand
residues 8-11	first loop
residues 12-25	first α -helix
residues 26-32	second loop
residues 33-44	second α -helix
residues 45-48	third loop
residues 49-54	second β -strand
residues 55-63	third α -helix
residues 66-81	fourth α -helix
residues 83-89	third β -strand

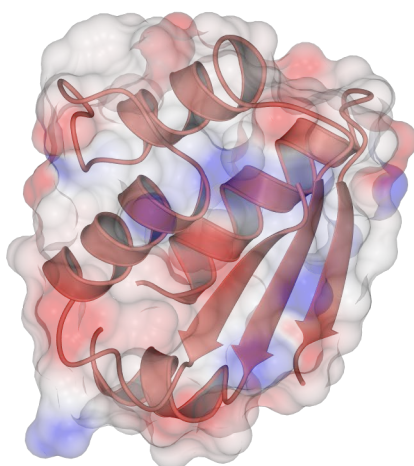


Figure 10: Crystal structure of barstar. Created in CCP4MG, PDB code 1BRS.

The major structural difference to barnase is the presence of two cysteine residues featured in the sequence of barstar. As has been revealed in structural studies on the

inhibitor these are, however, neither structurally relevant, nor play a significant role in binding interactions towards barnase. Mutating both Cys residues to Ala provided a crystal structure showing more than 11 Å distance between the two AAs, which makes the formation of a disulfide bridge unlikely.⁵⁴ Hence, this mutation is commonly applied in research. In later sections this mutation is also described in this thesis. Removing both cysteines from the sequence additionally simplifies the synthesis of barstar, as it removes possible issues arising from oxidation of the thiols. It was furthermore the mutated sequence that was first used to solve the crystal structure of the barnase-barstar complex.⁵⁵

1.1.3 Barnase-Barstar Complex

Mimicking an RNA-substrate, barstar interacts with barnase via a selected group of AAs. Research performed by Schreiber and Fersht provided the AAs showing the strongest interactions: Lys27, Arg59, Arg87, and His102 of barnase, and Asp35, Asp39 and Glu76 of barstar.⁵⁶⁻⁵⁸ Barstar has a considerably larger footprint on barnase than does a typical RNA substrate, with a surface area of 800 Å² compared to 305 Å² for a model d(CGAC) nucleotide, potentially aiding in the very tight binding observed for the complex.⁵⁹

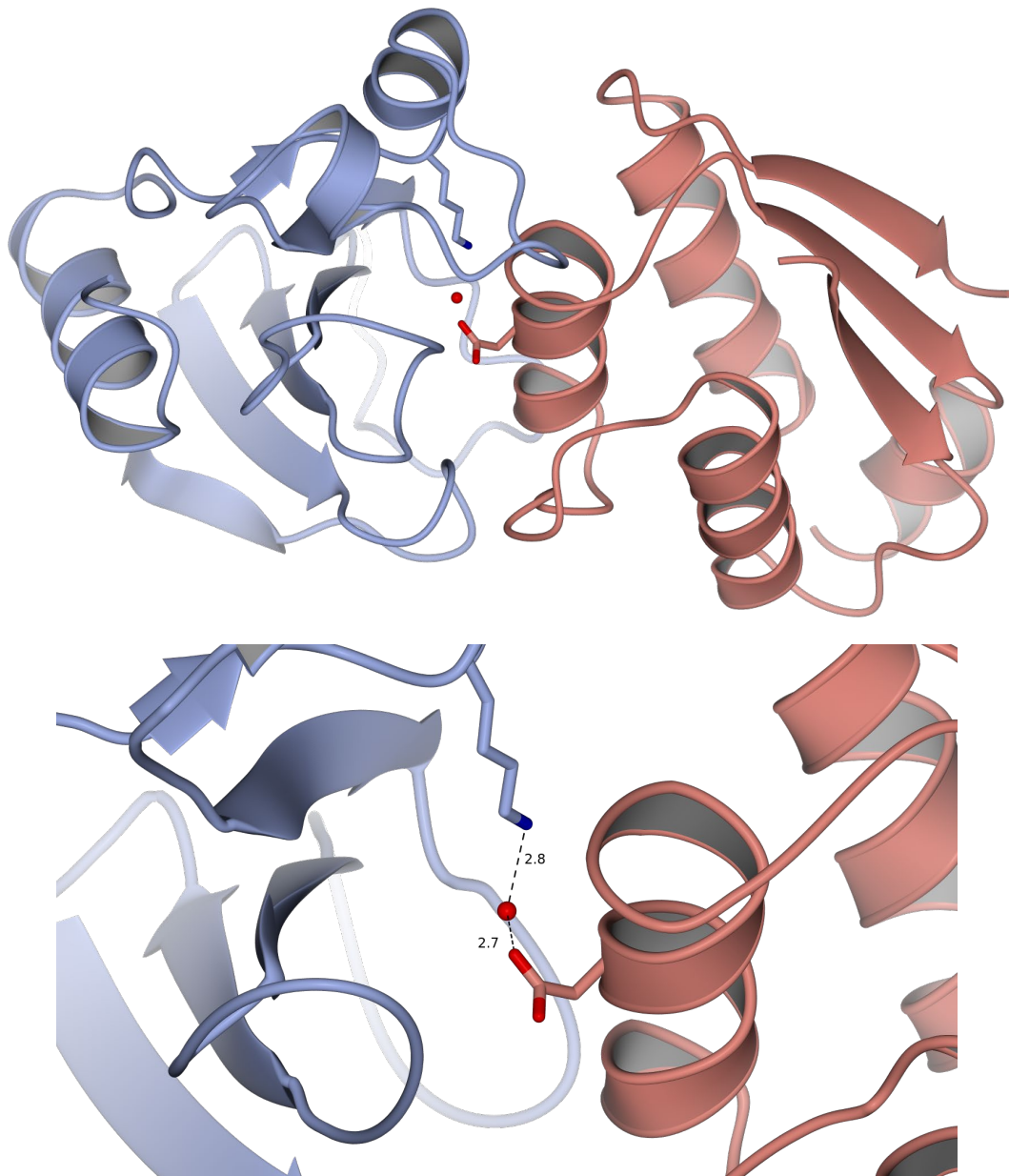


Figure 11: (Top) Crystal structure of barnase (left) and barstar (right) complex highlighting interaction between Lys27 of barnase and Asp39 of barstar facilitated by structural water molecule H₂O-121. (Bottom) Zoom in on interacting AAs Lys27 and Asp39 highlighting H-bonds between both AAs and structural water molecule H₂O-121 and their respective bond length. Created in CCP4MG PDB code 1BRS.

Specific interactions between barnase and barstar are formed amongst the charged AA residues. In the mimicking process, Asp39's carbonyl group of barstar acts as the substrate's phosphate, thus interacting via hydrogen bonds with Arg83, Arg87 and His102 of barnase.⁵⁹ A structural water molecule (H₂O-121) facilitates the interaction between Lys27 and the Asp39 side chain.⁴⁷ (Figure 11) This particular interaction is one of

the strongest contributions with an energy of $4.8 \text{ kcal mol}^{-1}$ despite its distance of 4.5 \AA .⁵⁹ It caught our attention, as its nature was assumed to be comparable to interactions found in the enzyme-inhibitor complex of protease-BPTI, which will be discussed in a later section of this thesis. The association rate constant of the barnase-barstar complex is $3.7 \times 10^8 \text{ s}^{-1}\text{M}^{-1}$; as expected, this is decreased two-fold when mutating any of the crucial acidic side chains listed above. The dissociation constant (10^{-14} M) is increased by five orders of magnitude when mutating Asp39 to Ala; however, in this case the stability of barstar increases by $2.1 \text{ kcal mol}^{-1}$.⁵⁸ Nonetheless, these mutations are not of significance in the presented thesis, hence the reader is kindly referred to the profound work of A. Fersht, G. Schreiber, R.W. Hartley, or A.M. Buckle for more detailed information on folding, stability and complexation involving barnase.

2 Fluorine - élément extraordinaire

Fluorine is the 24th most abundant element overall, the 13th most abundant element in the earth's crust and thus the most abundant halogen, however its natural occurrence outside of minerals or salts like CaF_2 (Fluorit), $\text{Na}_3[\text{AlF}_6]$ (Cryolite) or $[\text{Ca}_5(\text{PO}_4)_3]$ (Fluoroapatite) is rare.⁶⁰⁻⁶² In fact seawater, which makes up 0.02% of earth's mass, contains less than 1% of earth's fluorine budget,⁶³ accumulating at 1.3 ppm within the hydrosphere, a very small value compared to chloride at 20000 ppm.⁶⁴ Nevertheless, inorganic fluorine can be found outside of sedimentary materials. Significant quantities of fluorine have been found within the sponge *Halichondria moorei*, in the form of potassium fluoride.⁶⁵ Furthermore, plants in fluoride-rich areas were also found to contain increased amounts of fluoride.⁶⁶ Even naturally occurring elemental fluorine (F_2), has only been observed in inclusions in antozonite, a radioactive mineral, resulting from the decay of uranium salts.⁶⁷ Due to its low bioavailability and its low solubility in water, fluorine's occurrence in natural organofluorine compounds is rare and it has only been identified in a limited number of plants and microorganisms.⁶⁸ To date approximately 3800 organohalogens have been isolated, of which the majority contain either chlorine or bromine, at 2200 and 1950 compounds respectively. Only approximately 100 compounds contain a fluorine substitution.⁶⁹ While increasing amounts of organohalogens, e.g.

containing chlorine, have also been isolated from higher animals and humans,⁶⁹ no natural organofluorine compounds could be described within these kingdoms.⁶² The first ever isolated natural fluorinated product was fluoroacetate (FA) in 1943. It was initially found in *Dichapetalum cymosum* and has now been identified in over 40 different plants.⁷⁰

Despite nature mostly ignoring fluorine, or rather fluorinated building blocks, it has already been of key interest to chemists for approximately 500 years.⁷¹ Since the first description of fluorite dating back to 1529 by Georgius Agricola,⁷² scientists have generally acknowledged fluorine's immense potential due to its inherent exceptional properties. It has a relatively small size of 1.47 Å, which is between hydrogen (1.20 Å) and oxygen (1.52 Å),⁷³ thus it is frequently used as a hydrogen substitution.

Table 3: Physicochemical parameters of fluorine compared to frequently occurring elements.

	vdW Volume ⁷³	Electronegativity ⁷⁴	Electronaffinity ⁷⁴
F	1.47	3.98	328.2
Cl	1.75	2.55	348.5
Br	1.85	2.96	324.5
H	1.20	2.20	72.8
O	1.52	3.44	141.4
C	1.70	2.55	153
N	1.55	3.40	-6.3

Even though fluorine is approximately 20% larger than hydrogen, it is generally seen as bioisosteric.⁷⁵ This, however, changes with the degree of fluorination and is debated in literature, as the steric demand of fluorocarbon groups seems to increase nonlinearly. Thus, the steric demand of a trifluoromethyl group is on one hand described as comparable to a simple methyl group⁷⁶, an isopropyl group⁷⁷, a *sec*-butyl group, or even a phenyl or *tert*-butyl group⁷⁸. This discrepancy could possibly be explained with complications in distinguishing between steric and electrostatic contributions when observed in a chemical reaction or interactions.^{79, 80}

With an electronegativity value of 4.0 according to Pauling⁸¹ it is the most electronegative element. Owing to its small atomic size of 50 pm⁸² fluorine shows very high reactivity, thus compounds generated by its reactions show remarkable thermal stability.⁷¹ Interestingly, when looking at fluorocarbons, the binding affinity of C-F bonds

growths with the degree of fluorination. Hence the C-F bond in CH₃F shows a binding affinity of 453 kJmol⁻¹ but 546 kJmol⁻¹ in CF₄. This trend is not seen for any other halogen. Furthermore, fluorination increases C-C bond strength but decreases C=C bond strengths.⁸³ Thus, with its bond dissociation energy (BDE) of 105 kcal mol⁻¹ the C-F bond can be considered the strongest single bond in organic chemistry.⁷⁵ As a consequence of the aforementioned high EN value of fluorine, resulting carbon-fluorine bonds are highly polarized and are thus more of an electrostatic than covalent nature, exhibiting ionic character due to electron density being focused at the fluorine atom.⁸¹ When compared to the C-H bond, this leads to an inversion of polarity; C^{δ+}-F^{δ-}, C^{δ-}-H^{δ+}.⁸⁴ This in turn results in the already described strong binding between carbon and fluorine, but also affects overall bond length. The C-F single bond has a length of 1.4 Å, which is significantly longer than the C-H bond with 1.09 Å. It is however comparable to C-O (1.43 Å). Other carbon-halogen bonds show bond lengths of 1.77 Å (chlorine) and 1.97 Å (bromine).⁸⁴ Similar to bond strength increasing with degree of fluorination, mentioned above bond length decreases from CH₃F to CF₄, due to the increasing positive charge density at the carbon center.⁸¹ Furthermore, high polarization of the C-F bond also introduces a large dipole moment, which can have both inter- and intramolecular consequences.^{81, 84} Again, the strength of the dipole moment increases with the degree of fluorination, being 1.85 D in fluoromethane and 1.97 D in difluoromethane. Intramolecularly, the C-F bond induced dipoles tremendously influences the conformation of the compound. Thus, a simple α-fluoroamide shows a strong preference towards *trans* conformation. (**Figure 12**)

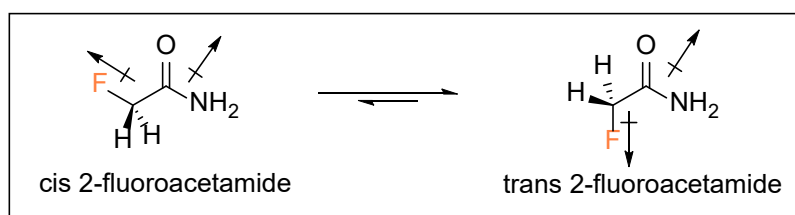


Figure 12: α-fluoroacetamide dipole moment. Adapted from O. Hagan et al.⁸¹

Intermolecularly, the high polarization of the C-F bond facilitates various dipole-dipole interactions, and literature controversially discusses the ability of a C-F bond to act

as a good hydrogen bond acceptor. This assumption was made based on the presence of three lone pairs as well as the high polarization of fluorine.

Table 4: Properties of different carbon bonds.⁷⁵

	Bond length [Å]	Dipole moment μ [D]	Bond dissociation energy [kcal/mol]
C-H	1.09	0.4	98.8
C=O	1.23	2.33	85
C-OH	1.43 CH ₃ OH	2.87	84
	1.48 CH ₃ CH ₂ OH	1.66	
C-F	1.35	1.41	105.4
C-Cl	1.77	1.87	78.5

While evidence is scarce, however, reported fluorine involving hydrogen bonds are generally weaker than their hydrocarbon analogues, with 2.0–3.2 kcal mol⁻¹ (F--H) compared to 5-10 kcal mol⁻¹ (O--H).^{85, 86} This can be explained with fluorine's higher electronegativity (EN) and its poor polarizability compared to oxygen, decreasing its electrostatic influence and thus making it a worse hydrogen bond acceptor.⁸⁵ Nevertheless, multiple cases of weak fluorine involving hydrogen bond interactions, termed "weak dipolar interactions" have been found and reported, with C-F ---H-C being the most common.^{85, 87} Intriguingly, fluorine's contribution to electrostatic or polar interactions has been widely accepted in organic, more specific all medicinal chemistry, showing a beneficial impact.⁸⁸

Owing to fluorine's strong EN it can exert a strong inductive effect on neighboring groups like carboxyl or hydroxyl groups, lowering their pK_a values and increasing overall acidity. In the case of amines, however, basicity is reduced. This in turn shows a strong influence on parameters like binding affinities and biological activity.⁸⁸ Compared to other halogens, the influence of fluorine is significantly stronger.

2.1 Fluorine, a tool for rational design of small and macromolecules

Thanks to the above presented unique properties of fluorine, its relative absence in natural organic compounds has become an intriguing opportunity for scientists to modify or expand the existing repertoire of organic molecules in agrochemicals and

pharmaceuticals. Tremendously altering properties like hydrophobicity, lipophilicity, receptor binding, activity and metabolic stability of small drug molecules and macromolecules alike, it has become a valuable design tool. It is thus not surprising that to date 20% of all pharmaceuticals, approximately 370 total compounds as of 2020, contain at least one fluorine atom.⁸⁹ Since the first fluorine containing pharmaceutical Florinef (Florinef acetate) was reported in 1954, a significant increase in annually approved fluorine-containing drug molecules can be observed. (Figure 13)

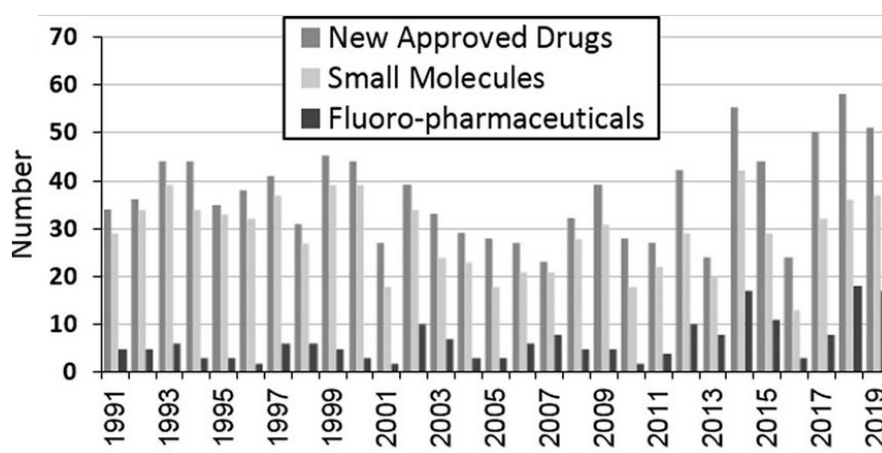


Figure 13: Globally registered fluoro-pharmaceuticals between 1991-2019. Reprinted from Inoue et al.⁸⁹

These increases, especially over the past two decades, are driven by new developments in fluorination processes, increasing the scope of available fluorinated compounds.⁸⁸ Further noteworthy fluoropharmaceuticals generated since FlorineF or Fludrocortisone are Levofloxacin, developed in 1993 as an antibacterial inhibitor of DNA gyrase and topoisomerase⁹⁰ and Lipitor, developed in 1997 for the treatment of cardiovascular diseases.⁹¹

Similar trends in the increasing amount of fluorinated compounds can be seen in the development of agrochemicals, with 53% of newly registered compounds and 16% of overall approved compounds containing at least one fluorine atom. Interestingly, for the last two decades, roughly 50% of all compounds approved for commercial use per year, are fluorine containing molecules.⁹²

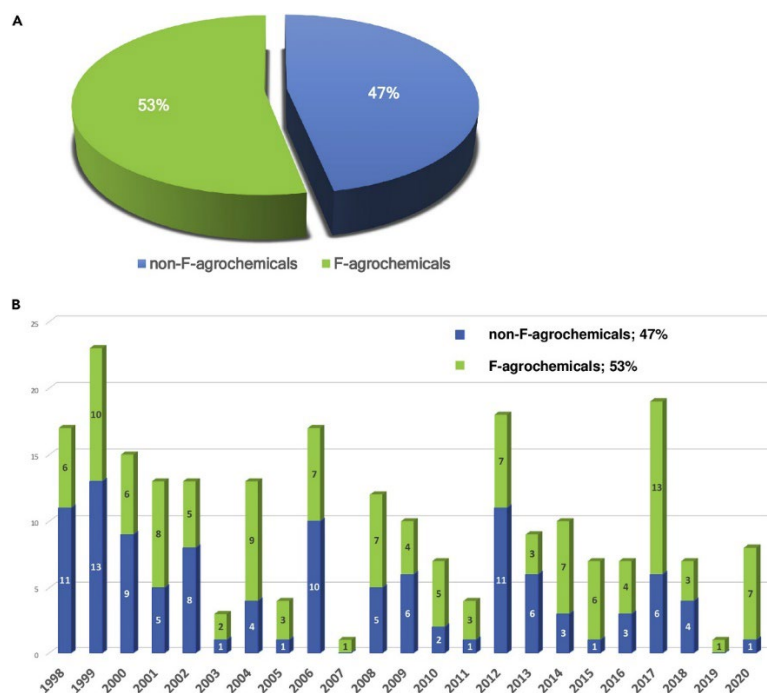


Figure 14: A) Pie chart showing the ratio between approved fluorine containing and non-fluorine agrochemicals since 1998. B) Bar chart illustrating ratio between fluorine containing and non-fluorine agrochemicals approved per year since 1998. Reprinted with permission from Ogawa et al.⁹² © 2020 The Author(s).

Despite offering great potential in the above mentioned fields of pesticides, (per)fluorinated reagents also pose an environmental risk, since due to their increased stability they persist as pollutants in soil and water for prolonged periods of time, or do not decompose at all, leading to accumulation.⁹³ Perfluorooctane sulfate (PFOS), a common product of insecticide application,⁹⁴ and perfluorooctanoic acid (PFOA), are frequently mentioned examples of such perfluorinated compounds, and part of very critically discussed per- and polyfluoroalkyl substances (PFAS).⁹⁵ According to the German Federal Institute for Risk Assessment (BfR), PFOS and PFOA have been prohibited in the European Union since 2006 and 2020, respectively, due to their toxicity towards humans and animals.

Apart from direct disease treatment, through fluorinated drug molecules, or frequent use in agrochemicals like insecticides, fluorine also offers a convenient probe for imaging. Thanks to the short half-life of the radioactive ¹⁸F isotope of 109.8 min⁹⁶ and its positron emission it is commonly used for positron emission tomography, a method of imaging biochemical processes.⁹⁷ Therefore, ¹⁸F is administered in the form

^{18}F -Fluorodeoxyglucose ^{18}F -FDG, (**Figure 15**) a glucose derivative that is preferably taken up by neoplastic cells.⁹⁸

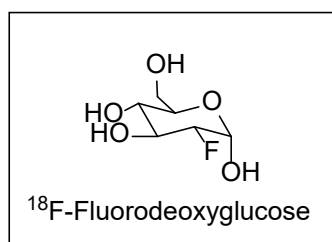


Figure 15: Chemical structure of ^{18}F -Fluorodeoxyglucose in chair conformation.

Furthermore, thanks to ^{19}F 's favorable NMR properties, like 100% natural abundance, spin of $\frac{1}{2}$ and a sensitivity of 83% with respect to a proton,⁹⁹ this natural isotope is a promising nucleus for magnetic resonance imaging.¹⁰⁰

However, not only medicinal and agricultural chemistry have profited from the great potential fluorination has to offer. In the field of peptide and protein engineering, it has also proven to be a versatile tool to tailor inter- and intramolecular features, as will be discussed in the following chapters.

2.2 Fluorinated amino acids – a tool for rational protein design

As discussed above, fluorination has gained increasing interest as a tool to modify and tailor certain parameters in small molecules and biomolecules alike. Furthermore, thanks to its fascinating properties, properties of proteins like hydrophobicity, lipophilicity or secondary structure formation can also be altered significantly.¹⁰¹

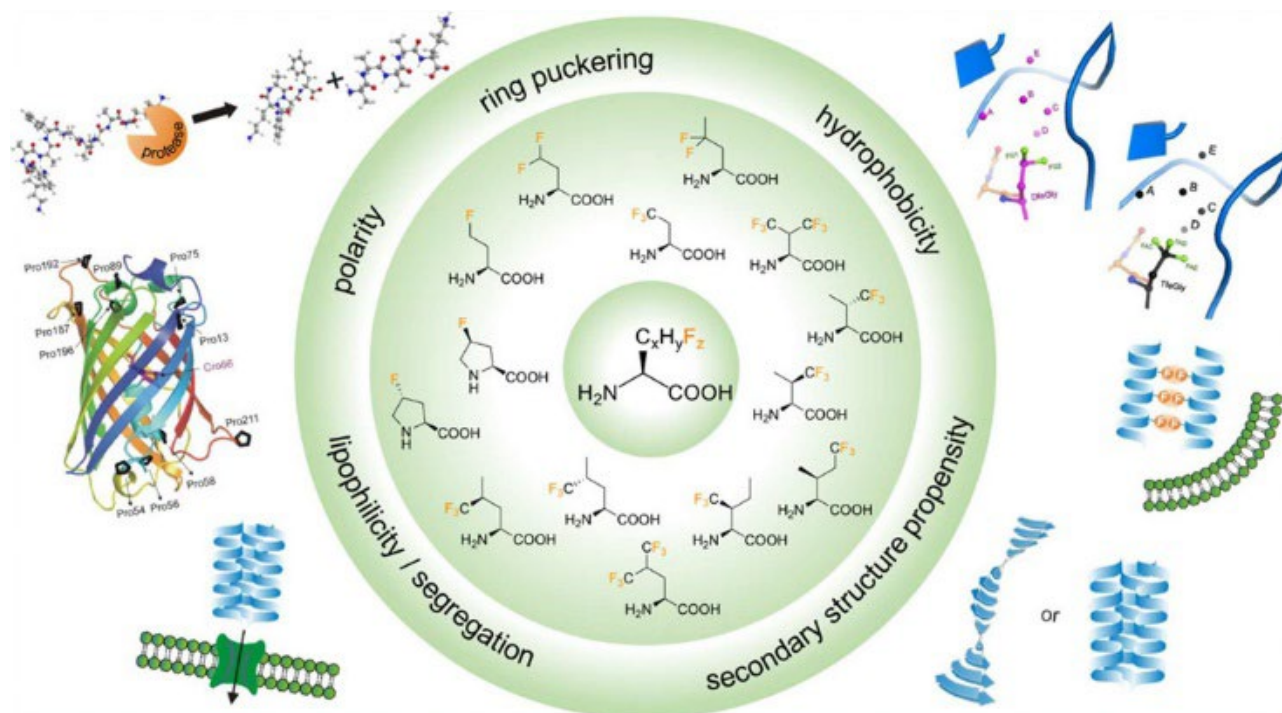


Figure 16: Overview of fluorinated amino acids (fAAs) and the properties fluorine can potentially affect on the AA itself, as well as the biomolecules it gets incorporated into. Reprinted from Berger et al. ¹⁰¹

Moreover, fluorine can have a tremendous impact on protein-protein interactions, which is of critical relevance in the ultimate goal of the here presented thesis.

2.2.1 Fluorinated amino acids – a tool to rational protein design

In the context of peptide and protein engineering fluorine is commonly introduced in the form of fluorinated building blocks like AAs, which can be implemented into sequences by biological and chemical means. To make this special element usable for peptide and protein synthesis two general approaches can be found, bottom-up and top-down. During a bottom-up approach, which was also followed in this thesis, the peptide or protein sequence is build up from the bottom using common techniques of chemical or biological

protein synthesis. Fluorine is thereby introduced in the form of fluorinated building blocks, like AAs. During the top-down approach however, fluorine is incorporated into existing peptide sequences by late-stage fluorination using external fluorine-sources.¹⁰²

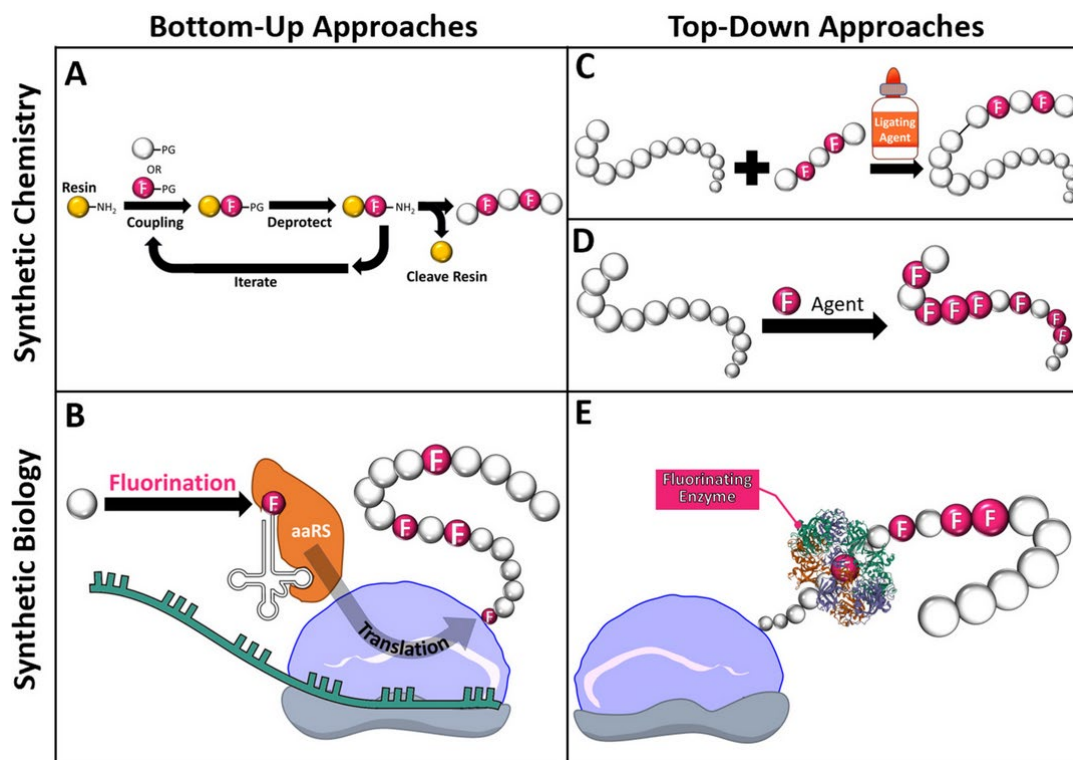


Figure 17: Illustration of the different methods that can be applied to introduce fluorine into biomolecules. A) Bottom-Up approach by means of SPPS. B) Bottom-Up approach by means of biosynthetic methods. C) Top-Down approach introducing fluorine by ligation methods using fluorinated peptides. D) Top-Down approach by means of late-stage fluorination using fluorination agents. E) Top-Down approach by means of late-stage fluorination using enzymatic machinery. Reprinted from Monkovic et al.¹⁰²

Herein we focus on the bottom up approach. A major advantage of this approach is the very selective site-specific incorporation of fluorine. However, fluorine in the form of fAAs must be made readily available. Since next to no natural biological fluorinated compounds, let alone AAs have been isolated,⁶² a need for synthetic access to enantiopure AAs grew. A vast variety of synthetic approaches was comprehensively described by Moschner et al.¹⁰³ One specific approach will be discussed in the following section, since it was applied to generate all fAAs utilized in this thesis.

Synthesis of fluorinated amino acids using chiral Ni-complexes

A very versatile approach to the synthesis of the fAA trifluoroethyl glycine (TfeGly) was reported by Soloshonok et al.¹⁰⁴⁻¹⁰⁶ This strategy makes use of a chiral Ni-complex, first reported by Belokon et al,¹⁰⁷ to generate access to TfeGly in a gram-scale¹⁰⁸ which is crucial for the development of SPPS-strategies. These Ni-complexes have since found extensive application to generate numerous aliphatic AAs.¹⁰⁹ The complex is built up from a tridentate proline-based Schiff-base and the natural AA glycine, which can be easily reacted with alkyl iodides.¹¹⁰

Recently Hohmann et al. reported the adaptation of the Ni-complex to the gram-scale synthesis of multiple fluorinated aliphatic AA in their Fmoc-protected form, thus vastly increasing the synthetic scope of this approach.¹¹¹ Their route consists of three steps starting with the synthesis of the Ni-glycine Schiff base, followed by alkylation with the desired fluorinated iodo-alkyl chain. In a final step both hydrolysis of the complex and N-terminal protection using Fmoc-O-Succinimide are performed. (**Figure 18**)

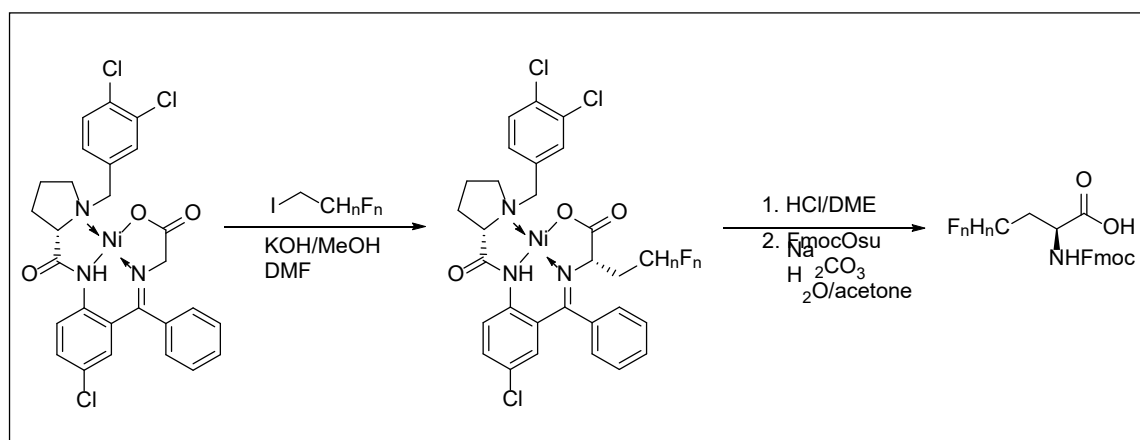


Figure 18: General reaction pathway of generating Fmoc-L-fAA-OH using the Soloshonok Ni-complex. Following this general scheme all fluorinated Abu variants can be achieved.¹¹¹

Utilizing this procedure all AAs discussed in this thesis were synthesized and kindly provided by T. Hohmann and S. Chowdhary.

2.2.2 Fluorinated amino acids in SPPS

As initially discussed, the bottom-up approach allows site specific incorporation of the desired fluorine substituent. However, a few different issues still limit this approach. Even though the Soloshonok Ni-complex solves the problem of limited access to fluorinated aliphatic AAs, their availability is not comparable to that of the canonical AAs. Thus, special synthesis cycles during SPPS need to be applied to reduce the equivalents required during each coupling cycle. This will be further discussed in a later section of this thesis. Furthermore, while fluorination is generally investigated with beneficial effects in mind, it also significantly affects synthesis procedure in a negative way. Due to fluorine's high EN it shows a very strong inductive effect, drawing electrons from a given system.¹¹² Thus, it can for example significantly reduce the nucleophilicity of an AA's N-terminal amine. This in turn leads to severely deteriorated synthesis properties, as can be seen in the use of α -trifluoromethylated alanine (α -TfmAla). The fluorinated analogue of aminoisobutyric acid (Aib) features a trifluoromethyl substituent in α -position, which is in the direct vicinity of the N-terminal amine, and thus reduces nucleophilicity significantly,¹¹³ rendering common SPPS approaches ineffective. Synthesis involving these kinds of AAs are thus approached by building block methods¹¹³ that generate dipeptides in solution-phase synthesis by acid chlorides¹¹⁴ or mixed anhydrides.¹¹⁵ These building blocks can then be incorporated into peptides utilizing SPPS methods, even though applied strategies are still not straight forward.¹¹⁴

2.2.3 Fluorine's impact on peptide engineering

A critical factor in peptide and protein chemistry is the change in hydrophobicity that comes with the modification/substitution of certain AAs. It is thus important to evaluate how fluorination affects hydrophobicity at the level of the smallest unit of a peptide, the AA. To date there are a multitude of different methods to estimate hydrophobicity,¹¹⁶⁻¹¹⁹ of which RP-HPLC based methods are a common approach. In previous work, Kokschi and coworkers investigated the hydrophobic properties of a wide range of fAAs, amongst which are also the derivatives of Abu used in this thesis. Their results, in general, show the expected trend of increasing hydrophobicity upon fluorination of AAs, however, a few trend-breaking AAs are apparent.

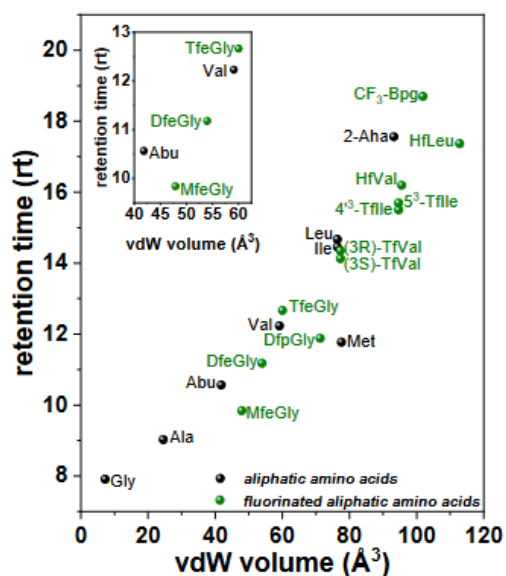


Figure 19: HPLC based assay plotting retention time of AAs against their van-der-waals-volume to evaluate their hydrophobicity of AAs. Adapted from S.A. Samsonov et al.,¹¹⁹ H. Erdbrink et al.¹²⁰ and U.I.M. Gerling et al.¹²¹

It was thus described that single fluorination of Abu (MfeGly) causes a decrease in hydrophobicity. Trifluorination however increases hydrophobicity compared to Abu, as expected.¹¹⁹ In addition, DfpGly shows lower-than-expected hydrophobicity in contrast to the size-comparable AAs Leu and Ile. Ile's fluorinated analogues in turn show lower hydrophobicity than their size-comparable AA 2-Aha; compared to their non-fluorinated analogue, however, their hydrophobicity is increased. A possible explanation for the decreased hydrophobicity, especially of MfeGly, is the introduction of a strong dipole moment as well as the present highly polarized geminal C-H bonds.¹⁰¹ While a general trend can be observed when only considering one factor at a time, showing increased hydrophobicity in both increased fluorine content, and increased spatial demand, trend-breakers are observed when considering multiple factors. These observations underline that hydrophobicity of fAAs is indeed dependent on more than simply fluorine content. Similar results have been shown in studies conducted by Robalo et al. In initial studies investigating the impact of CH₃ – CF₃ substitutions the authors described the increased spatial demand of CF₃ over CH₃ as not being the leading cause in observed hydrophobicity increases. However, reduction of possible hydrogen bonds, as well as increased steric hindrance of backbone-water hydrogen bonds by CF₃ seem to play a crucial role.¹²²

Further studies including also CH₂F and CHF₂ substitutions further support the above-discussed discrepancies in hydrophobicity trends. By evaluating hydration free energies, an indicator for hydrophobicity,¹²³ of fAAs with varying degree of fluorination, both positive and negative values were observed, indicating increased hydrophobicity and decreased hydrophobicity respectively. These unexpected, yet well supported, results were explained by changes in polarity, which plays a significant role in hydrophobicity.¹²⁴

Closely linked, hydrophobicity¹²⁵ and increased steric demand¹²⁶ of fAAs side chains also affects secondary structure propensities. Utilizing a model peptide developed by Chakrabarty et al.¹²⁷ the Kocsch group investigated a variety of fAAs to evaluate their α -helical propensity. Concluding these investigations it was found that fAAs generally show decreasing α -helical propensities compared to their non-fluorinated analogues, and with respect to increasing degree of fluorination.^{120, 121, 126} **Table 5** shows determined values for herein used Abu derivatives.

Table 5: Comparison of helical propensities of Abu and its fluorinated analogues.¹²¹

Amino Acid	Helix propensity
Abu	1.22
MfeGly	0.873
DfeGly	0.497
TfeGly	0.057

Following a conclusion by Cheng et al.,¹²⁵ fAAs show only low α -helical propensities and should favor β -structures. Yet, most investigations on structural impact have been conducted in coiled-coil or single-helix model peptides, indicating stabilizing effects when introducing fAA into the hydrophobic core of coiled-coils. For example, Tirrell et al. investigated the influence of trifluoroisoleucine (TfIle) and trifluorovaline (TfVal) when introduced into different positions of the hydrophobic core of GCN4. Their investigations revealed increased thermal stability in both cases.¹²⁸ Following the rationale of Cheng et al., however, Gerling et al. investigated the transition of a coiled-coil based model peptide to amyloid structures upon introduction of fluorinated AAs. This transition was already observable in the parental peptide, however the authors were able to report increasing amyloid formation rates when substituting solvent exposed positions

containing valine by MfeGly, DfeGly, TfeGly and trifluorovaline. As expected, helix propensity decreases with increased fluorine content, which in turn is reflected in reduced transition times. No change in the amyloid structure, however, was detected for the fAA substitutions.¹²¹ Aside from thermal stability, increased hydrophobicity due to fluorination can also affect proteolytic stability as well as bioactivity, as has been shown in studies by Gottler et al. In their study on antimicrobial peptides (AMP) MSI-78 the authors assumed that increasing hydrophobicity, and thus better stability could also benefit the proteolytic stability of the AMP.¹²⁹ Showing an unstructured profile, the peptide assembles into an α -helical *coiled-coil* when in contact with lipid bilayers.¹³⁰ Here it is thought to form torus-shaped holes, leading to its antimicrobial activity.¹³¹ By substituting Ile and Leu throughout the sequence with hFLeu, the authors were able to show that their fluorinated analogue retained its antimicrobial activity, even showing increased activity towards bacterial strains *Klebsiella pneumonia* and *Staphylococcus aureus*.¹²⁹ Furthermore, while testing stability towards the proteases trypsin and chymotrypsin, the authors observed increased proteolytic stability while the peptide is in its *coiled-coil* form. However, no effect was observed in its unstructured form.¹²⁹

2.2.4 Fluorine's impact on protein engineering

With recent advances in the generation of proteins bearing non-natural AAs, either by chemical or biological methods,¹³² fluorination can be considered an interesting tool for tailoring protein properties.¹³³ While in the context of peptides the incorporation of fAAs can have an immense impact on overall structure of a peptide, their introduction into proteins is in general well accommodated, generally leading to minimal structural perturbation.¹³⁴ Fluorine's influence on thermal and chemical stability, biological activity, and folding kinetics is controversial.

Fluorine's impact on protein stability

Stabilizing effects of fluorine substitutions have been reported, for example, by More et al.¹³⁵ who incorporated trifluoroleucine (tfLeu) into *coiled-coil* forming proteins. These proteins contain seven tfLeu units throughout their heptads.

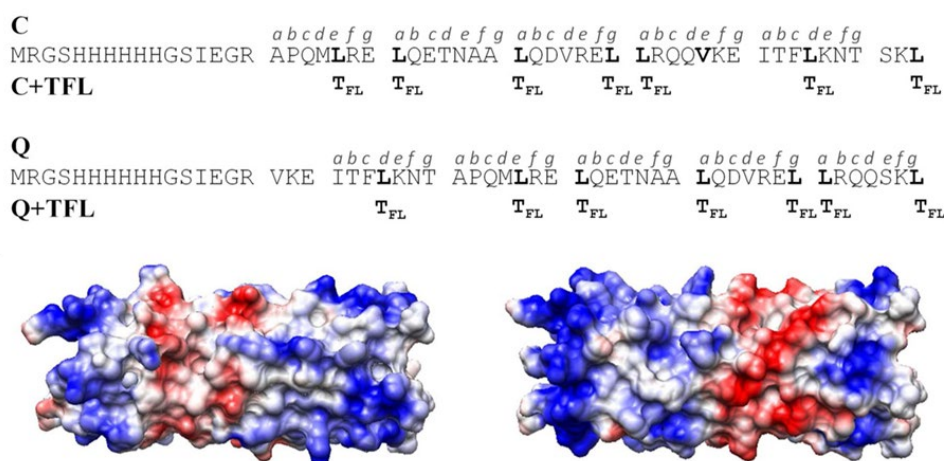


Figure 20: Sequences for engineered proteins as well as fluorinated mutants. (top); electrostatic surface of both fluorinated proteins. Reprinted with permission from More et al.¹³⁵ Copyright © 2015, American Chemical Society

To investigate their influence on overall structure and protein stability, the authors performed CD-experiments. These showed increased helical content for both strands of the coiled-coil protein. Further, thermal denaturation studies also confirmed that both protein strands show increased melting points compared to their non-fluorinated counterparts. Compared amongst each other, melting temperatures were comparable. These results revealed that fluorination not only increases stability, but also enhances secondary structure formation, similar to reports by the Kumar group on GCN4 derived coiled-coils.¹³⁶ Interestingly the formed *coiled-coil* fibers of fluorinated proteins were thicker and more stable, showing the significant influence of fluorine.¹³⁵

Opposing trends have, however, been reported by Alexeev et al.¹³⁷ In their study they investigated modified ubiquitin containing 5-fluoroleucine (MfLeu) at two positions of its hydrophobic core, substituting the proximal pair Leu50 and Leu67 with the fluorinated derivative. Initial NMR investigations showed similar dispersion when compared to wild-type ubiquitin indicating native folding. This was further supported by far-UV CD-

spectroscopy. Furthermore, 2D-NMR analysis showed that fluorinated side chains are similarly buried inside the hydrophobic core, showing no significant deviation from the native structure. Consistent with literature, this shows that the fluorination is again accommodated with next to no structural changes. Analysis of thermal stability using differential scanning calorimetry (DSC), however, showed that FLeu50/67-Ub, while retaining a typical unfolding profile, has a reduced midpoint T_m , which is about 8°C lower than wild-type protein (**Figure 21**).

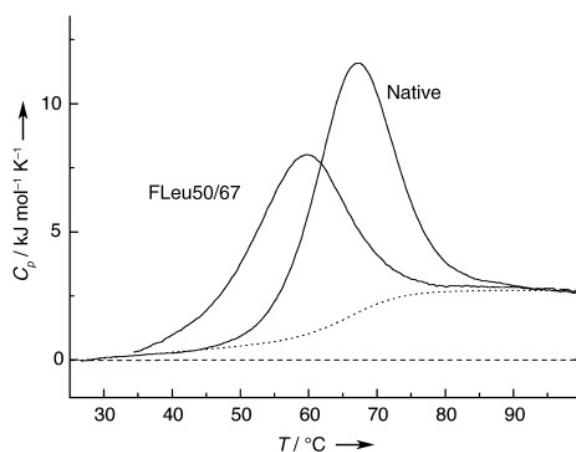


Figure 21: Comparison of the thermal stability of WT and FLeu50/67-Ub by DSC. 1 mg/mL at pH 3.0. Reprinted with permission from Alexeev et al.¹³⁷ Copyright © 2003 WILEY-VCH Verlag GmbH & Co. KGaA, Weinheim.

The authors explain this change with “fundamental changes in solvation thermodynamics (hydrophobicity)”.¹³⁷ Interestingly, FLeu50/67-Ub’s ability to form protein conjugates is retained, further supporting the assumption that MfLeu is incorporated with no structural perturbation.

Fluorine's impact on folding kinetics

In their studies on NTL-9, an α/β -protein, Horng and Raleigh¹³⁸ introduced 4,4,4-trifluorovaline into the two positions Val3 and Val21 (**Figure 22**).



Figure 22: Cartoon of the crystal structure of NTL-9, highlighting Val21 and Val3. Reprinted with permission from Horng and Raleigh.¹³⁸ Copyright © 2003, American Chemical Society.

CD-experiments on modified NTL-9 showed only minimal changes in the proteins overall structure. These results were further confirmed by NMR experiments that showed C_{α} proton shifts with a maximum deviation of 0.3 ppm, with respect to the wild-type protein. Similar to the above presented studies, fAAs are accommodated with minimal perturbation. Further denaturation experiments then revealed increases in stability for the investigated NTL-9 mutants. (**Table 6**)

Table 6: Thermodynamic parameters for NTL-9, NTL-9Val3TfVal and NTL-9Val21TfVal. Adapted with permission from Horng and Raleigh.¹³⁸ Copyright © 2003, American Chemical Society.

Protein	ΔG_u° (kcal mol ⁻¹)	M (kcal mol ⁻¹)	C_M (M)	T_m (°C)
NTL9	4.17 ± 0.07	1.35 ± 0.1	3.08 ± 0.1	79.8
tfV3	4.96 ± 0.05	1.31 ± 0.1	3.78 ± 0.1	81.9
tfV21	5.61 ± 0.11	1.35 ± 0.1	4.07 ± 0.1	83.7

Conducted stopped-flow experiments to investigate folding kinetics showed expected V-shaped chevron plots, confirming the two-state folding mechanism reported for NTL-9¹³⁹ in all cases. Furthermore, present unfolding of both tFVal mutants occurred slower, while refolding occurred at increased rates, with respect to the wild-type protein.

Reduction in unfolding rates suggests that the $-\text{CF}_3$ substitution does not cause a major strain on the native state,¹⁴⁰ while the increase in refolding rates suggests a stabilizing effect on the transition state by hydrophobic interactions induced by $-\text{CF}_3$.¹³⁸

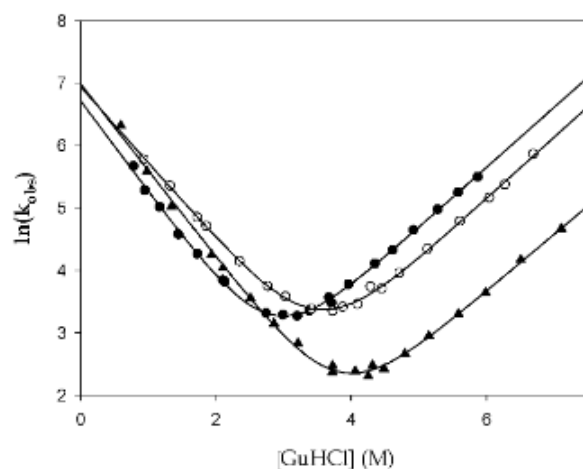


Figure 23: Chevron plot of observed $\ln(k_{\text{obs}})$ vs conc. of denaturing agent GnHCl. ● WT, NTL, ○ tfV3, ▲ tfV21, pH 5.4, at 25°C. 100 mM NaCl, 20 mM sodium acetate. Reprinted with permission from Horng and Raleigh.¹³⁸ Copyright © 2003, American Chemical Society.

Fluorine's impact on protein-protein interaction and subsequent activity

Another parameter that can be influenced by fluorine is the protein-protein, or more specifically, enzyme-inhibitor interaction. The following section aims at discussing this using a model system investigated by the Kokschi group, as this system also builds the foundation for the here presented research on barnase-barstar complexes. A crucial requirement when investigating the influence of site-specific mutations on protein-protein interaction is a profound understanding of the wild-type or parental system. Bovine Pancreatic Trypsin Inhibitor (BPTI) matches these requirements and has thus been studied thoroughly in the past.¹⁴¹⁻¹⁴³ BPTI is a rather small protein with a chain length of 58 AA. Similar to barnase it shows an α/β -fold;¹⁴⁴ it is however supported by the three disulfide bonds Cys5/55, Cys30/51 and Cys14/38 (**Figure 23**).

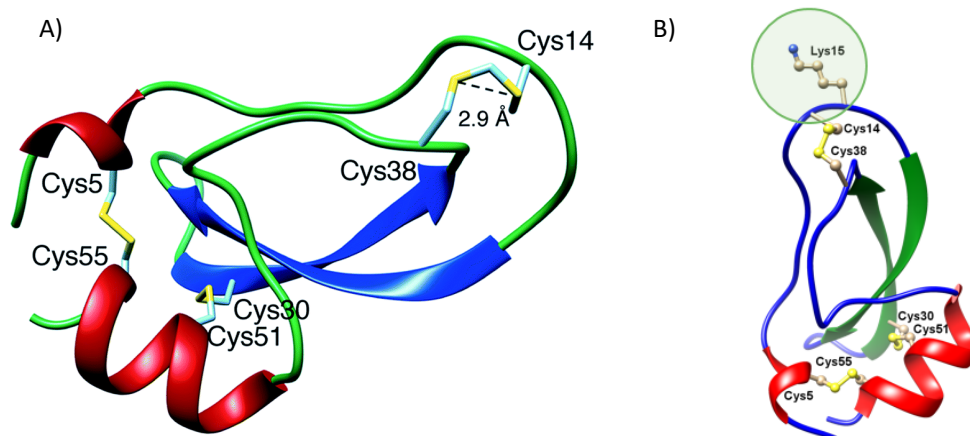


Figure 24: Crystal structures of BPTI, a) highlighting the three disulfide bridges Cys14/38, Cys5/55, and Cys30/51¹⁴¹ b) highlighting Lys15 which is crucial for interaction to proteases. Reprinted (adapted) from Mousa et al.¹⁴¹

BPTI is a serine protease showing a broad range of interaction partners, like trypsin and chymotrypsin, and its active site P1-P1' is located in a loop at Lys15 and Ala16.¹⁴⁵ **(Figure 24)** Crystal structure analysis conducted by Capasso et al. showed that the positively charged Lys side chain interacts via water-mediated hydrogen bonds with negatively charged residues in the S1 position of trypsin-like enzymes, however, in the case of α -chymotrypsin interaction occurs with the carbonyl oxygen atoms of, e.g., Ser217 and Gly216.¹⁴⁶ Further investigations performed on BPTI-trypsin and BPTI-chymotrypsin complexes by Tschesche et al. then showed significant loss of BPTI's inhibitor activity towards trypsin and chymotrypsin upon site-specific Lys15 substitution with canonical AAs, proving its crucial role in binding.¹⁴⁷ **(Table 7)**

Table 7: Concise summary of BPTI-mutants dissociation constants complexed with trypsin and chymotrypsin.(-) indicates no complex, (+) complex formed, illustrating the significance of Lys15. Adapted from Beckmann et al.¹⁴⁷

[Xaa15]BPTI	K _d for Trypsin [M]	K _d forChymotrypsin [M]
Lys	< 1 x 10 ⁻¹¹	7.2 x 10 ⁻⁸
Gly	-	-
Ala	+	-
Abu	+	+
Val	-	-
Ile	-	-

As it has been shown in the Kocsch study that Abu in position 15 of BPTI leads to complex formation but, not to retention of inhibitory activity of wild-type levels, the system lends itself as a valuable starting point to investigate the influence on fluorine in protein-protein interaction. Using the fluorinated Abu derivatives DfeGly and TfeGly Ye et al. set out to synthesize different fluorinated P1 variants of BPTI by a combination of SPPS and native chemical ligation (NCL).¹⁴⁸ This family of AAs also offers the possibility to investigate the influence of the varying degree of fluorination while retaining the side chain connectivity. Consistent with the literature, these modifications did not cause significant structural perturbations, which was shown by initial CD spectra. Furthermore, denaturation experiments revealed that fluorine has a stabilizing effect on the structure of BPTI; Abu, however, shows lower stability, which is in agreement with studies conducted by Krowarsch et al.¹⁴⁹ Thus the stabilizing effect of TfeGly and DfeGly cannot be explained merely with hydrophobic effects but also facilitated electrostatic interactions due to the strong bond polarization.¹¹⁹

Most strikingly, performed activity assays with bovine β -trypsin showed inhibitory activity which is comparable to wild-type BPTI. The performed Abu substitution again showed results in agreement with literature. **Table 8** summarizes observed association constants of all variants.

Table 8: Association constants of BPTI-P1 variants in comparison to WT-BPTI.¹⁴⁸

Protein	Association constant
WT-BPTI	$5.17 \times 10^7 \text{ M}^{-1}$
Lys15DfeGly-BPTI	$3.88 \times 10^7 \text{ M}^{-1}$
Lys15TfeGly-BPTI	$5.20 \times 10^7 \text{ M}^{-1}$

Crystal structure analysis was performed on all variants, revealing additional water molecules in close proximity to the hydrophobic sidechains (**Figure 25**).

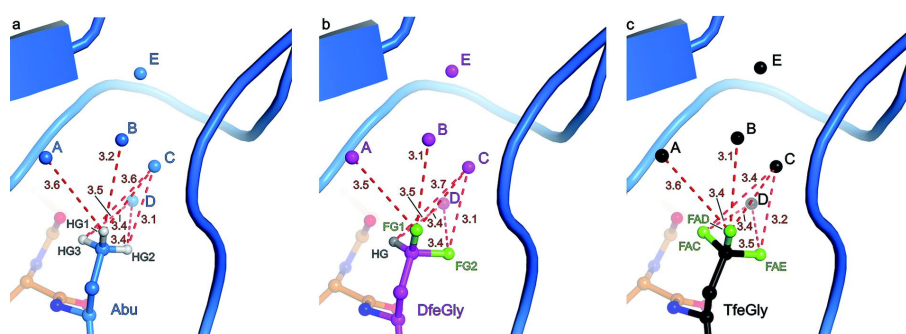


Figure 25: Crystal structure of BPTI active site, illustrating immediate vicinity of fluorinated side chains and possible interaction with water molecules A to E. Reprinted with permission from Ye et al.¹⁴⁸

These additional water molecules (B and C), filling space which otherwise would be occupied by the Lys15 side chain, were thought to be involved in a more energetically favoured fluorine-induced H-bonding network. This was supported by comparison of the calculated *B*-factors (**Table 9**) that showed that waters D and C were apparently more tightly hold in the fluorinated complexes compared to the Abu variant. This was thought to provide an explanation for the restoration of inhibitory activity.

Table 9: B-factors comparing average values for BPTI protein complexes and water molecules in S1 pocket. Adapted from Ye et al.¹⁴⁸

	WT	Lys15Abu	Lys15DfeGly	Lys15TfeGly
Average B-factor of protein complex	20.7	21.3	19.6	21.2
Water molecules on average	31.0	33.8	31.2	32.0
Water molecules in S1 pocket				
A/A'	-/13.5	21.8/-	17.5/-	18.4/-
B	-	27.7	20.0	20.5
C	-	31.2	22.2	20.7
D/D'	-/15.4	23.0/-	17.8/-	17.9/-
E/E'	-/14.1	20.7/-	19.1/-	19.4/-

The theory was, however, disputed by a recent study of Leppkes et al.¹⁵⁰ Improvements were made to the synthesis and refolding methods, and the library of P1 modified BPTI variants was expanded by incorporating also fluorinated variants of norvaline, difluoropropyl glycine and pentafluoropropyl glycine, and completing the trilogy of Abu variants by incorporating MfeGly. Similar to the Ye results, potential structural perturbation was investigated, displaying retained structural integrity for all variants. Furthermore, thermal and chemical stability was investigated for MfeGly15-BPTI, showing slightly reduced T_M of 74 ± 0.1 °C and 70.2 ± 0.1 °C for 8M urea and 6M GnHCl, respectively. This is a difference of 6.2 °C and 3.8 °C, respectively, compared to WT-BPTI under similar conditions. In contrast to the work presented by Ye et al. inhibitory activity was assessed using α -chymotrypsin instead of β -trypsin. Nevertheless, the observed trends were similar. All fluorinated BPTI-P1 variants showed restoration of inhibitory activity up to wild-type level, the Abu variant fell behind slightly. (**Figure 26**)

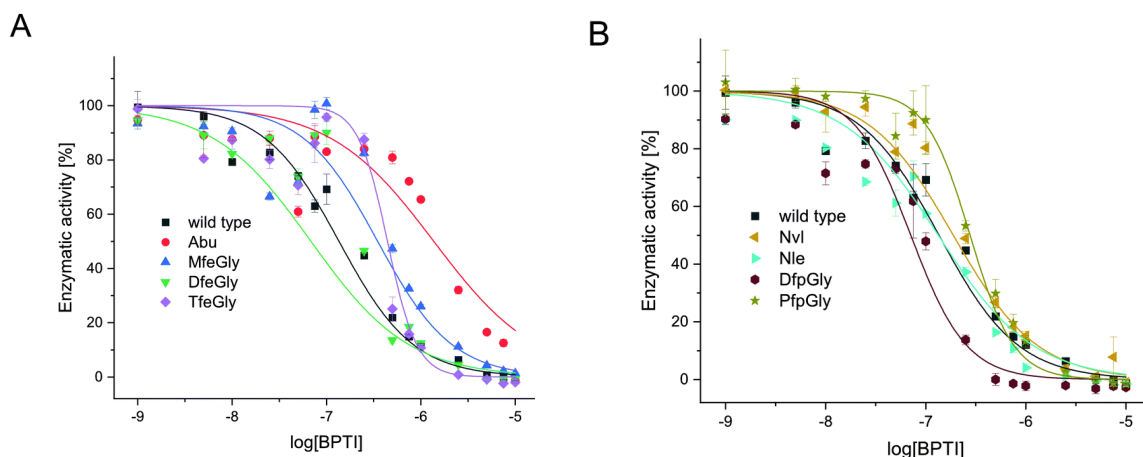


Figure 26: Inhibition of chymotrypsin measured as loss of activity vs. $\log[\text{BPTI}]$. Adapted from Leppkes et al.¹⁵⁰

Calculation of inhibitory constant K_i revealed DfeGly-BPTI as the most potent variant, followed by DfpGly. In general lower K_i were observed in all fluorinated cases compared to the Abu variant, showing the significant impact of fluorination. However, no direct trend could be seen with regard to the degree of fluorination, e.g., comparing results for TfeGly and DfeGly BPTI.

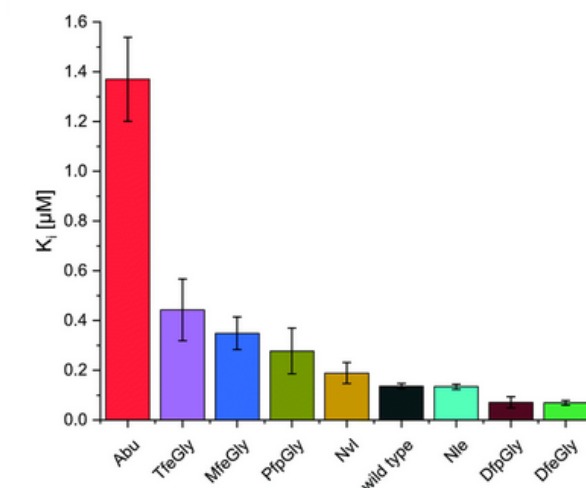


Figure 27: Determined K_i in $[\mu\text{M}]$ for all BPTI-variants, illustrating DfpGly and DfeGly as the most potent inhibitors. Adapted from Leppkes et al.¹⁵⁰

Mere increased hydrophobicity and increased steric demand can thus not be the only explanation. The authors additionally argue that fluorine's induce polarity plays a

crucial role. Further X-ray diffraction experiments also revealed structures in agreement with above presented results, featuring structural water molecules (**Figure 28**).

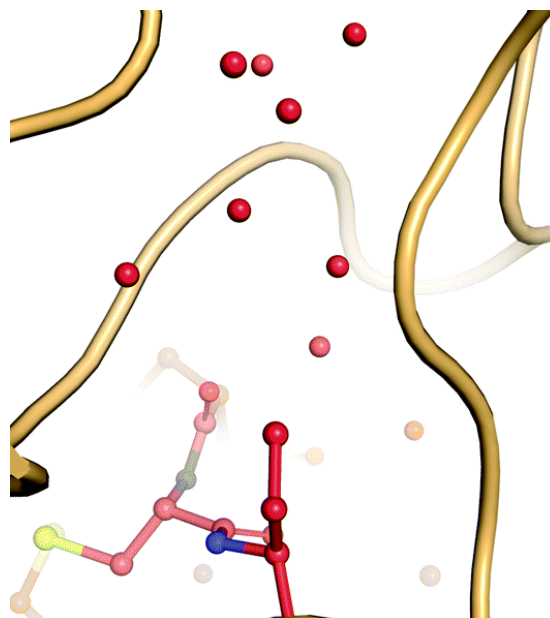


Figure 28: Crystal structure of BPTI-MfeGly15 active pocket. Adapted from Leppkes et al.¹⁵⁰

However, *in silico* studies performed in collaboration with the Keller group showed that these water molecules, despite earlier discussed *B*-factors, do not appear to be involved in observed interactions. While the *B*-factors suggested tighter binding compared to the BPTI variants, the *in silico* experiments by Wehrhan et al. suggest that these are not bound, but rather enter and leave the binding pocket liberally.¹⁵¹

These studies, as well as above presented research on fluorine's impact on peptides, impressively show that the incorporation of fluorine can generally have beneficial consequences. Its impact, however, cannot be predicted in the majority of cases.¹⁰¹

3 Aim

The here presented thesis aims at investigating the influence of fluorine on enzyme-inhibitor interaction. Based on earlier results of the Kocsch group, which show an interesting trend in the influence of fAAs on the enzyme-inhibitor interaction in Bovine Pancreatic Trypsin Inhibitor (BPTI), it will be investigated on another complex, barnase-barstar, whether the observed effects are generalizable or specific for BPTI. Fluorination of barnase will be achieved by the site-specific incorporation of fAAs in position 27.

These fluorinated variants will contain fluorinated analogues of Aminobutyric acid MfeGly, DfeGly, TfeGly, as well as DfpGly and PfpGly, which are the analogues of norvaline. Fluorinated AAs were kindly provided by Hohmann and Chowdhary. To date no fluorinated variants of either barnase or barstar have been described.

In order to facilitate investigations of these fluorinated barnase variants, synthesis methods utilizing microwave-assisted SPPS (MW-SPPS) will be established. Synthesis success will be continuously ensured by analytical HPLC and ESI-MS methods. Following the synthesis suitable purification methods will be established, making use of a combination of protein folding and SEC techniques. Once synthesis and purification have been established, pure proteins will be subjected to structural investigation to ensure correct folding. This will be done by CD spectroscopy as well as NMR-techniques. Finally, proteins with native conformation will be studied in fluorescence-based activity assays to generate a basis for future investigations regarding interaction with the native inhibitor barstar, resulting inhibitor efficiency, and crystal structures. Recombinant barstar_{CCAA} as target inhibitor will be provided by M. Krummhaar (MPI). Furthermore, fluorinated barnase-barstar complexes will be examined towards changes in their binding affinities by ITC measurements, to further elucidate fluorine's impact on protein-protein interactions. Finally, all variants in complex with barstar_{CCAA} will be crystallized and analyzed by X-ray diffraction, to gain further information on the three dimensional structure of the fluorinated complexes.

4 Results and Discussion

4.1 Barnase as system to investigate fluorine's impact on protein-protein interaction

As discussed above, the barnase-barstar complex was chosen to investigate the influence fluorine might have on protein-protein interaction. Therefore, choosing a well-characterized system is indispensable, and thanks to the efforts of researchers like Allen Fersht, barnase is such a system. To investigate fluorine's impact on this protein, the aim is to site-specifically substitute Lys27. As discussed previously, this position plays a key role in the interaction of barnase with both its inhibitor, and substrate. While substitution with canonical AAs leads to loss of activity but an increase in folding stability⁴⁵, the goal here is to investigate how partially fAAs impact these characteristics.

Typically, proteins, being sizeable biomolecules, are synthesized using methods of protein expression. In spite of the fact that site-specific incorporation of custom AAs is possible by these methods, access through Solid-Phase Peptide Synthesis (SPPS) was the method of choice. Historically, chemical access to barnase was granted through a combination of SPPS and NCL, which to date is used to chemically synthesize large proteins, even up to 90 KDa¹⁵². However, with recent advances in MW-assisted SPPS¹⁵³ establishing a total synthesis for barnase and modified barnase variants seemed feasible. To our knowledge, only NCL-based procedures had been reported until early 2020, when a flow-based SPPS strategy was reported by N. Hartrampf, stating successful synthesis of proteins up to 170 AA.¹⁵⁴ This further encouraged the attempts, since flow-based SPPS, while still utilizing the general mechanisms of SPPS, can still be considered a different method of synthesis.

4.2 Access to fluorinated derivatives of aminobutyric acid

In previous work the group of Prof. Dr. Kocsch already put extended efforts in establishing gram-scale access to fAAs. The synthesis of these is discussed in **Section 2.2.1** and the AAs used in this project were thus kindly provided by T. Hohmann and S. Chowdhary. The AAs used in this thesis are primarily derivatives of aminobutyric acid (Abu): Monofluoroethyl glycine (MfeGly), Difluoroethyl glycine (DfeGly) and Trifluoroethyl glycine (TfeGly).

Furthermore, derivatives of the AAs norvaline were incorporated into barnase, these being Difluoropropyl glycine (DfpGly) and Pentafluoropropyl glycine (PfpGly) (**Figure 29**).

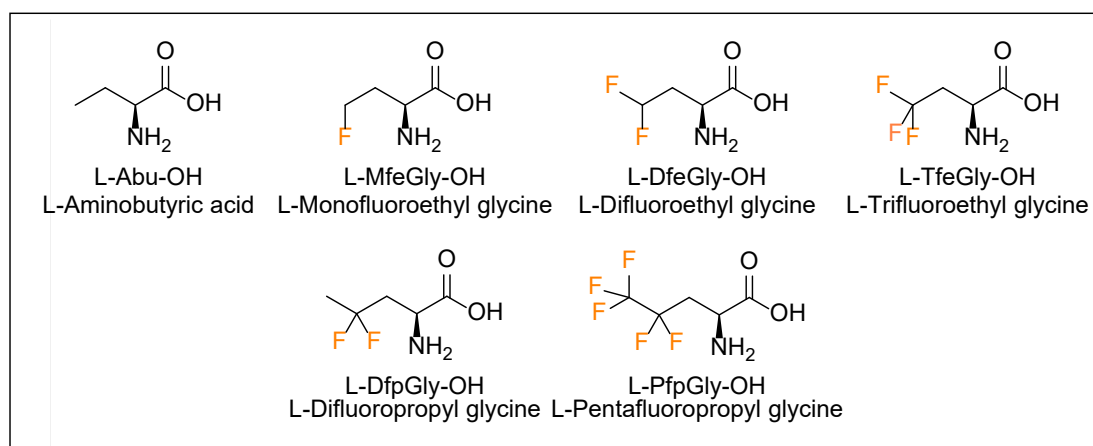


Figure 29: Chemical structures of Aminobutyric acid and its fluorinated analogues (top row), and fluorinated analogues of Norvaline (bottom row).

4.2.1 Microwave-assisted SPPS

With its chain-length of 110 AAs, barnase poses a significant synthesis challenge in the context of SPPS, as this method has historically been limited to synthesis of up to 30-50 AAs. This limit is linked to decreased coupling or deprotection efficiency, decreased crude purity, and a significant increase in side-product formation during synthesis, mainly being truncated sequences or deletion products as the outcome of incomplete couplings. The main cause of these side products lies in the increasing strength of interactions between growing peptide chains, ultimately leading to aggregation on the solid support and impeding further coupling reactions. In manual and early automated synthesis this was met with the use of so-called pseudoprolines (**Figure 30**), dipeptide building blocks which, due to their rigid conformation, cause a kink in the peptide chain and thus, making the otherwise buried N-terminus available for further coupling. They are, however, limited to dipeptides containing Ser, Thr or Cys derivatives, as these are needed for the cyclisation. During TFA mediated cleavage from the solid support this cyclic structure is opened to generate the desired peptide sequence.¹⁵⁵

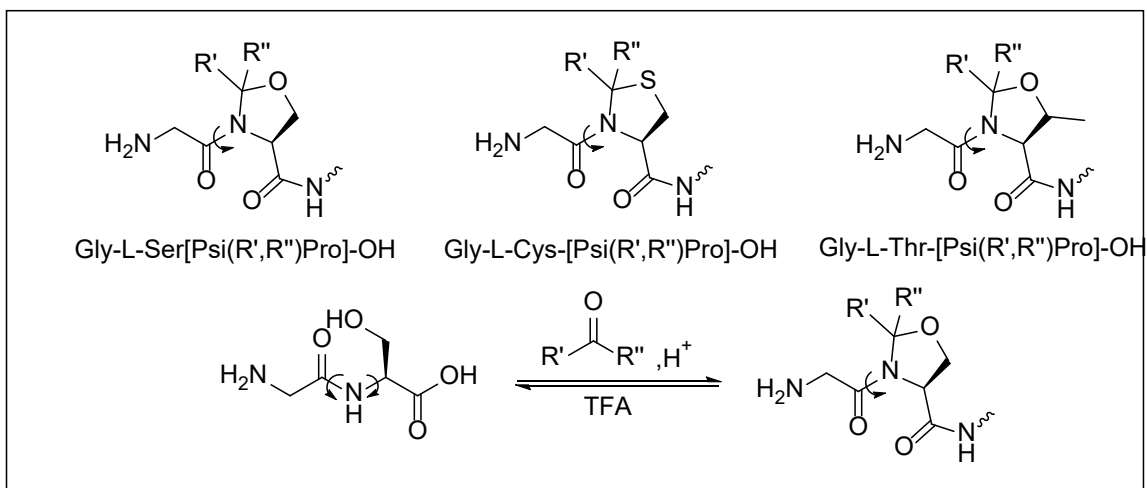


Figure 30: (Top) Exemplary illustration of pseudoproline dipeptides resulting in GlySer, GlyCys, GlyThr. (Bottom) Illustration of pseudoproline generation and removal resulting in desired peptide sequence. Adapted with permission from Dumy et al.¹⁵⁵ Copyright © 1997, American Chemical Society.

A more recent approach to battling aggregation and related issues during synthesis is the development of MW-assisted SPPS. Using this method, synthesis of peptides up to 100 AAs, like ubiquitin or barstar, were reported.¹⁵³

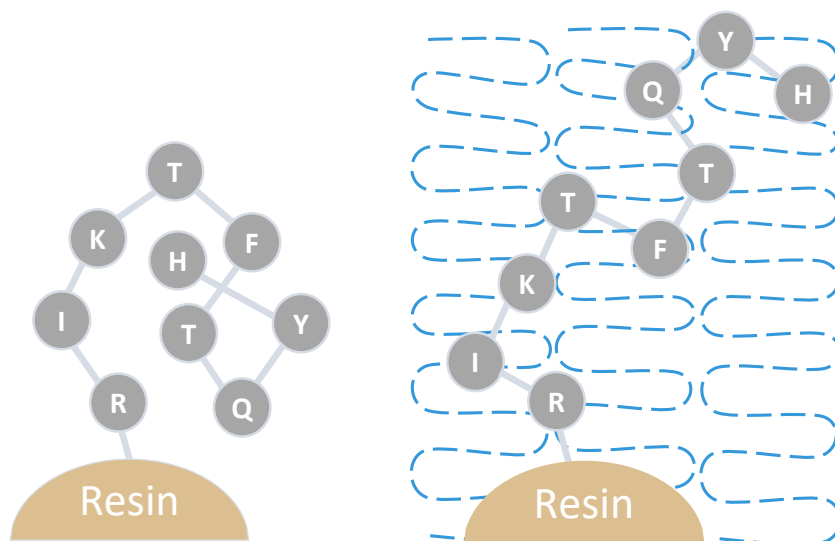


Figure 31: Expected impact of microwave-radiation on peptide-resin complex during SPPS. Adapted with permission from Palasek et al.¹⁵⁶ Copyright © 2006 European Peptide Society and John Wiley & Sons, Ltd.

Different to conventional automated SPPS, a common theory on the mode of action attributes the main advantage to MW-assisted SPPS to the direct interaction of MW-irradiation with the large dipole moment of the peptide backbone. Through dipole rotation, this interaction causes a direct energy transfer or heating which enhances a

multitude of processes. Furthermore, it is theorized that this interaction also prevents aggregation of the peptide chains on resin. While significant positive effects on synthesis efficiency are observed, it is widely discussed whether this is merely a thermal effect through irradiation, as similar results in synthesis up to 24 AAs were achieved utilizing consistent external heating.¹⁵⁷ To date however, no total synthesis approach to large peptides, like the herein discussed barnase or barstar have been reported, utilizing only conventional heating.

4.2.2 Establishing a MW-assisted SPPS approach to barnase

Even though SPPS offers very well established methods to synthesize peptides, every synthesis approach to a new molecule shows its individual intricacies. And while using MW-assisted SPPS generates a facile process to synthesize even proteins up to 100 AAs, its major advantage can also be considered a major drawback. Using fast coupling cycles with temperatures up to 90°C evidently increases coupling efficiency; however, also undesired side reactions benefit from these conditions. Thus, the total synthesis of barnase poses a significant challenge in different aspects.

The first challenge to any peptide synthesis is the choice of the resin. With regards to microwave methods an optimized Cl-MPA resin (**Figure 32**) was chosen, as it offers the ideal properties in terms of swelling profile, temperature resistance at prolonged times, low loading capacity, which reduces inter-chain interactions,¹⁵⁸ and acid lability, as suggested by the manufacturer CEM GmbH. Loading of the resin occurs in the presence of DIPEA and KI, following a simple Finkelstein exchange¹⁵⁹ (**Figure 32**), and can be performed for any AA as the first cycle of the synthesis.

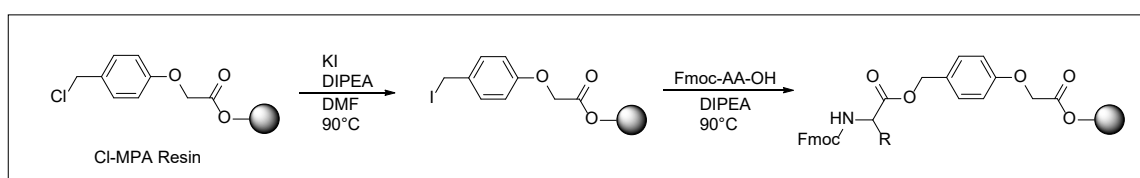


Figure 32: Schematic representation of chloride loading as carried out during MW-SPPS.

Since no established MW-assisted synthesis scheme, apart from standard MW-SPPS methods used in the synthesis of smaller proteins and peptides, existed to the synthesis of barnase, the protein was separated in eleven 10-AA blocks as a starting point. This is summarized in **Table 10**. While in general the stepwise synthesis of wild-type barnase by adding 10 AA followed by immediate reaction control by analytical RP-HPLC went without many difficulties a few very common side-reactions had to be eliminated, and will be discussed in the following sections.

Table 10: Summary of establishing a synthesis of barnase by step-wise addition of blocks of 10 AA.

10	20	30	40	50	60	70	80	90	100	110
AQVINTFDGV	ADYLQTYHKL	PDNYITKSEA	QALGWVASKG	NLADVAPGKS	IGGDIFSNRE	GKLPKGSGRT	WREADINYTS	GFRNSDRILY	SSDWLIYKTT	DHYQTFKIR
										← 10 ¹ D-110R
									← 91S-100T	← 10 ¹ D-110R
								← 81G-90Y	← 91S-100T	← 10 ¹ D-110R
							← 71W-80S	← 81G-90Y	← 91S-100T	← 10 ¹ D-110R
						← 61G-70T	← 71W-80S	← 81G-90Y	← 91S-100T	← 10 ¹ D-110R
					← 51I-60E	← 61G-70T	← 71W-80S	← 81G-90Y	← 91S-100T	← 10 ¹ D-110R
				← 41N-50S	← 51I-60E	← 61G-70T	← 71W-80S	← 81G-90Y	← 91S-100T	← 10 ¹ D-110R
		← 31Q-40G	← 41N-50S	← 51I-60E	← 61G-70T	← 71W-80S	← 81G-90Y	← 91S-100T	← 10 ¹ D-110R	
	← 21P-30A	← 31Q-40G	← 41N-50S	← 51I-60E	← 61G-70T	← 71W-80S	← 81G-90Y	← 91S-100T	← 10 ¹ D-110R	
← 11A-20L	← 21P-30A	← 31Q-40G	← 41N-50S	← 51I-60E	← 61G-70T	← 71W-80S	← 81G-90Y	← 91S-100T	← 10 ¹ D-110R	
← 1A-10V	← 11A-20L	← 21P-30A	← 31Q-40G	← 41N-50S	← 51I-60E	← 61G-70T	← 71W-80S	← 81G-90Y	← 91S-100T	← 10 ¹ D-110R

Histidine epimerization

One of the most common side reactions are the epimerization of histidine and cysteine. Since no cysteines are present in barnase, only His is discussed in this section. As mentioned before, increased temperature and microwave-irradiation does not only enhance desired product formation, but also increases the probability of side reactions like epimerization.¹⁶⁰ Early studies suggested the imidazole π -nitrogen to be the cause of this reaction.¹⁶¹ Two mechanisms had been proposed on how this side reaction occurs.¹⁶⁰ (**Figure 33**) Following pathway A, during carbodiimid activation, the α -acidity of the backbone C_{α} -proton is increased and is thus attacked by imidazole π nitrogens. This leads to the formation of a C=C double bond. Opening this double bond leads to the formation of (*R*) and (*S*) conformations of the AA. The alternative mechanism (**Figure 33B**) proposes an internal nucleophilic attack of π -nitrogen leading to a cyclisation, which can open up to (*R*) and (*S*) conformations.

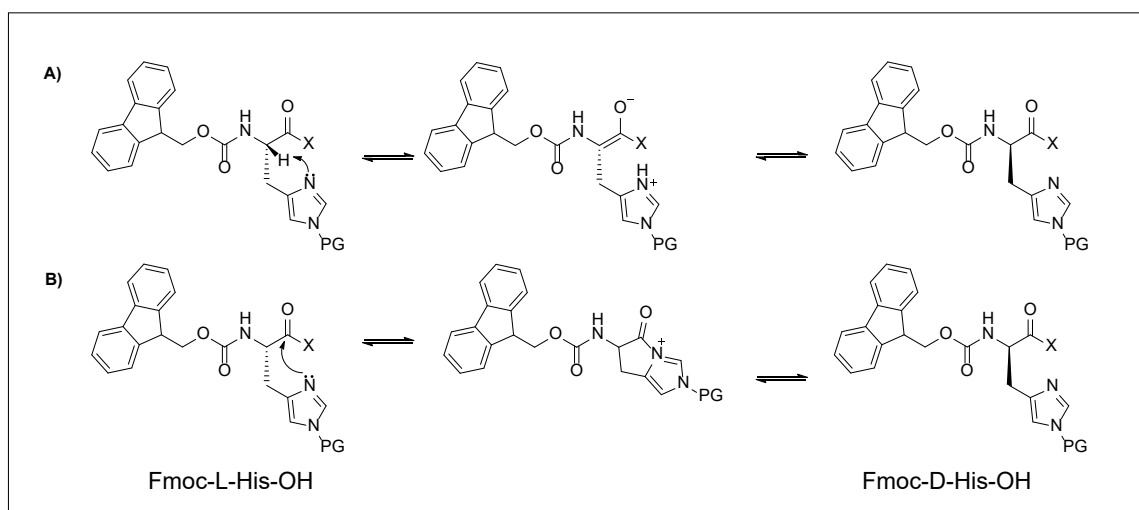


Figure 33: Suggested mechanisms to His epimerization during SPPS. A) shows intramolecular deprotonation leading to formation of a C=C double bond. Opening results in epimerization. B) shows intramolecular nucleophilic attack at carboxylic function leading to cyclization. Opening results in epimerization. X= Leaving group.

In general, His is therefore coupled at reduced temperatures compared to standard couplings, e.g., 50°C as opposed to 90°C, applied in MW-methods. However, the overall reaction time is prolonged to keep coupling efficiency consistent.

Despite the use of this method, epimerization could be observed in the presented work, as shown in **Figure 34**. Protecting group chemistry was modified to further reduce epimerization. Instead of the most commonly used Fmoc-His(Trt)-OH, the Fmoc-His(Boc)-OH derivative (**Figure 34**) can be used. Here, the imidazole τ -nitrogen is protected with a Boc-group, thus deactivating the π -nitrogen due to the introduced electron withdrawing effect, reducing likelihood of C_{α} deprotonation. Another option is the protection of π -nitrogen using Fmoc-His(Mbom)-OH (**Figure 34**). In this case a bulky protecting group is installed that blocks any reaction occurring at this position.

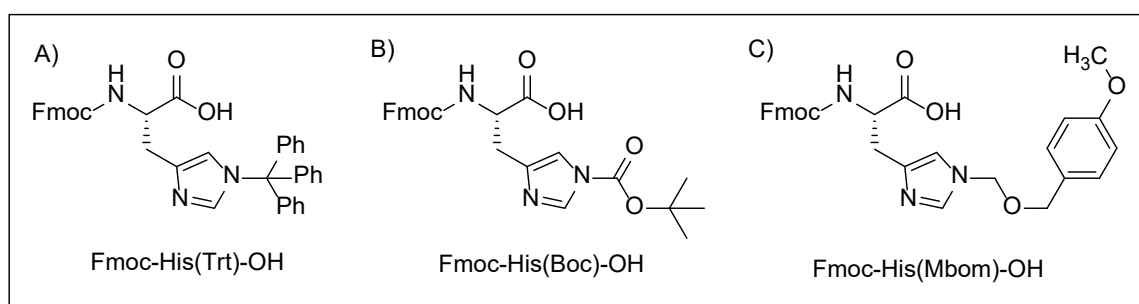


Figure 34: Chemical structure of protected His-derivatives A) Fmoc-His(Trt)-OH B) Fmoc-His(Boc)-OH C) Fmoc-His(Mbom)-OH

All protecting groups are cleaved during standard cleavage procedures using TFA. In this presented work Fmoc-His(Boc)-OH was used instead of Fmoc-His(Trt)-OH, reducing the observed epimerization by approximately 5%.

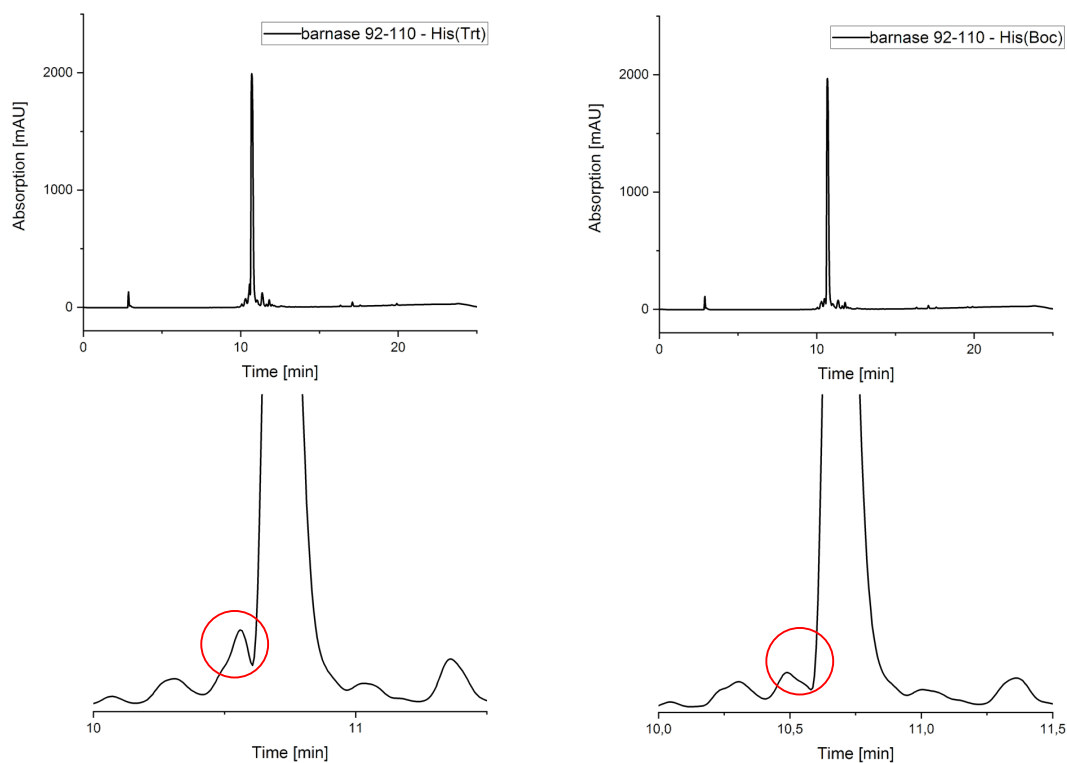


Figure 35: Analytical HPLC chromatograms displaying reduction in His epimerization when using Fmoc-L-His(Boc)-OH (right) instead of Fmoc-L-His(Trt)-OH (left). Zoom in on both signals (bottom) clearly shows diminished signal at $R_t=10.55$ min.

However, it has to be mentioned that none of the above-described procedures was able to completely prevent epimerization from the synthesis, but reduced it considerably.

Aspartimide formation

Another very common side reaction, which unfortunately cannot be avoided entirely is the aspartimide formation, which can occur at any aspartic acid residue, however its probability varies, depending on e.g. sterical demand of aa side-chains. In chemical synthesis, aspartimide formation will occur after cyclization of Asp-residues during Fmoc-removal under basic conditions.¹⁶² Due to the cyclic nature of SPPS this undesired side reaction can arise at any point during the synthesis, though as mentioned above its probability varies depending on neighboring AAs. A very crucial example, which is also present in the barnase sequence, is the Asp-Gly dipeptide.

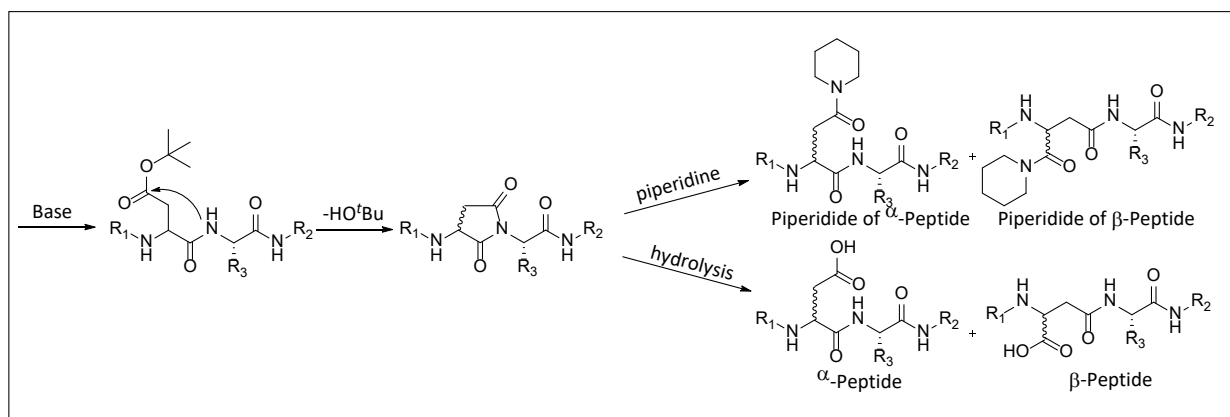


Figure 36: Mechanism of aspartimide formation at Asp-X AA pair. Adapted with permission from Mergler et al.¹⁶³ Copyright © 2003 European Peptide Society and John Wiley & Sons, Ltd.

Under the basic conditions of Fmoc-removal, backbone amides can be deprotonated, generating a nucleophilic nitrogen, which can then attack the carboxy-group of the Asp side chain and remove the $t\text{Bu}$ -ester, which is generally used as protecting group. This will lead to the aforementioned cyclisation of both neighboring AAs. At this point two possible pathways can occur; In the presence of piperidine, which is commonly used for Fmoc-removal, the ring can open up to form α or β piperidide. On the other hand, the ring can open up by hydrolysis generating an α or β peptide.

When analyzing these side products in HPLC and ESI-MS the intermediate shows as second signal in HPLC and $-18 m/z$ difference to the expected average mass of the desired product (**Figure 37**).

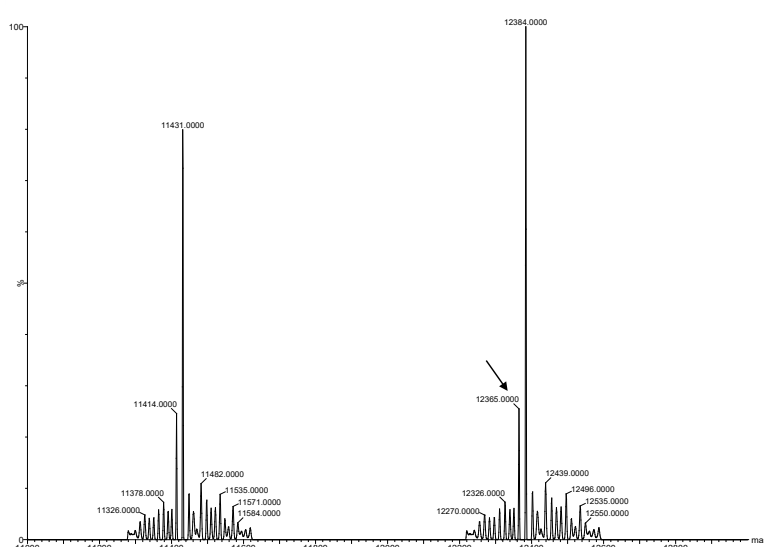


Figure 37: Mass spectroscopy revealing $-18 m/z$ with respect to the expected mass showing the potential formation of aspartimide for WT barnase. m/z Values round up during deconvolution.

The piperidine adducts, however, generate a +67 m/z signal in ESI-MS relative to expected results, however, such signal was not observed in the presented study, as no piperidine was used. Similar to His epimerization aspartimide formation cannot be fully eliminated, only minimized. Fortunately a variety of countermeasures can be applied during synthesis. The most common of which is the use of piperazine over piperidine due to its lower pK_a value (piperidine $pK_a = 11.1$ at 25°C, piperazine $pK_a = 9.73$ at 25°C).¹⁶⁴ Common deprotection solutions contain 2-20% (v/v) of piperidine in DMF, while piperazine is prepared at 10% (w/v) in a mixture of NMP/EtOH 9:1. Overall basicity of deprotection solutions can be further reduced by the addition of 0.1 M HOBt or OxymaPure, thus further reducing chances of aspartimide formation to occur. Similarly to His also the sidechain protecting group can have a tremendous influence on avoiding side reactions. A common strategy is the use of bulky sidechain protecting groups instead of a standard t Bu ester. These could be Fmoc-Asp(OMpe)-OH, as used in this work, Fmoc-Asp(OEpe)-OH or Fmoc-Asp(OBno)-OH, further increasing bulkiness of the side chain (**Figure 38**).

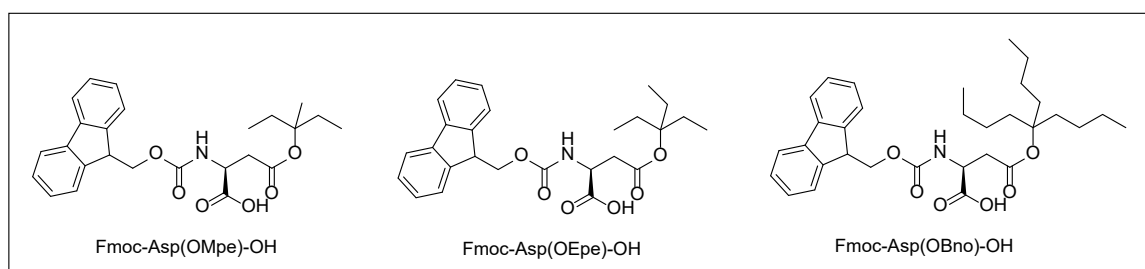


Figure 38: Chemical structures of side chain protected aspartic acid A) Fmoc-Asp(OMpe)-OH, B) Fmoc-Asp(OEpe)-OH, C) Fmoc-Asp(OBno)-OH.

Another very effective countermeasure is the dimethoxybenzyl- (DMB) backbone protecting group, which is commonly used in the Asp-Gly dipeptide; Fmoc-Asp(O t Bu)(DMB)Gly-OH. Using this group, no deprotonation can occur during Fmoc-removal, thus eliminating the chance of aspartimide formation. Due to the complexity of the protein, aspartimide formation could not be observed directly during synthesis steps, however, since it is a very common side reaction, above discussed countermeasures were applied nonetheless.

4.2.3 Results after optimization and adapting for unnatural amino acids

Under consideration of possible side reactions, a straight forward scheme for the successful synthesis of barnase was established. (**Figure 39**) With a total reaction of approximately 21 hours wild-type barnase was successfully synthesized using the LibertyBlue™ MW-Synthesizer. After approaching the synthesis in blocks of 10 AAs, confirming success, synthesis is then conducted in two steps starting with a block of 60 AA followed by adding a block of 50 AA's. Established procedures can be easily scaled up to 0.1 mM, and were also applied in the successful synthesis of the first unnatural variant of barnase containing aminobutyric acid.

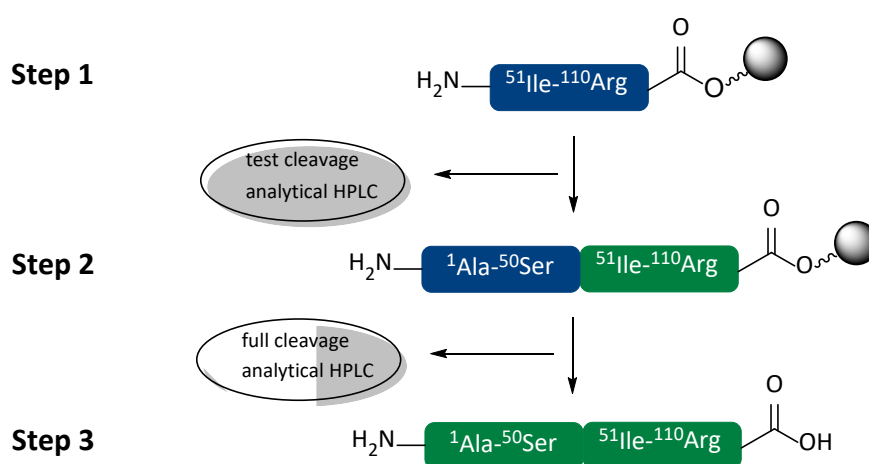


Figure 39: Synthesis scheme for wild-type barnase.

With established methods in hand the synthesis of fluorinated barnase variants was tackled. A major issue to this task is the position of substitution itself. Aiming for the substitution of Lys27, this meant modification of a coupling step, which happened quite late in the synthesis, reducing overall efficiency of coupling reactions. Already prior to this project, a coupling cycle for special AAs using the MW-synthesizer was established. Since fAAs are not as abundantly available as their natural counterparts are, this cycle aims at the dramatic reduction of amount of artificial AA's needed, and thus calls for two equivalents. In comparison, natural AAs are coupled at five equivalents. This reduction is made possible by additional washing steps, and thus eliminating the risk of quenching by remaining deprotection solution. To compensate for reduced equivalents of AAs the overall reaction time was extended to ten minutes. However, a reduction in overall yield

and crude purity was noticed in the case of BarDfeGly27 and BarMfeGly27, hence equivalents for fAAs should be kept at five, if possible.

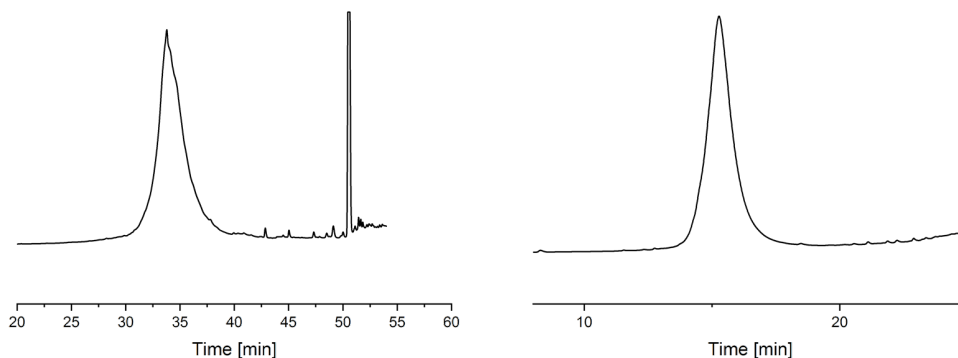


Figure 40: Crude chromatogram WT barnase (left) coupled at five equivalents vs. DfeGly (right) coupled at 3 equivalents. Chromatograms illustrate significant broadening of the peaks, suggesting increasing amounts of truncated species when reducing equivalents.

To ensure coupling of the fluorinated AA, and thus reduce the possibility of truncated barnase variants, further adjustments were made to the overall synthesis pathway. While the synthesis can be approached similarly to wild-type barnase, starting with a fragment of 60 AAs, the next step only includes 22 AAs, ending at position 29. The next step involved merely the addition of AAs 28 and 27, which is the point of substitution. AA 28 is coupled just before the fAA to ensure that all external conditions, like temperature and take-up of AAs, are met properly. The successful addition of unnatural AAs is verified by immediate test-cleavage followed by HPLC and MS analysis. If the result is positive, the final 26 AAs are coupled to finish the barnase sequence. **Figure 41** summarizes the synthesis scheme after including unnatural AAs to the sequence.

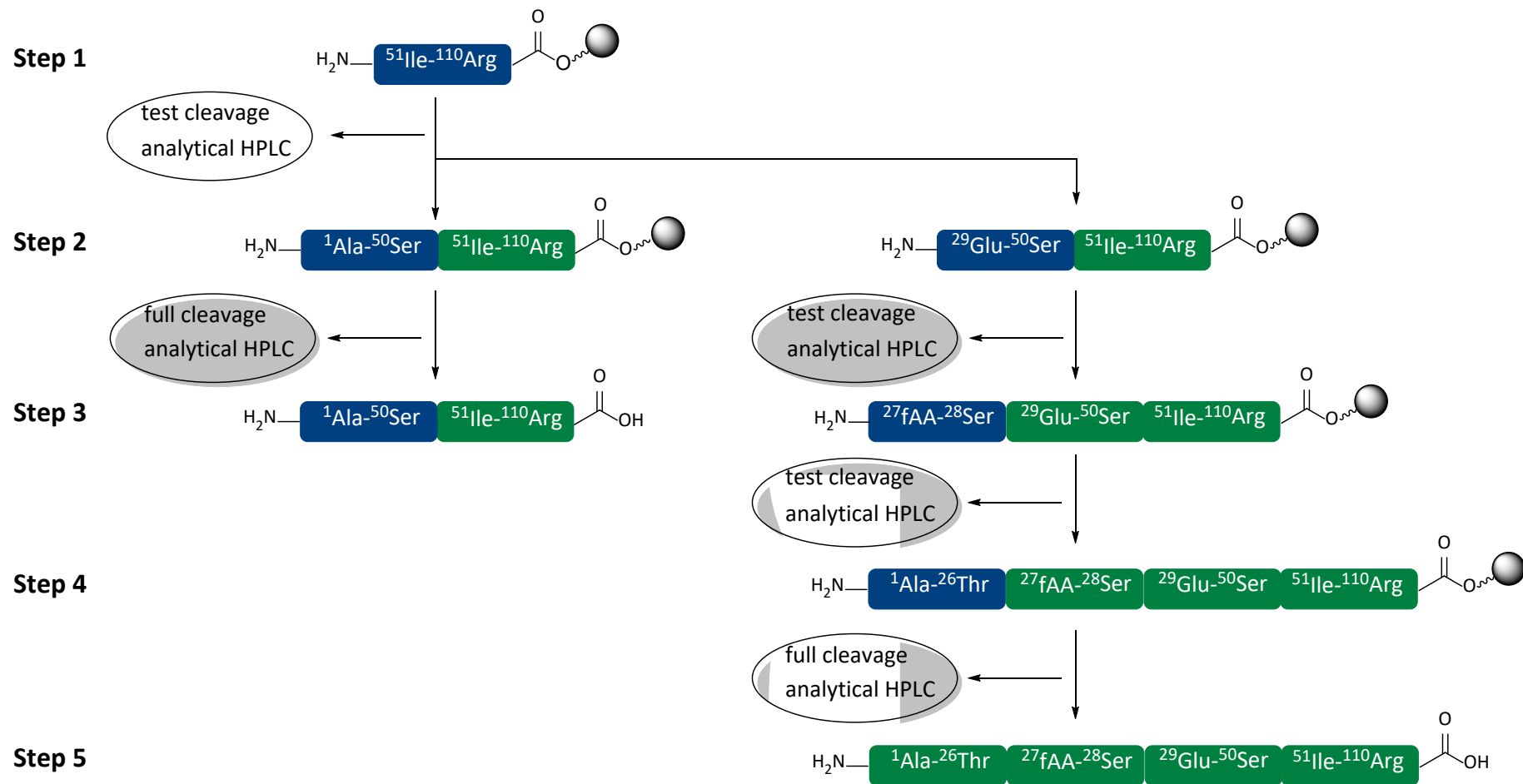


Figure 41: Extended synthesis scheme of barnase including non-natural AAs (fAA).

Applying these methods, successful synthesis of BarLys27, BarAbu27, BarMfeGly27, BarDfeGly27 and BarTfeGly27 variants can be reported in this work.

4.2.4 Purification of Barnase – from HPLC to SEC

Having established applicable methods to the synthesis of different barnase variants, and verifying their success by analytical HPLC methods, the next major issue is the purification of these proteins. In preparation proteins were cleaved of the resin using a standard TFA (Trifluoroacetic acid) containing cleavage cocktail, as described in **Section 9.6.1**. Due to significant amounts of His and Trp residues, which are prone to oxidation, it is crucial to use EDT (ethanedithiol) as scavenger. Already early on during full- and test cleavages it was noticed that all proteins generate a HPLC signal with similar retention time, which in ESI-MS analysis identifies as +44 m/z relative to the expected value. This side product stems from incomplete side chain deprotection of Trp residues and is removed by incubation of crude peptide samples under acidic conditions. (**Figure 42**)

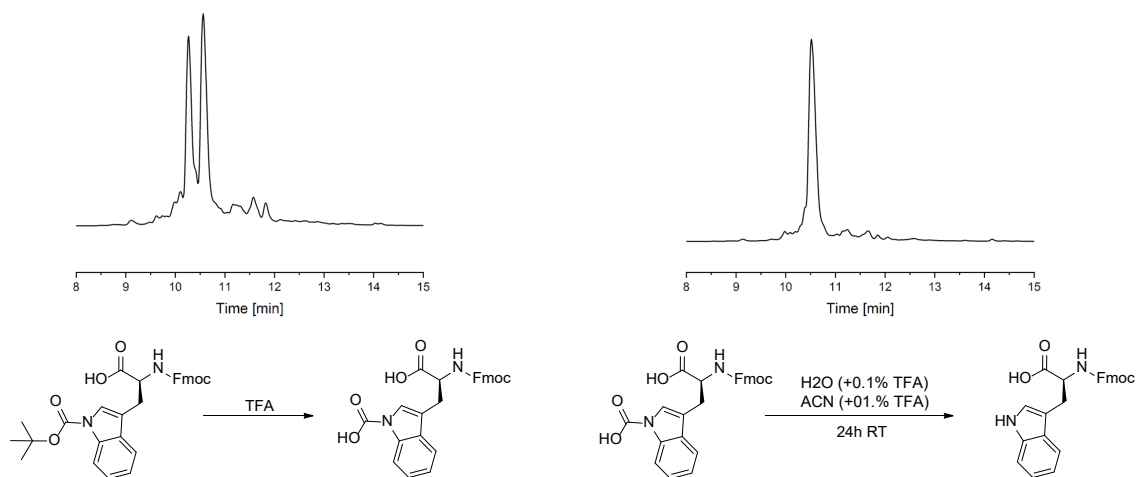


Figure 42: (Top) Chromatogram of a barnase 20mer before and after incubation in acidic conditions. (Bottom) Expected Trp-deprotection during full cleavage and incubation.

Hence, in preparation of purification, crude proteins were dissolved in 1:1 mixture of H₂O:MeCN, each containing 0.1% TFA, and incubated overnight. While analytic purification was possible, generating minimal amounts of pure protein, transfer to preparative methods was troublesome. In the first attempts, a Jupiter C18 column 300 Å

was used, due to protein size; however, the results did not match previously performed analytical HPLCs in this work using the same conditions.

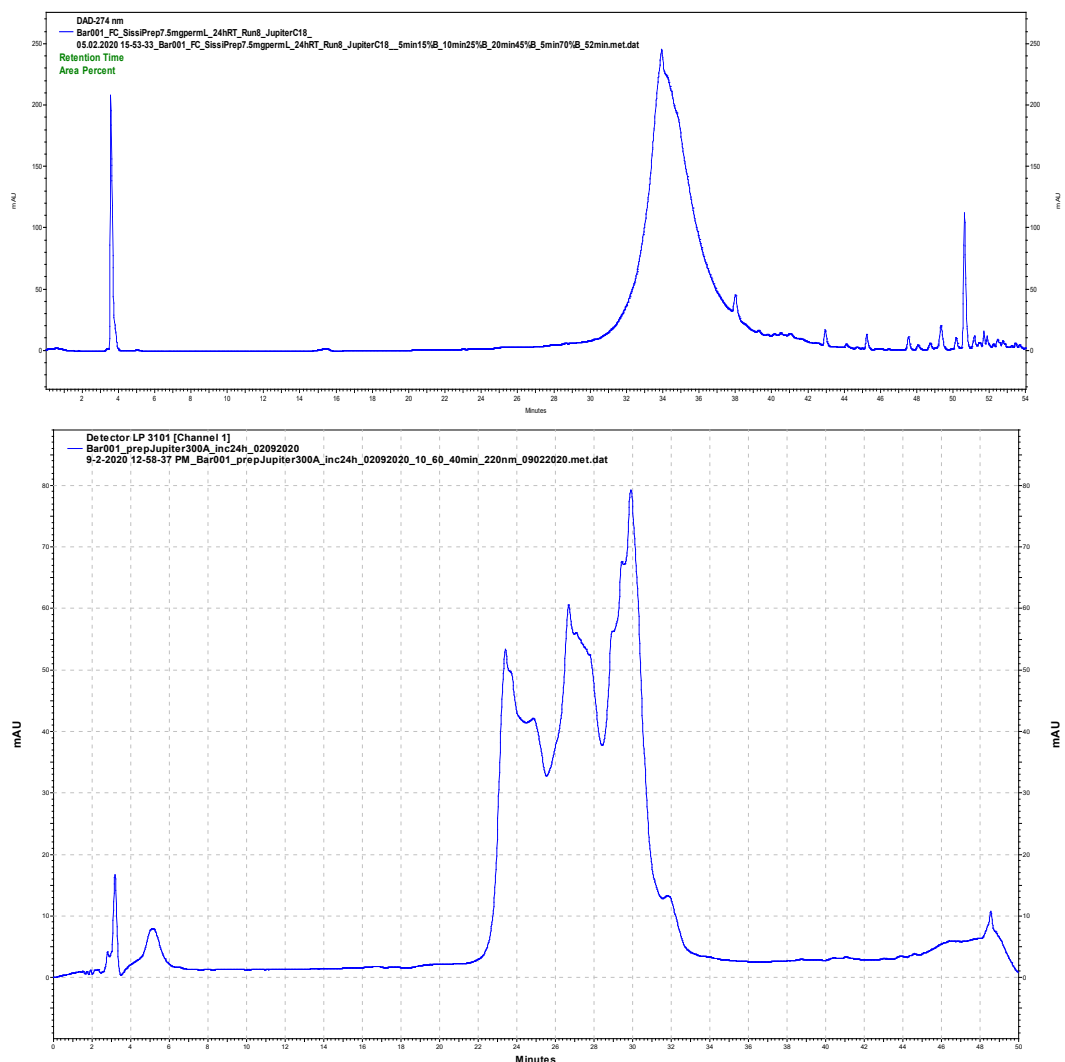


Figure 43: Analytical HPLC chromatogram (top) compared to preparative HPLC chromatogram wild-type barnase (bottom).

Using these conditions as a starting point, a vast variety of conditions were tested: increases and reduction of applied peptide crude mass, ranging from 5 to 20 mg/mL with a total injection volume of 2 to 5 mL; increases and reduction of percentage of TFA added to eluents H₂O and MeCN, ranging from 0 to 1%; and substitution of MeCN for MeOH. It has to be noted that according to manufacturer's suggestion no more than 1% TFA should be applied to the column material. Even though, on first glance, it seemed like progress in terms of purification conditions, and reproducibility was made (**Figure 44**), with elevated TFA concentrations to 0.5% proposedly showing the best results, it was theorized, that by

reducing the amount of TFA in the mobile phase to 0.05%, instead of generating better separation, the contrary happened and product signals were compressed.

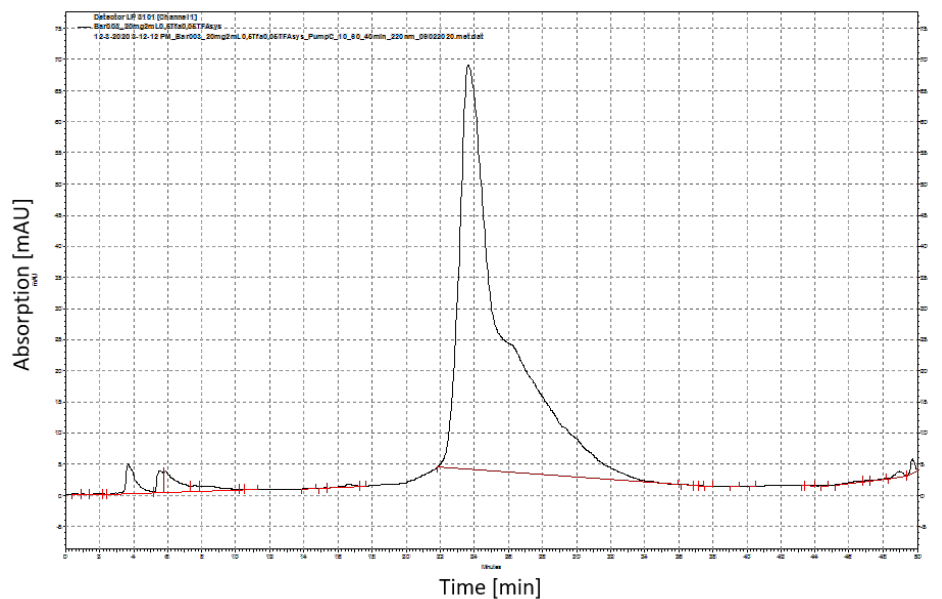


Figure 44: Illustration of supposedly achieved optimization; preparative HPLC chromatogram of xx mg crude peptide applied to the column, purified in ACN:H₂O adding 0.5% TFA to the eluents.

This is supported by recent results provided by CEM, testing the purification of wild-type barnase on their HPLC device *Prodigy*. (**Figure 45**)

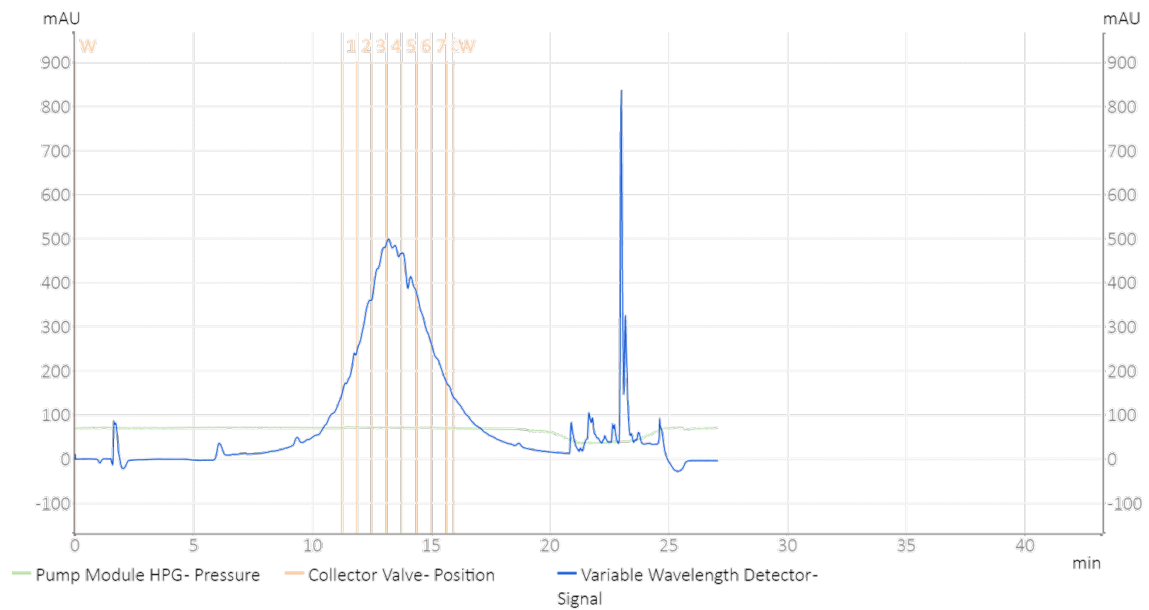


Figure 45: CEM chromatogram by Monika Swiontek. Wild-type barnase C4 column, the advantage of heating during HPLC. Compared to the most successful attempt in this work.

Without making significant progress in the RP-HPLC based purification of barnase, and having to report damage to the column operated, alternative methods had to be established. Fortunately, a very common and promising alternative for the purification of proteins is size-exclusion chromatography (SEC). Unlike RP-HPLC methods where separation is based on polarities, in SEC methods molecules are separated based on their molecular size. However, this comes with a crucial disadvantage: truncated sequences of next to similar size due to incomplete couplings of just a few AAs during SPPS, cannot be separated by SEC. This can be circumvented when making use of barnase's simple and reversible folding mechanism. Similar to other peptide and proteins barnase can be forced into an unfolded state by adding chaotropic salts, like GnHCl, to a buffered solution. Slowly removing these salts allows barnase to fold into its native conformation. Deletion sequences as well as truncated variants cannot adopt a proper folding and thus become insoluble in decreasing amounts of GnHCl. Until reaching less than 1 M GnHCl concentration these misfolded or unfolded variants continuously precipitate and can be filtered off. The remaining protein solution can then be purified by SEC. A similar effect of

precipitation can be observed during thermal denaturation, however dissolving the crude protein poses a significant challenge.

In the first iteration of a purification method 200 mg crude wild-type barnase was dissolved in 10 mL 200 mM phosphate buffer at pH 6.5, containing 6 M GnHCl, properly dissolving the protein using ultra sonication. Afterwards the solution was diluted stepwise with buffer, to reduce the concentration of GnHCl to less than 1 M, ending at a total buffer volume of 80 mL. The solution was left at RT overnight, allowing proper folding, afterwards the precipitate was removed. To avoid partial unfolding, before SEC, remaining GnHCl was removed using a standard desalting column. Therefore the total volume was reduced to 50 mL utilizing Amicon® Ultra spin filter with a 3 kDa cutoff. During this procedure further precipitation was observed and removed. The final solution was desalted and again concentrated to 50 mL using the same procedure, bringing the total time investment until this point to approximately three days from full cleavage. The final concentrated solution can then be applied on a preparative Sephadex S75 column. Purification was performed in single runs with an injection volume of 1.7 mL, using a two hour isocratic gradient of 10 mM phosphate buffer pH 6.4, 50 mM Na₂SO₄, overall taking approximately three days. Afterwards all fractions are collected and concentrated to 1 mL. The final purity can be assessed by analytical HPLC and MS. **Figure 46** summarizes this procedure while **Figure 47** shows an exemplary chromatogram of performed SEC and HPLC for different barnase variants. Furthermore, **Figure 47** shows the successful application of this procedure for BarAbu27 and BarTfeGly27.

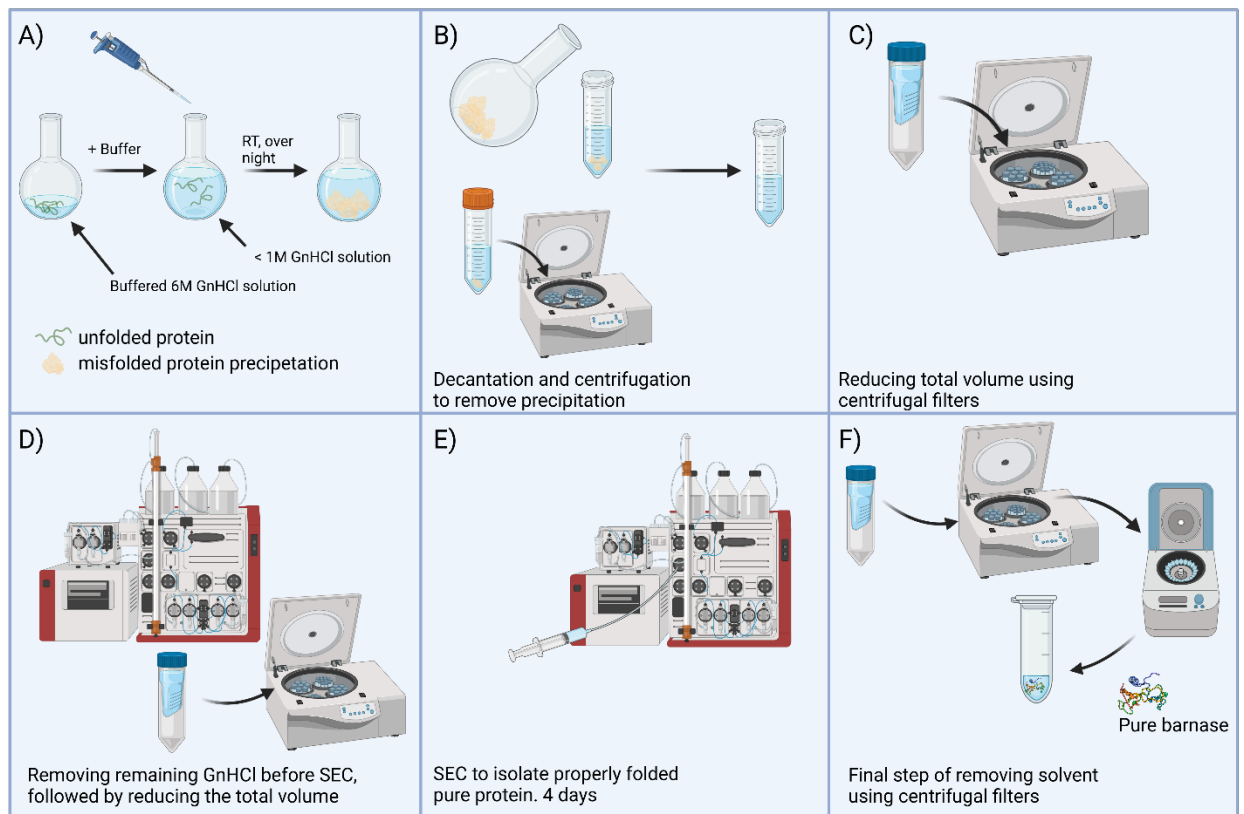


Figure 46: Illustration of the full procedure to purify barnase variants by refolding and SEC. A) Protein is dissolved in buffered 6M GnHCl solution, then diluted with buffer and left overnight. B) Precipitate is removed by decantation and centrifugation. C) Buffer is reduced to reach a maximum volume of 50 mL. D) Remaining GnHCl is removed by desalting column, gained total volume is reduced again. E) Protein is purified by SEC. F) Final step of removing buffer to retrieve purified protein. Created in BioRender.

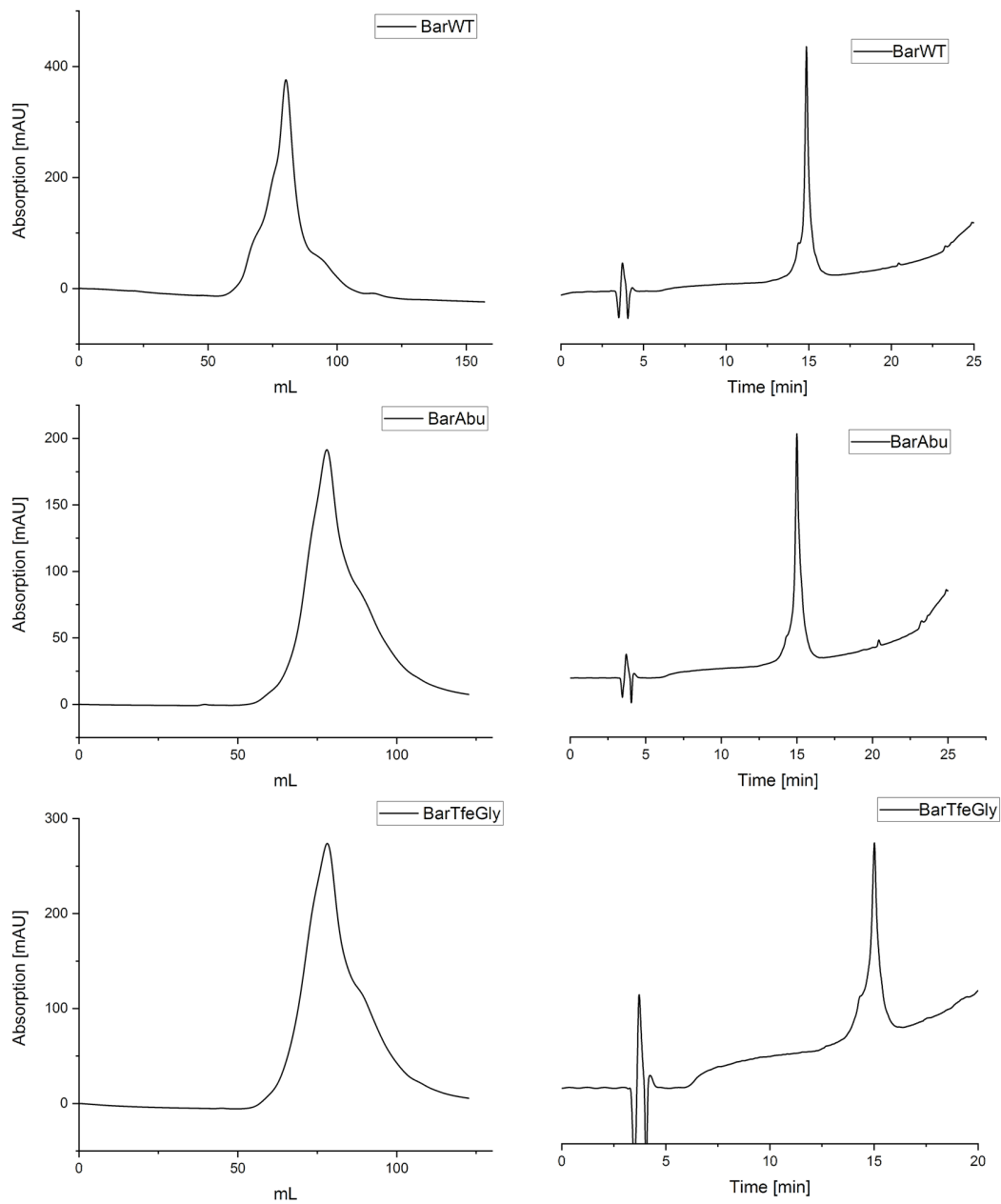


Figure 47: (Top) SEC chromatogram of wild-type barnase and purified protein as verified by analytical HPLC, (middle) SEC chromatogram of BarAbu and purified protein as verified by analytical HPLC, (bottom) SEC chromatogram of BarTfeGly and purified protein as verified by analytical HPLC. Single injection, flow rate 1mL/min.

When applying this strategy to variants BarDfeGly27 and BarMfeGly27, however, it was observed that these two proteins seemed to behave differently when applied on the stationary phase, showing as peak broadening which could be explained with slightly

different folding behavior. During analytical HPLC it then became apparent, that this approach is not optimal for these two variants compared to the Abu and TfeGly species.

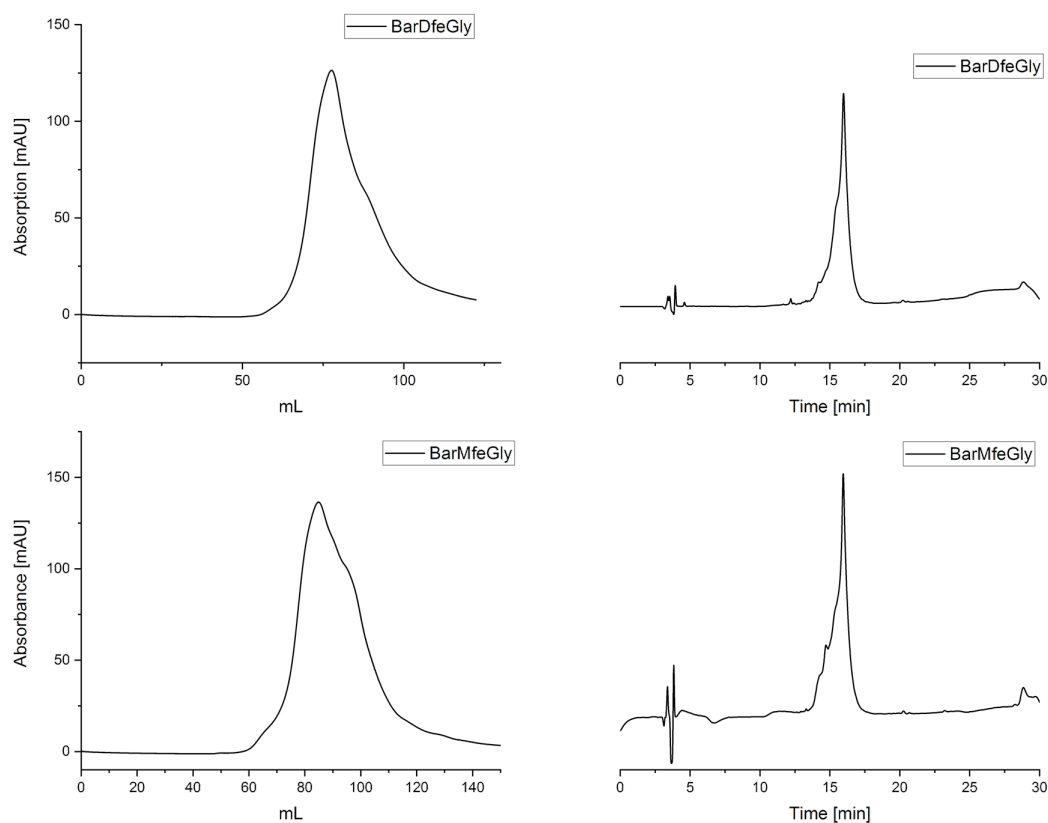


Figure 48: (Top) SEC chromatogram of BarDfeGly27 (left) and analytical HPLC of the protein without further purification (right). (Bottom) SEC chromatogram of BarMfeGly27 (left) and analytical HPLC of the protein without further purification (right).

Unfortunately, repeated SEC attempts did not increase purity, hence additional purification steps using analytical RP-HPLC methods were performed. (**Figure 48**) While this resulted in significantly increased purity (**Figure 49**), it also lead to loss of a significant amount of product. Due to the acidic conditions applied during HPLC of 0.1% TFA, barnase is unfolded, and thus needs additional manual refolding by GnHCl-driven dilution. This was performed analogously to above described folding procedures. Afterwards, the protein is manually desalted using PD-10 columns. **Figure 49** shows chromatograms of both BarDfeGly27 and BarMfeGly27 after additional purification, refolding and desalting.

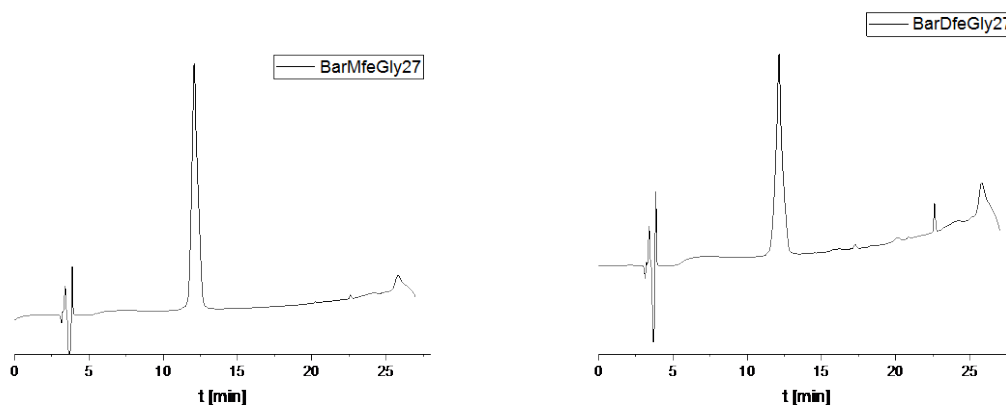


Figure 49: Analytical HPLC chromatograms after purification and refolding of BarMfeGly27 (left) and BarDfeGly27 (right).

Since applied purification methods need up to seven days, it became apparent that optimization is inevitable. Two significant possibilities for improvement are desalting and reducing the resulting total volume that had to be purified by SEC. In the first approach to optimizing these parameters, the time needed for purifying the proteins by SEC should be decreased. Therefore, hydrophobic interaction chromatography was utilized prior to SEC, to reduce the overall volume that needed purification. During this procedure the protein binds to a stationary phase by hydrophobic interactions. Using a decreasing gradient of 1 to 0 M $(\text{NH}_4)_2\text{SO}_4$ the sample can be eluted in minimal volumes, thus reducing overall time consumed during SEC. While this attempt worked as intended for BarLys27 and BarAbu27, no significant improvement was observed for fluorinated variants. However, purity of tested fluorinated samples was significantly reduced, hence this approach was discarded without further investigation. In the third iteration of an overall purification approach the refolding procedure and removing the GnHCl were combined, by performing this step by means of dialysis.

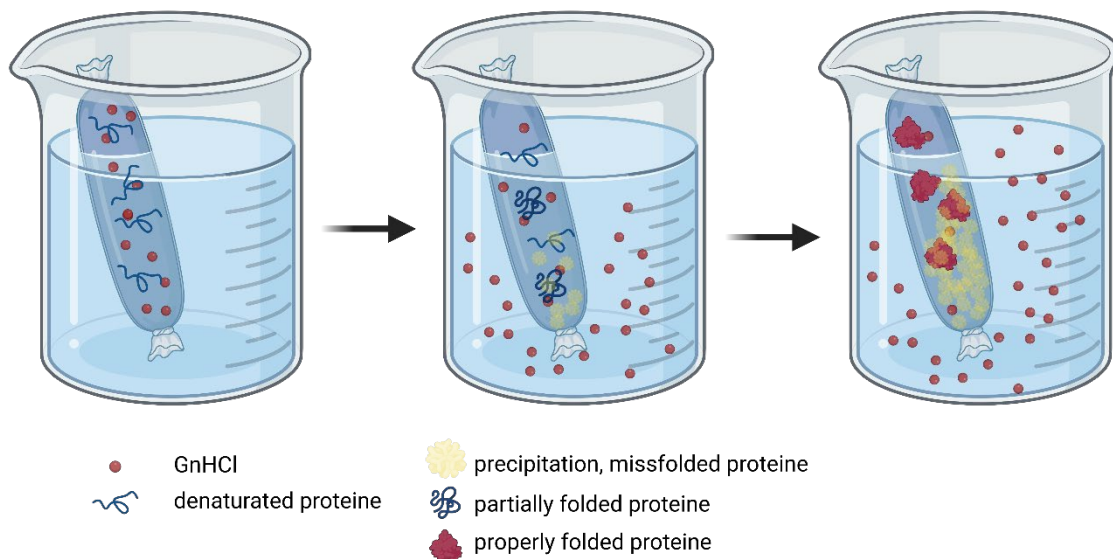


Figure 50: Refolding process via dialysis. Precipitation can be removed by decantation or filtration. Created with BioRender.

This resulted in significantly reduced volumes, 1/2 to 1/3 of initial volumes purified during the first iteration, and thus reduced the time needed for SEC of approximately three days to less than 24 hours. The resulting proteins showed purities comparable to prior attempts, but still needed additional HPLC based purification according to standard conditions. Furthermore, SEC-methods were set up in a five to one ratio, meaning that one run included five injections, followed by cleaning the column with 0.1 M NaOH and equilibration with desired buffer, further slightly reducing the overall required time. **Figure 51** shows the injection profile of one purification attempt, confirming reproducibility.

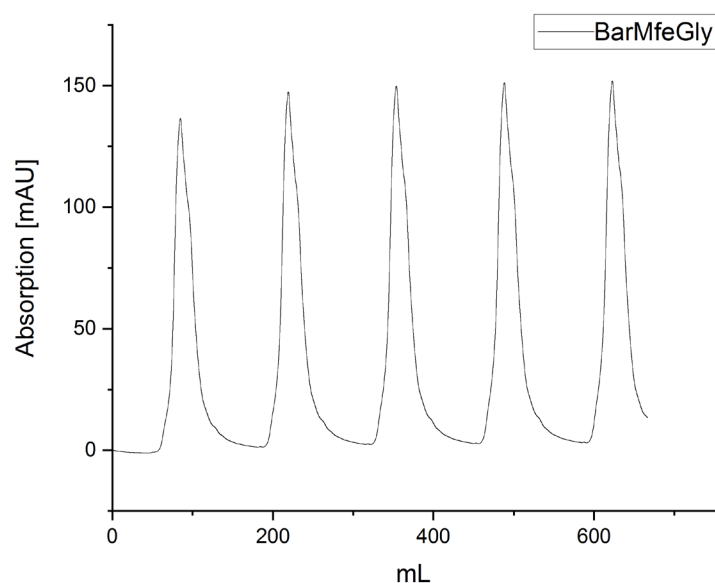


Figure 51: Exemplary SEC chromatogram of five injections of BarMfeGly. Flow rate 1mL/min, injection volume 1.5 mL.

Using this final iteration to the purification procedure, all protein variants were successfully isolated. Their purity was confirmed by ESI-MS analysis. Unfortunately, this presented another issue. While all expected products were verified by ESI-MS, received spectra were difficult to interpret due to low intensities. Significant amounts of protein were needed to receive satisfying results, which ultimately reached the limits of detection possible by ESI-ToF MS. This was however solved when using a SYNAPT G2 Si UPLC-MSMS. Unfortunately this method also revealed significant impurities, consistent in all variants, which were not detectable in ESI-MS nor by applied HPLC-methods. A comprehensive overview of analytical HPLCs as well as mass analysis will be presented in the experimental section. (**Tables 20-30, Chapter 6.14.1-6.14.7**)

However, as will be discussed in the next sections, the impurities revealed by MS/MS did not impair performed activity assays, nor can they explain the significant differences between BarLys27 or BarTfeGly27 when compared to BarAbu27, BarMfeGly27 or BarDfeGly27, in CD spectroscopy. Concluding this section, a successful synthesis method can be reported, that opens the access to fluorinated barnase variants by MW-assisted SPPS. The applied purification methods however should be further investigated in a follow up project, to further improve purity as well as reduce the overall time

requirement. One possible approach to this is the use of C4 RP-HPLC columns, as can be seen in both the results provided by CEM, and UPLC chromatograms gained during MS/MS analysis performed by A. Springer. (**Figure 52**)

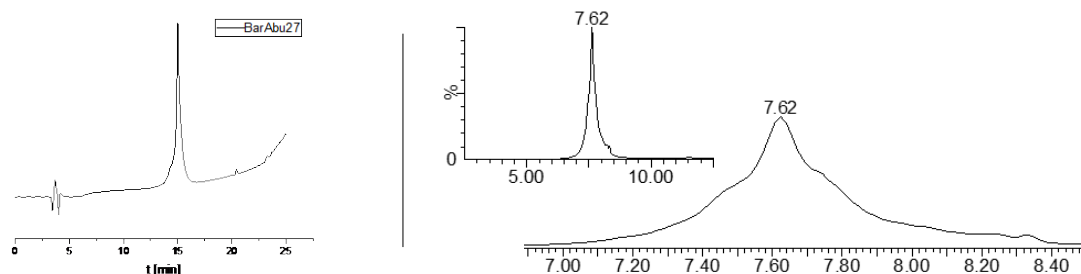


Figure 52: Analytical HPLC chromatogram of BarAbu27, performed on C18 Jupiter column (left) compared to a chromatogram gained from UPLC performed on a Acquity UPLC Protein BEH C4 column (right), demonstrating the importance of suitable RP column material.

4.3 NCL vs. full-length synthesis

All final experiments towards developing a ligation approach for the synthesis of barnase were conducted by Sina Schmidt during her bachelor thesis under the guidance of Alexander Langhans.

Due to complex issues in the purification of full-length barnase using only HPLC methods, ranging from column material to HPLC conditions, the synthesis of barnase by NCL was approached as a viable alternative. With the established methods described in **chapters 4.2.1 – 4.2.3**, smaller fragments as needed for ligation were readily available in good yields and purity, thus reducing complexity of the final purification. Due to the lack of natural cysteine, multiple ligation sites can be suggested. Based on data available in literature, reporting ligation in three steps¹⁶⁵, ligation in the presented work was attempted from two fragments. A common approach to ligating peptide fragments without natural cysteines is the use of so-called cysteine surrogates (**Figure 53**). Additional desulfurization steps can transform these into the desired AA. The most common example is the Cys-Ala pair,¹⁶⁶ which was chosen in the presented work.

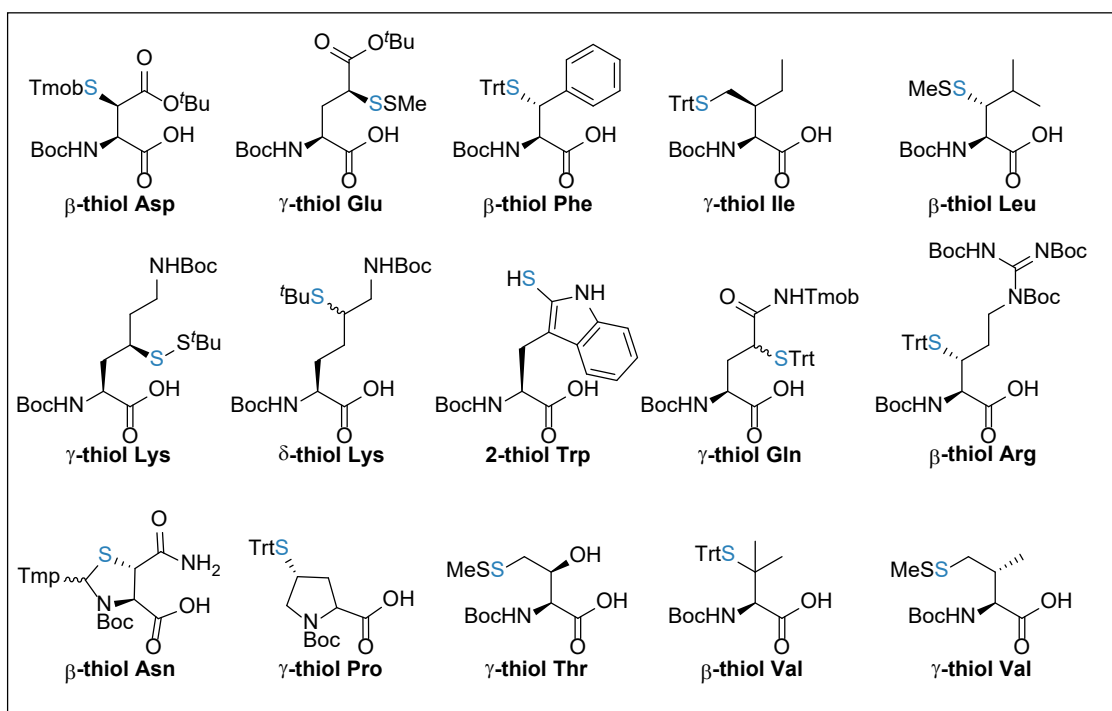


Figure 53: Cysteine surrogates. AAs are Boc-protected as they are incorporated N-terminally, thus, leading to final deprotection during full cleavage.¹⁶⁷⁻¹⁶⁹

Ligation sites and thereby peptide fragments were chosen depending on the position of unnatural AAs (Fragment Bar1/2) for the synthesis of barnase variants, and overall fragment length (Fragment Bar3/4). (**Table 11**)

Table 11: Summary of barnase sequence and fragments used in ligation approaches.

10	20	30	40	50	60	70	80	90	100	110	
AQVINTFDGV	ADYLQTYHKL	PDNYITKSEA	QALGWVCSKG	NLCDVAPGKS	IGGDIFSNRE	GKLPGKSGRT	WREADINYTS	GFRNSDRILY	SSDWLIYKTT	DHYQTFTKIR	
<p>Bar1 </p>			<p>Bar2 </p>								
AQVINTFDGV	ADYLQTYHKL	PDNYITKSEA	QALGWV	CSKG	NLADVAPGKS	IGGDIFSNRE	GKLPGKSGRT	WREADINYTS	GFRNSDRILY	SSDWLIYKTT	DHYQTFTKIR
<p>Bar3 </p>			<p>Bar4 </p>								
AQVINTFDGV	ADYLQTYHKL	PDNYITKSEA	QALGWVCSKG	NL	CDVAPGKS	IGGDIFSNRE	GKLPGKSGRT	WREADINYTS	GFRNSDRILY	SSDWLIYKTT	DHYQTFTKIR

To perform the ligation, two crucial parameters need to be addressed. The first as described above is the existence of a thiol functionality, usually from cysteine. The second functional group needed is a C-terminal thioester, which in general is prepared *in situ* as the NCL is considered a one-pot reaction. In classical NCL approaches the preparation of thioesters required fully protected peptide chains to avoid side reactions at unprotected AA side chains. In recent years however, a variety of thioester surrogates like the Dawson linker¹⁷⁰, hydrazides^{171, 172} or the SEA-Ligation¹⁷³ were developed avoiding this additional step. Even thioester-free approaches to the ligation of unprotected peptide fragments were developed, like the KAHA-ligation¹⁷⁴ or the serine/threonine ligation (STL).¹⁷⁵ Describing each method in detail, however, is well beyond the scope of this thesis, hence only the applied well-established and proven method¹⁷⁶ of hydrazide based NCL will be discussed further. A general procedure of a NCL using hydrazides as thioester surrogates is presented in **Figure 54**.

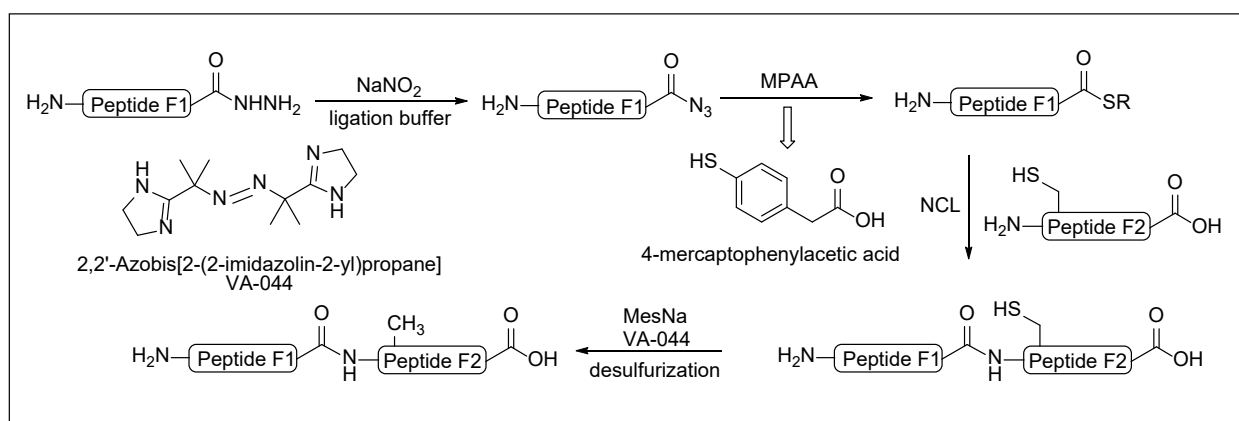


Figure 54: General reaction scheme of hydrazide based NCL.

Peptide hydrazides were readily available by using commercial non-loaded hydrazide resins. (**Figure 55**) These resins can then be manually loaded following standard manual SPPS procedures.

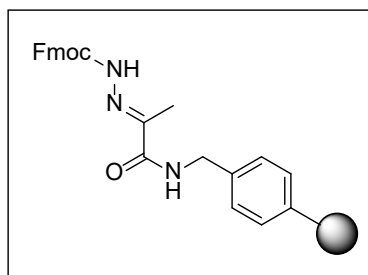


Figure 55: Chemical structure of Fmoc-NHN=Pyv resin (Fmoc-hydrazono-pyruvyl-aminomethylpolystyrene resin).

1 eq. of deprotected resin is reacted with 10 eq. of desired AA over 24 hours. Adjusting the coupling time allows slight control over the final loading. Fmoc based loading determination¹⁷⁷ revealed a loading of 0.42 mmol/g for Fmoc-Val-NHNH₂ and 0.36 mmol/g for Fmoc-Leu-NHNH₂ respectively. For the following MW-assisted SPPS no further optimization was needed and purification of all fragments was executed using standard RP-HPLC methods, which is a significant advantage over the full-length approach.

As depicted in the general reaction scheme hydrazide fragments Bar1 and Bar3 are oxidized using sodium nitrite, thus generating a reactive azide moiety, which is reacted with mercaptophenyl acetic acid (MPAA) to generate the thioester.



Figure 56: Two-step conversion of barnase fragments Bar1 and Bar3 into the respective thioester.

The ligation was first attempted with fragments Bar1 and Bar2. General reaction pathways are however analogous for Bar3 and Bar4. As mentioned before, NCL is usually performed in a one-pot reaction, which is generally kinetically driven.¹⁷⁸ However, due to poor oxidation of Bar1 N-terminus, already reported by Mong et al,¹⁶⁵ of the fragment Bar1 it is suggested to isolate the thioester before any further steps. This way a defined starting point for the following ligation reaction can be set up, though remaining peptide-hydrazide does not negatively affect the reaction. Established purification methods were then also adopted for fragment Bar3. Though the thioesters are stable, they should not be stored more than a few days at -20°C. Successfully isolated thioesters are then

redissolved in 20 mM NaHPO₄ buffer at pH 6.5 containing 6 M GnHCl. Again following the procedure reported by Mong et al. at this point all necessary steps were carried out under inert atmosphere (N₂). In a first attempt the second thiol containing peptide fragment was dissolved in equal amounts of buffered solution and mixed with the thioester. To follow the reaction progress small amounts of reaction solution were taken at different time points and quenched with 1 M DTT solution. Using standard RP-HPLC methods the turn-over can be evaluated. **Figure 57** shows chromatograms of the starting material in comparison to the reaction mixture at the beginning and over a period of 80 hours.

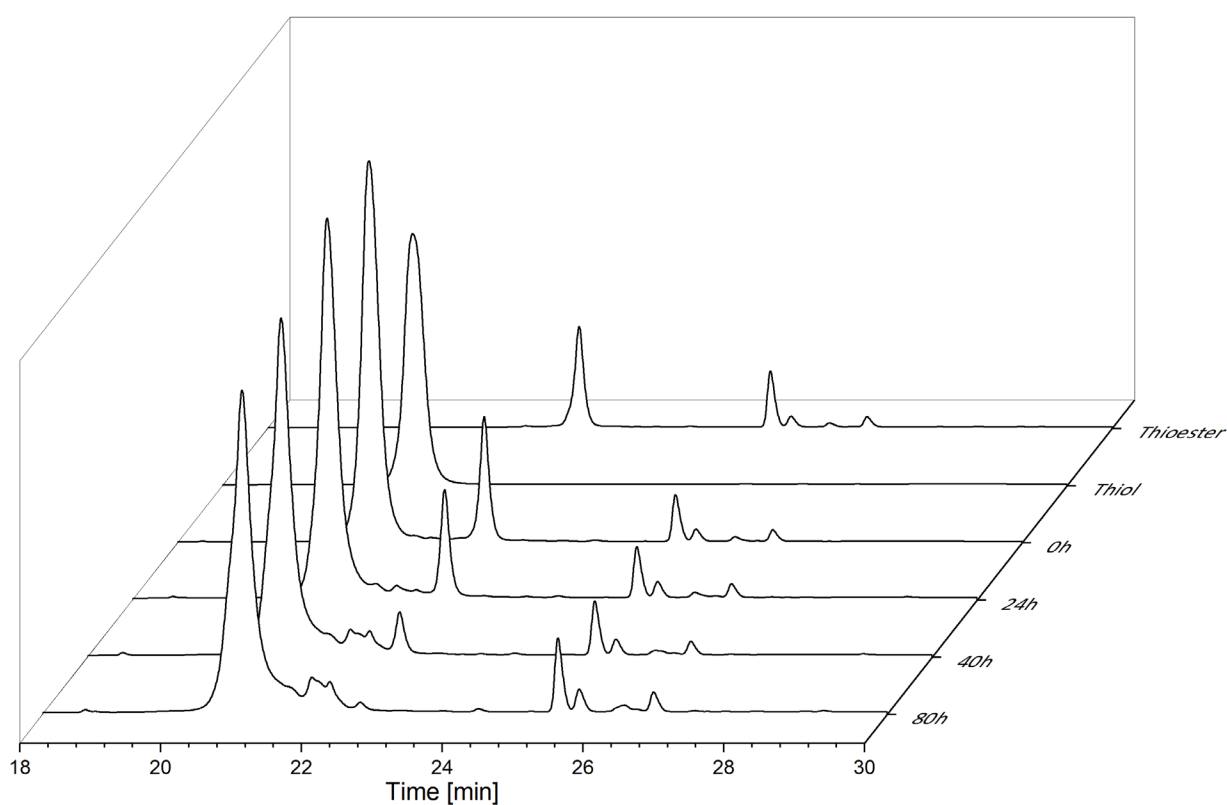


Figure 57: Back to front: Bar ¹Ala-³⁶Val-SR (Bar1) before mixing, Bar ³⁷Cys-¹¹⁰Arg (Bar2) before mixing. Turn-over of Bar-Thioester fragment (Bar1) over the course of 80 hours. A new growing signal can be observed between 21.5 and 22.0 min.

In the beginning both fragments are easily recognizable: Bar1 at R_t=22.4 min and Bar2 at R_t=20.7 min. Over the course of the reaction these signals stay visible, however a consumption of thioester fragment Bar1 can be observed. Additionally, a new broader

signal becomes visible at a retention time between 21.5 min and 22.0 min. This supposed product signal can be isolated using the same HPLC methods and then characterized by ESI-MS. Unfortunately, no product could be identified in the first attempts. Investigating the signal revealed auto-hydrolysis of the thioester, which is a common side-reaction that competes with the ligation at a faster rate. This reaction is favored at pH values lower than 6.5; hence, the careful control of pH becomes crucial. Furthermore, in ongoing attempts the thiol-fragment was no longer dissolved separately. A key answer to this issue is the use of excess MPAA, acting as a catalyst during the ligation.^{179,178} This leads to hydrolysis and reformation of thioester being in a thioester-favored balance facilitating the ligation step. **Figure 58** shows chromatograms of the successful ligation of fragments Bar1 and Bar2, after the addition of 10 eq. MPAA, over the course of 42 hours.

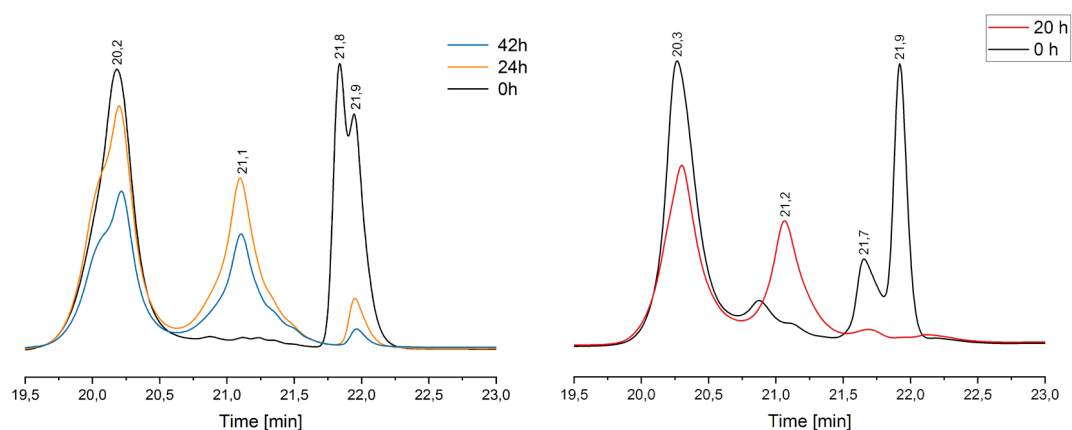


Figure 58: HPLC chromatogram of attempted ligation Bar1 & Bar2 (left) with MPAA. Middle signal $R_t=21.1$ min increasing product. Bar3 & Bar4 (right) product forming over 20 hours $R_t=21.2$ min .

The established methods were then applied on the ligation of fragments Bar3 and Bar4 showing similar results at faster reaction rates. (**Figure 58**) This can be explained with the steric demand of C-terminal AAs of the thioester-fragment; valine, being a β -branched AA, features a more rigid side-chain, while leucine offers a more flexible side-chain. The ligation product can be readily isolated using analogous RP-HPLC methods; due to the small reaction volumes, however, it was done in analytical scale. In a final step Cys is desulfurized to the corresponding Ala. To achieve this, isolated protein is dissolved in minimal amounts of ligation buffer (200 mM NaHPO₄, 6 M GnHCl) at pH 7, adding TCEP·HCl

and MesNa. Finally, the radical initiator VA-044 is added and the pH is maintained at 7.0. Due to the minimal change in the sequence by removing the thiol no change in retention time is noticeable and the reaction cannot be followed by HPLC methods. The final product has to be characterized by ESI-MS. **Figure 59** summarizes a proposed mechanism for the desulfurization.¹⁸⁰ Unfortunately, no successful attempt can be reported.

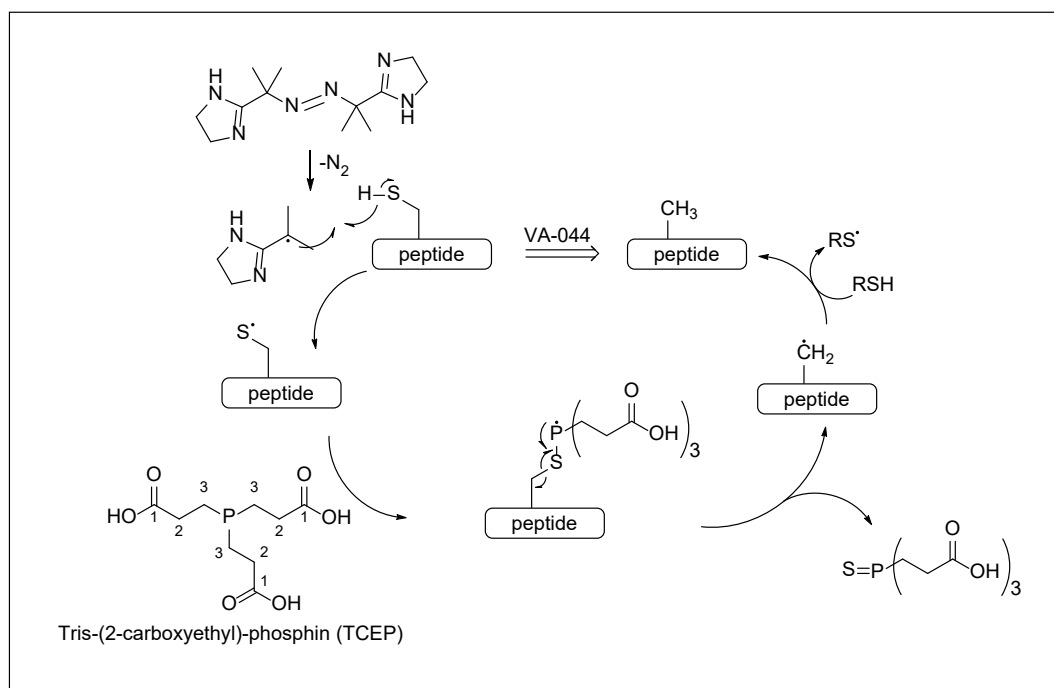


Figure 59: Proposed mechanism of VA-044 initiated radical desulfurization. Adapted from Jin et al.¹⁸⁰

Despite the evident potential of NCL and the here presented results, a few drawbacks were identified in this work, leading to the progression of a total-synthesis approach to barnase. These drawbacks lay primarily in elevated time requirement, due to additional purification steps of the fragments and the ligation products alike, additional synthetic efforts made to generate thioester-fragments as well as desulfurized final products, and the overall reduction to yields. Considering early successes in MW-assisted synthesis approaches these drawbacks did not make ligation worthwhile for this project at this time. However, a reassessment of these results, taking into account the problems with full-length barnase purification discussed in **chapter 4.2.4**, leads to the conclusion that NCL, especially the additional purification steps, provides a solid basis to eliminate many of these problems. Therefore, during a continuation of this project, in addition to the optimization of the purification methods, efforts should also be put into the optimization of the NCL approach, specifically the scale-up of the process. Finally, yields

of both methods seemed comparable, even though the yield of desulfurization cannot be estimated.

4.4 Structural investigations – CD Spectroscopy

Synthesized barnase variants were investigated in the context of fluorine's influence on secondary structure. Therefore CD-spectroscopy was conducted at 20°C. All samples were prepared in 10 mM phosphate buffer at pH 6.4 containing 50 mM sodium sulfate. Protein concentration was determined based on UV-absorbance at 280 nm according to the Lambert-Beers Law, using the literature reported extinction coefficient $\epsilon=27411$.¹⁸¹ CD-spectra were taken at 20 μM or 30 μM protein concentration; however, no significant differences were observed between these two concentrations. **Figures 54** and **55** show groups of comparable CD profiles of all Bar variants at 30 μM . Spectra were again measured after 24 hours to evaluate stability of the enzymes, yet no significant differences could be observed indicating a stable structure.

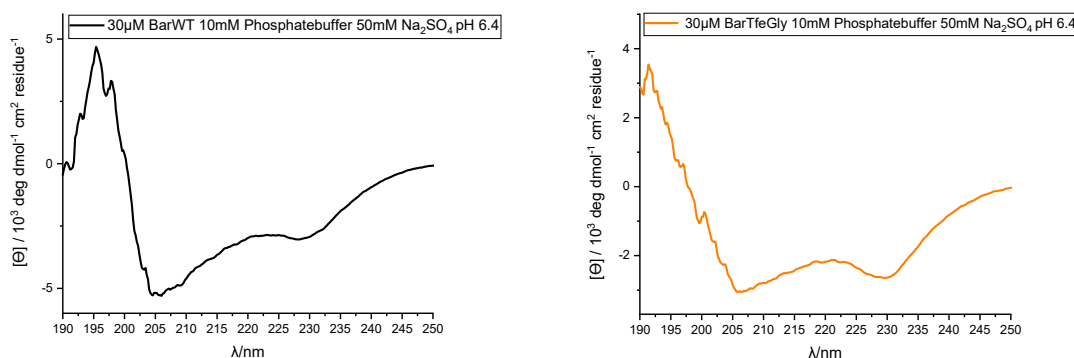


Figure 60: CD-Spectra of wild-type barnase (left) and BarTfeGly27 (right). Spectra were recorded at pH 6.4 in 10 mM Phosphate buffer + 50 mM Na₂SO₄. Spectra are normalized.

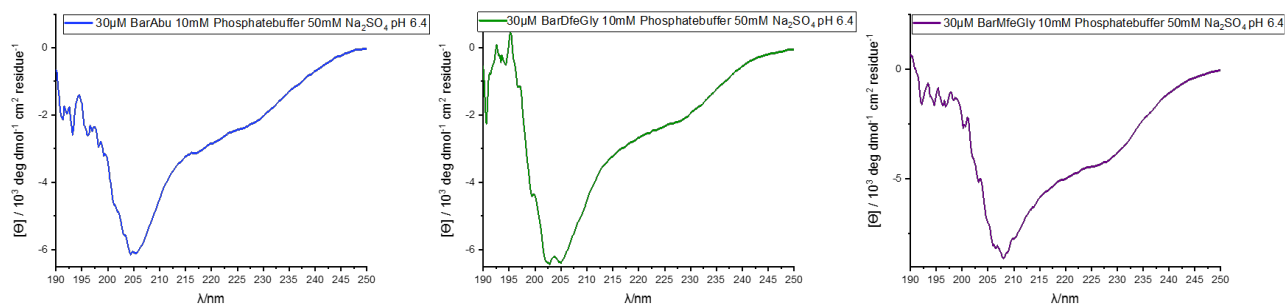


Figure 61: CD-Spectra of BarAbu27 (left), BarDfeGly27 (middle), BarMfeGly27 (right). Spectra were recorded at pH 6.4 in 10 mM Phosphate buffer + 50 mM Na₂SO₄. Spectra are normalized.

On first sight, it is apparent that two profiles can be described, nevertheless, all variants show the expected global conformation of α - β -proteins, indicated by the characteristic minima of 208 nm and 222 nm.¹⁸² It should be noted that these minima are 205 nm in case of BarAbu27 and BarDfeGly27. In all cases the second minima is shifted to 228-230 nm consistent with published CD spectra for barnase.¹⁶⁵ Only the synthetic wild-type barnase and BarTfeGly27 variant show ideal profiles. BarAbu27, BarDfeGly27 and BarMfeGly27 show a more pronounced minimum at 205-208 nm, while the overall profile is still comparable. This may be a consequence of the different purification methods. The latter three variants needed an additional HPLC purification step resulting in an extra unfolding step followed by refolding as described in **section 3.2**. Furthermore, impurities in form of wrong peptide sequences may result in increased amounts of unstructured peptides that might also affect the curve profile. Though this should be consistent throughout all variants, as UPLC-MSMS showed side-products in all synthesized variants of barnase (see **section 3.2**). The issues regarding purity need to be solved to further elucidate differences in structure. The analysis of the potential structural differences is essential to evaluate the influence of fluorinated side-chains in barnase. Thus other methods, for example NMR or X-ray diffraction should be considered, but both techniques require higher amounts of pure protein, which was beyond the scope of this thesis. Nevertheless, no significantly disturbed structure was observed, indicating that the fluorinated AAs are overall well accommodated by the proteins, which is also reflected in observed activities discussed in the following chapter.

4.5 Activity assays

Enzyme activity can be taken as an indicator for correct protein folding. To investigate barnase's inherent RNase activity, a commercially available, fluorescence based assay kit was chosen. It contains a fluorescence-labeled and dark-quenched RNA oligomer. According to patent data published 2003 and 2007,¹⁸³ the exact sequence should be: „Fl-AugggcA-QSY-7”; „Fl” being the fluorescence tag 6-Carboxyfluoresceine, A being 2'-O-methyl ribonucleotides, flanking the actual RNA strand, to reduce autohydrolysis of the oligonucleotide, and QSY-7 (QSY™ 7 Carboxylic Acid, Succinimidyl ester) as the dark quencher to reduce background fluorescence.

However, the exact structure used the commercially available kit from IDT Integrated DNA technologies is not known. It is thus used only as an assumed substrate design to discuss concepts arising from presented results.

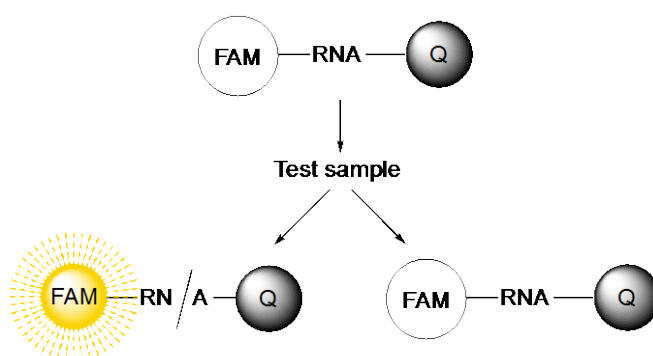


Figure 62: Expected principle of function; FAM = 6-Carboxyfluoresceine, Q = dark quencher. Adapted from IDT RNaseAlert™ Substrate instruction manual. Left; in the presence of RNase the RNA substrate is cleaved which can be detected via a fluorescence signal. Right; without the presence of RNase the substrate stays intact and not fluorescence signal can be detected.

Figure 62 shows an illustration depicting the expected principle of function. The assay can be set up to either provide qualitative evidence, i.e., whether laboratory space or devices are contaminated with RNases, or to provide quantitative data following standard Michaelis-Menten kinetics. A simple “positive or negative” read out can be achieved by incubating a test sample with RNaseAlert™ substrate. Upon cleavage the dark quencher is removed and fluorescence can be observed either visually or using a fluorimeter. To evaluate constants like k_{cat} or K_M , however, a continuous assay has to be designed, for example utilizing 96-well plates and a plate reader. In order to assess the

RNase activity for all synthesized barnase variants in comparison to synthetic wild-type protein, a kinetic assay was designed based on varying substrate concentration. [S] should reach a saturation state at which reaction speed remains unaffected by further changes in [S] to obtain Michaelis-Menten kinetics. Enzyme aliquots were prepared at 10 μM concentration by dilution series. Concentration was determined based on UV-absorption analogous to the procedure described in the experimental section. **Figure 63** comprehensively shows the dependency of initial velocity v_0 on the substrate concentration. In all cases substrate saturation was not achieved and therefore full Michaelis-Menten kinetic parameters cannot be obtained. This means, that K_M for all barnase variants is still well above the highest measured substrate concentration of 600 nM.

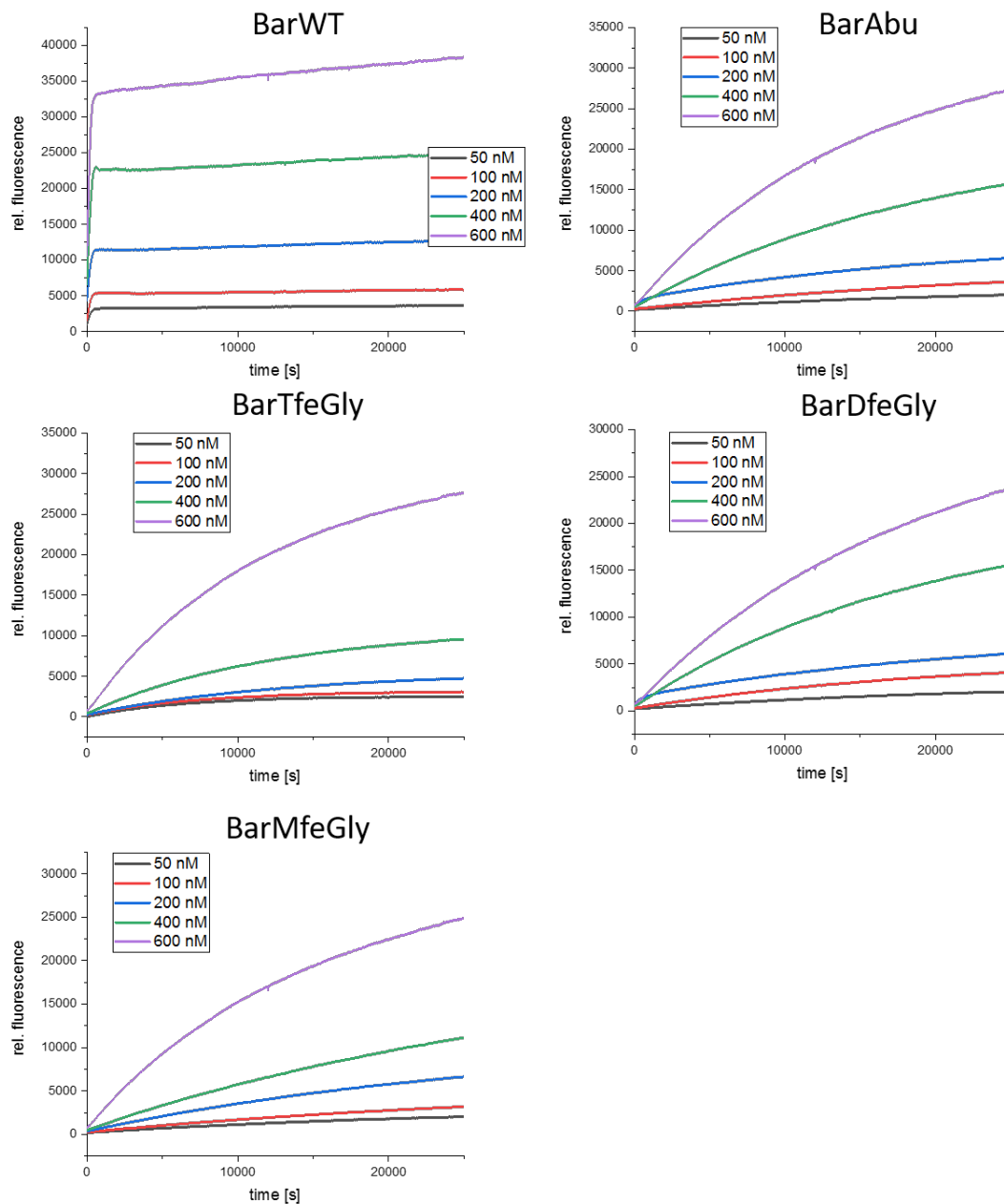


Figure 63: Initial kinetic graphs showing relative fluorescence vs. time for all purified barnase variants. Each graph contains curves for $[S] = 50 \text{ nM}$, 100 nM , 200 nM , 400 nM and 600 nM . Samples were prepared from $10 \mu\text{M}$ enzyme aliquots, resulting in final $[E] = 8 \mu\text{M}$. Measurements were performed in 10 mM Phosphate buffer + 50 mM Na_2SO_4 at pH 6.4 and 37°C over the course of 7-10 hours.

These results complicate the evaluation, because k_{cat} and K_M cannot be determined under these conditions. Unfortunately, a detection limit in terms of rel. fluorescence is reached when the substrate concentration is further increased. An attempt to decrease the enzyme concentration led to a sensitivity issue and the small changes could not be detected reliably. Hence only values for k_{cat}/K_M , which describes the catalytic efficiency, can be derived from these measurements, according to the following equation 1.

$$v_0 = \frac{k_{cat}}{K_M} \cdot [E] \cdot [S] \quad (1)$$

With the assumption of $[S] \ll K_M$, $[E]$ is equivalent to $[ES]$, the enzyme-substrate complex, and $[E]$ can be described as $[E]_{total}$, total enzyme concentration. It thus becomes independent of enzyme active fraction or any previous described impurities, and $[E]_{total}$ can be assumed as the concentration calculated by UV-absorption following Lambert-Beer's law.

$$v_0 = \frac{k_{cat}}{K_M} \cdot [E]_{total} \cdot [S] \quad (2)$$

Thus k_{cat}/K_M can be determined according to equation 3.

$$\frac{v_0}{[E]_{total} \cdot [S]} = \frac{k_{cat}}{K_M} \quad (3)$$

Initial velocities v_0 are equal to the slope of the curves from plotting rel. fluorescence vs. time and can be readily determined using a linear fit. Following equation 3, k_{cat}/K_M was determined for all variants at different $[S]$. **Figure 64** representatively shows the initial plot for all enzymes at 8 nM $[S]$. **Table 12** comprises all deduced values for the catalytic efficiency.

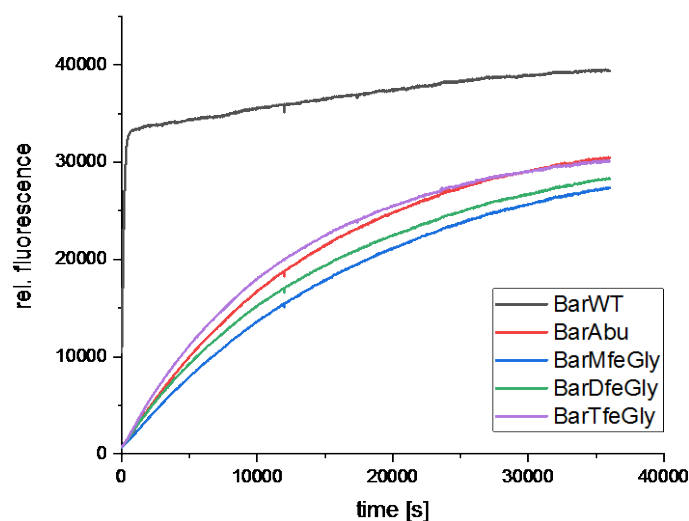


Figure 64: Relative fluorescence vs time [s] used to determine initial velocities within the first 600 sec. for all variants at $[E]_{total} = 8 \text{ nM}$, and $[S] = 600 \text{ nM}$.

Table 12: Determined values for k_{cat}/K_M for all investigated barnase variants at various substrate concentrations.

	BarWT $k_{cat}/k_M [x 10^7]$	BarAbu27 $k_{cat}/k_M [x 10^5]$	BarTfeGly27 $k_{cat}/k_M [x 10^5]$	BarDfeGly27 $k_{cat}/k_M [x 10^5]$	BarMfeGly27 $k_{cat}/k_M [x 10^5]$
50 nM [S]	2.12 ± 0.14	2.56 ± 0.73	1.82 ± 0.36	1.68 ± 0.34	5.76 ± 0.37
100 nM [S]	1.84 ± 0.29	1.81 ± 0.29	2.44 ± 0.15	1.44 ± 0.20	4.01 ± 0.33
200 nM [S]	1.72 ± 0.16	5.64 ± 0.21	2.06 ± 0.17	1.24 ± 0.36	3.98 ± 1.20
400 nM [S]	1.82 ± 0.07	2.41 ± 0.37	2.47 ± 0.45	1.16 ± 0.42	7.69 ± 1.30
600 nM [S]	1.95 ± 0.11	3.92 ± 0.11	2.91 ± 0.25	2.42 ± 0.25	5.96 ± 0.90

From **Table 12** it becomes apparent that all variants show decreased activity towards the RNA substrate, however, no clear trend can be seen in relation to the fluorine content throughout the non-natural variants. These results do not correlate with the acquired CD spectra. Even though BarTfeGly27 displayed a CD curve which was comparable to BarWT, differ by two orders of magnitude. Rather BarTfeGly27 is comparable to all other synthetic variants showing distorted CD spectra. Nevertheless, all synthesized variants possess the expected RNase activity. Yet the variant BarMfeGly27 exerts slightly higher activities throughout all substrate concentrations. The acquired k_{cat}/k_M values are in good agreement with values published in literature showing a drastic decrease in activity for Lys27 mutations,⁴⁹ highlighting Lys27 critical role in stabilizing RNA

phosphate O⁻ during the transition state.⁵⁰ (**Chapter 1.1.1, Figure 8**) Furthermore, this indicates that the structure of the active site of all fluorinated variants seems largely intact, yet their substrate interaction is weakened. Similar effects have been described in literature.⁴⁵ Wild-type barnase on the other side exhibited catalytic efficiencies comparable to those reported in literature for both the synthetic $(7.6 \pm 0.2) \times 10^6$ and the recombinant variants $(1.3 \pm 0.4) \times 10^7$.^{154, 184} This shows the potency and suitability of MW-assisted SPPS as a chemical route to synthesize small proteins.

While the presented data show promising results, they have to be taken with caution, as a closer inspection of the curves in **Figure 64** shows that under the assumption of v_0 and v_{max} being independent of $[E]$, all enzyme variants should reach the same relative fluorescence maximum at different times depending on the enzyme efficiency. Clearly none of the variants are comparable to wild-type barnase in terms of their maximum fluorescence. To narrow down possible reasons for this behavior, firstly the thermal stability of the synthesized barnase variants was determined. The results are in agreement with the value reported in literature of 55°C at pH 5.5 for the wild-type enzyme.¹⁸⁵ Thus a lower stability of the synthesized variants could be ruled out. This is further corroborated by the fact that barnase can be unfolded by heating to 100°C with an automatic refolding during the cooling step with full recovery of the activity. To further rule out other reasons for enzyme inactivation, an assay was prepared in which fresh enzyme was added after the initial plateau was reached. Again no further increase was observed. Interestingly, adding wild-type enzyme lead to an increase of the fluorescence signal, driving the reaction to the same endpoint as the wild-type. (**Figure 65**) Thus, all non-natural variants show either an altered specificity towards the substrate, or cleavage products can inhibit the fluorinated variants, but not the wild-type enzyme.

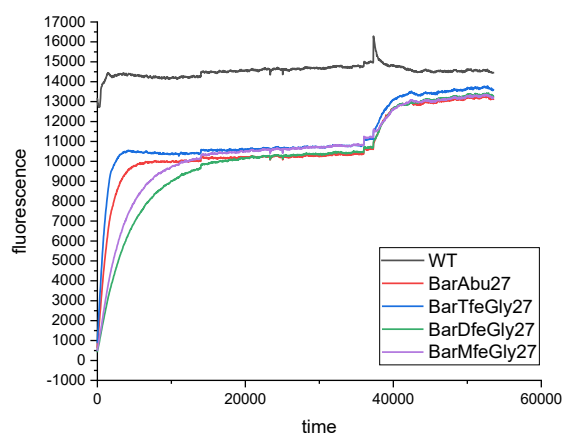


Figure 65: Relative fluorescence vs. time plot for all enzymes at initial substrate concentration of 200 nM. After approx. 10 hours wild-type barnase. Raw values are adjusted to consider drop in fluorescence intensity due to substrate dilution.

It is known that the wild-type enzyme has different specificity depending on the GpN's. (**Chapter 1.1.1**) Thus, since the exact composition of the substrate is not known but a mixture of all GpN's is likely, it is possible that the fluorinated variants can only interact with a subset of the substrate pool, which could explain the observed results. To resolve this issue custom designed substrate with only one of the four GpN's would be necessary to analyze the specificity of the fluorinated variants.

Furthermore the design of the here used substrate has another major weakness, harboring multiple cleavage sites, but only the first cleavage reaction can be detected. After the first cleavage fluorescence is triggered, any further cleavage happening at significant slower rates cannot be taken into consideration leading to biased values for k_{cat} , also described as the turnover number which is the number of conversions of substrate per second. Additionally, custom designed substrate could solve the issue of insufficient substrate concentrations for the accurate determination of a Michaelis-Menten kinetic.

Nevertheless, these results show that the introduced modification of fAAs does not impair the activity of the presented barnase variants beyond literature reported values for Lys27 mutants. This is a crucial prerequisite for further investigation towards enzyme-inhibitor interactions, to understand how fluorine might influence these interactions. The herein presented results can thus be used a starting point for future research which will be conducted on these barnase-barstar systems.

5 Summary and Outlook

In this thesis, fluorinated variants of the natural enzyme barnase were to be investigated on the influence of fluorine on structure, activity, and interaction with its natural inhibitor barstar. Therefore, a general synthesis procedure for full-length barnase was established, using MW-assisted SPPS methods. In order to avoid common side-reactions like aspartimide formation and epimerization, optimizations to the SPPS-synthesis had to be established. In the former case Asp standard side-chain protecting group $-O^t\text{Bu}$ was substituted for a sterically more demanding $-\text{OMpe}$ group. Furthermore, the known aspartimide forming dipeptide DG was substituted with a backbone DMB-protected building block. Finally, known His-epimerization was reduced by introducing Fmoc-His(Boc)-OH to the synthesis.

Parallel to the full-length synthesis, ligation based total syntheses were successfully applied to wild-type barnase, however, a final desulfurization step could not be performed. Due to the nature of ligation and the inherent increased purification steps, leading to reduced yields, it was decided to follow the total synthesis pathway.

The established MW-SPPS methods for the wild-type were then successfully transferred to the synthesis of various fluorine containing barnase variants. Thus, barnase variants BarTfeGly27, BarDfeGly27, and BarMfeGly27 were successfully synthesized. Applying a combination of RP-HPLC methods and SEC all variants were isolated. The simple folding mechanism of barnase was exploited during sample preparation: dissolving the protein variants in buffer containing 6 M GnHCl resulted in complete unfolding. After dialysis overnight only folded protein remained in solution, allowing for straight forward purification using size-exclusion chromatography. In some cases additional HPLC purification was necessary to isolate pure proteins. Close examination in terms of HR-MS using an UPLC-MS/MS ESI-QToF confirmed the success of applied synthesis methods. However, it also revealed significant amounts of side-products consistent through all synthetic variants. By current means of purification they could not be separated. Optimization of these strategies should be possible, for example by switching from a C18 300 Å column to a commonly used C4 300 Å, which is more suitable for protein purification.

Despite potential impurities, initial investigations were continued in terms of structural assessment and fluorine's influence on enzyme activity. Initial CD-spectra revealed expected secondary structure motifs for present α/β -proteins of which barnase is one. While all variants show the expected minima at 208 and 230 nm, which is in line with literature reported data,¹⁶⁵ significant differences can be found amongst the variants. Both wild-type barnase and BarTfeGly27 show similar ideal α/β -spectra, while variants BarAbu27, BarMfeGly27, and BarDfeGly27, still showing overall α/β -shaped spectra but feature increased intensities at their respective 208 nm minima. This could be attributed to differences in their previous purification, as described in **section 3.2**. However, as discussed in **section 3.4**, these differences are not reflected in subsequent performed activity assays. The overall spectra shape of these three variants implies an increased amount of unfolded protein, however literature supports increased stability for barnase variants featuring Lys27 mutations.⁴⁵ Furthermore mutation of Lys27 with any other canonical AA consistently lead to decrease in activity. This is reflected in the presented results, showing reduced activity for all fluorinated barnase variants as well as BarAbu27, in fluorescence bases RNase activity assays, which is in agreement with literature.⁴⁹

Performed measurements for synthetic wild-type barnase also showed k_{cat}/k_M values comparable to both synthetic and recombinant barnase described in the literature.¹⁵⁴ Overall this route demonstrates that chemical protein synthesis can compete with commonly practiced biological protein expression approach. Due to previously discussed impurities, however, these results have to be considered preliminary. Initial inhibition assays also showed that all variants interact with barstar, reducing overall activities. However, these results need further confirmation as well as profound investigation on potential differences in respective inhibition efficiencies.

In conclusion, additional emphasis should be put on the established methods of synthesis and purification, potentially further improving them. As they currently stand, further efforts should be taken in the direction of ligation-based methods. Synthesis of fragments needed for ligation showed significantly higher yields. Furthermore this also reduces side-products during final SEC-based purification improving overall purity.

One approach to further improve the success of MW-based methods could be the incorporation of pseudoproline into the sequences. Though initial CD-spectra and activity assays show promising results, additional steps towards increasing purities of all enzymes

are crucial, as in continuation of the research, the structure of enzyme-inhibitor complexes should be investigated by means of X-ray diffractions. Therefore synthesized barnase variants should be crystallized in complex with a barstar variant barstarCCAA. As described in literature⁵⁴ Cys contained in barstar is negligible to its inhibitory abilities, yet it removes the opportunity for oxidation, that would render barstar inactive.

Furthermore, the variants BarDfpGly27 and BarPfpGly27 synthesized in this thesis need to be further investigated. It is to be expected that activity results will resemble any other here presented fluorinated variant, due to even stronger steric demand of their side-chains, however, experimental results are still interesting for complete comparison, also towards previous BPTI research.

Finally the fluorescence based RNase assay used in this research offers potential for optimization. As discussed in **section 3.5** a tailor-made substrate would increase the accuracy of collected kinetic data. Furthermore, the determination of K_M could become possible, as with the current set up substrate concentrations reaching saturation could not be achieved, as reflected in **Figures 63** and **64**.

6 Materials and Methods

If not stated otherwise, reagents and solvents were ordered in highest quality and used as received without any further purification. Cl-MPA resin for SPPS, as well as Fmoc-His(Boc)-OH and Fmoc-Asp(O^tBu)-(Dmb)Gly-OH were purchased from CEM GmbH (Kamp-Lintfort, Germany). Standard Fmoc-protected AA derivatives were obtained from Carbolution (Carbolution Chemicals GmbH, St. Ingbert, Germany). Non-preloaded hydrazine resin was purchased from Iris Biotech GmbH (Marktredwitz, Germany). Fluorinated AA derivatives Fmoc-MfeGly-OH, Fmoc-DfeGly-OH, Fmoc-TfeGly-OH and Fmoc-DfpGly-OH were kindly provided by S. Chowdhary and T. Hohmann of AG Koksch. Coupling reagents Oxyma-Pure, DIC, Piperazine, DIPEA and KI were purchased from Carbolution (Carbolution Chemicals GmbH, St. Ingbert, Germany), Thermo-Fisher Scientific (Fisher Scientific GmbH, Schwerte, Germany), Iris Biotech GmbH (Marktredwitz, Germany) or Sigma-Aldrich (Merck KGaA, Darmstadt, Germany). Synthesis grade solvents for manual and automated peptide synthesis, as well as synthesis grade TFA were obtained from Thermo Fisher Scientific Scientific (Fisher Scientific GmbH, Schwerte, Germany), Carl Roth GmbH + Co. KG (Karlsruhe, Germany) and VWR (VWR International GmbH, Darmstadt, Germany). Ethanol was received from Berkel (Berkel AHK Alkoholhandel GmbH & Co. KG, Ludwigshafen, Germany), DCM from VWR VWR (VWR International GmbH, Darmstadt, Germany). EDT was purchased from Acros Organics Chemicals (Thermo Fisher Scientific, Geel, Belgium), TIS obtained from TCI Deutschland GmbH (Eschborn, Germany). Spectroscopy grade solvents MeCN, MeOH, ⁱPrOH for HPLC were obtained from Thermo Fisher Scientific Scientific (Fisher Scientific GmbH, Schwerte, Germany), spectroscopy grade TFA (Uvasol) from Merck (Merck Chemicals GmbH, Darmstadt, Germany).

Salts for buffer preparation were obtained from Grüssing GmbH (Filsum, Germany), Carl Roth GmbH + Co. KG (Karlsruhe, Germany) and Acros Organics Chemicals (Thermo Fisher Scientific, Geel, Belgium). Guanidine-Hydrochloride was obtained from Carl Roth GmbH + Co. KG (Karlsruhe, Germany). Water for buffer preparation and HPLC was prepared using a MilliQ Reference+ purification system (Merck KGaA, Darmstadt, Germany). RNase free water was purchased from Sigma Aldrich (Merck KGaA, Darmstadt, Germany)

PD10 Columns for protein desalting were obtained from Cytiva (). Float-A-Lyzer and Mini Dialyzer were purchased from Carl Roth Carl Roth GmbH + Co. KG (Karlsruhe, Germany). Amicon Ultra centrifugal filters were bought from Merck (Merck KGaA, Darmstadt, Germany)

RNaseAlter™ Substrate was purchased from IDT Integrated DNA Technologies (Integrated DNA Technologies, Inc., Coralville, Iowa, USA), and used as received.

6.1 Mass spectrometry

High-resolution mass spectrometry was conducted on an Agilent 6230 ESI-ToF LC-MS device (Agilent Technologies Inc., Santa Clara, CA, USA). Data collection and analysis was done on Mass Hunter Workstation version B.08.00 (Agilent Technologies, Santa Clara, CA, USA) and MestReNova version 10.0.1-14719 and version 14.2.2-28739 (Mestrelab Research S. L., Santiago de Compostela, Spain) were used.

Full length barnase purity was assessed on a UPLC-Synapt G2-S High Definition MS (HDMS) System (Waters, Milford, MA, USA) consisting of an Acquity UPLC running on a binary pump system suitable up to 1000 bar, a tempered autosampler, a column oven and a Photodiodearray (PDA) for UV-Vis detection. This device is coupled to the Synapt G2-S HDMS featuring a Q-ToF- and a ion mobility spectrometer. Data collection and analysis is done using the software Mass Lynx (Waters GmbH, 65760 Eschborn)

Monoisotopic and average masses, as well as mass to charge ratios were predicted using peptide mass calculator v3.2 (<http://rna.rega.kuleuven.be/masspec/pepcalc.htm>).

6.2 NMR-Spectroscopy

¹H-, ¹³C- and ¹⁹F-NMR spectra were recorded at room temperature using a JEOL ECX400 (¹H-NMR:

400 MHz, ¹³C-NMR: 101 MHz, ¹⁹F-NMR: 376 MHz, JEOL, Tokyo, Japan), a JEOL ECP500 (¹H-NMR: 500 MHz, ¹³C-NMR: 126 MHz, JEOL, Tokyo, Japan) or a JOEL ECZ600 S (¹H-NMR: 600 MHz, ¹³C-NMR: 126 MHz, JEOL, Tokyo, Japan). The analysis of received spectra was carried out using MestReNova version 14.2.2-28739 (Mestrelab

Research S. L., Santiago de Compostela, Spain). Chemical shifts δ are given in parts per million (ppm). Internal references are stated as used in individual experiments.

6.3 Manual Coupling protocol for resin loading

Hydrazone resins were loaded with Fmoc protected AAs according to an adapted procedure suggested by manufacturer Iris Biotech GmbH (Marktredwitz, Germany).¹⁸⁶

1 eq. Fmoc-protected hydrazone resin (Iris BioTech GmbH) was transferred into a fritted syringe reactor and swollen in 10 mL DMF for 30 minutes. Afterwards Fmoc protecting group was removed by adding 10 mL of 2% piperidine and 2% DBU in DMF for 10 minutes. This step was repeated three times, followed by filtration and washing the resin three times with DCM and DMF respectively. Afterwards 10 eq. Fmoc-AA-OH, 10 eq. HATU and 20 eq. DIPEA in 10 mL DMF were added. The coupling was conducted at room temperature over 20 hours. Afterwards the solution was removed, the resin dried in vacuum and the loading determined based on Fmoc UV-absorption procedures (**Section 6.4**).

6.4 Determination of resin loading

UV-spectra for resin loading determination were measured on a Varian Cary 50 spectrophotometer (Varian Medical Systems, Palo Alto, CA, USA). Samples were prepared using quartz cuvettes (10 mm path length, 3 mL max. Volume, Hellma Analytics Müllheim, Germany). Resin loading was determined according to a procedure adapted from Gude et al.¹⁷⁷ modified to suit smaller sample size by Sigma Aldrich.

General Procedure:

10 mg of dry Fmoc-protected loaded resin were agitated in 2 mL 2% DBU 2% piperidine in DMF in a 10 mL graduated flask. After 30 minutes the solution was diluted to 10 mL with MeCN. 2 mL of the resulting solution were transferred into a 25 mL graduated flask and further diluted to 25 mL. A blank sample was prepared in similar fashion without adding the resin. 3 mL of the final solution were transferred into a 3 mL quartz cuvette. Remaining

resin was allowed to sediment. Absorbance was measured at 304 nm. The Fmoc loading was calculated from equation 4.

$$\frac{\text{mmol}}{\text{g}} = (\text{Abs}_{\text{sample}} - \text{Abs}_{\text{reference}}) \cdot \frac{16.4}{\text{mg}} \quad (4)$$

6.5 Microwave assisted Solid Phase Peptide Synthesis

If not stated otherwise all proteins and protein fragments were synthesized following Fmoc strategy solid phase peptide synthesis on a microwave-assisted automated peptide synthesizer Liberty Blue™ (CEM Corporation, Matthews, NC, USA). Full length barnase variants as well as barnase fragment 37-110 were synthesized on Cl-MPA ProTide resin (CEM Corporation) with a loading capacity of 0.16-0.18 mmol/g, barnase fragment Bar1-36 was synthesized on a non-preloaded Fmoc-hydrazine resin (Iris BioTech GmbH) with a maximal loading capacity of 0.68 mmol/g. Individual resin loading is given in the respective synthesis section. AAs used for all syntheses were exclusively standard Fmoc protected L-derivatives.

Fmoc-His(Trt)-OH was substituted with Fmoc-His(Boc)-OH, Fmoc-Asp(O^tBu)-OH was substituted with Fmoc-Asp(OMpe), and the following building block Fmoc-Asp(O^tBu)-(DMB)Gly-OH was used.

6.5.1 Microwave Methods and Coupling Cycles

While both microwave methods and coupling cycles can be individually set up for each reaction scale, similar methods were applied for all proteins. The following **Tables 13** and **14** summarize heating profiles and reaction cycles, containing loading, coupling and deprotection.

Table 13: Microwave settings for temperature control.

	Temperature [°C]	ΔT [°C]	Power [W]	Time [s]
DCA (chloride) loading	80	2	75	60
	90	1	20	540
Coupling 10 min at 50°C	25	2	0	120
	50	1	35	480
Coupling 10 min at 90°C	75	2	217	15
	90	1	40	585
Coupling 2 min	75	2	178	20
	90	2	35	120
Coupling 4 min	75	2	217	15
	90	2	43	225
Deprotection	75	2	155	15
	90	2	35	120

If not changed manually all applied microwave methods are set up in two steps. To ensure consistent rapid heating the first step applies increased power for a short period of time, the second step applies lower power over a prolonged period of time to reach and hold the desired final reaction temperature. Within their respective reaction scale setting these methods are assigned to the coupling cycles of each AA respectively allowing for individual coupling conditions as needed.

Table 14: Coupling cycles used for protein synthesis.

	Cycle
Chloride loading	DCA (chloride) loading Wash through manifold 4x Wash
Single/Double coupling	Deprotection 4x Wash 1(2)x Coupling Wash
Double Deprotection, single/double coupling	2x Deprotection 4x Wash 1(2)x Coupling Wash
Single coupling extra wash	Deprotection 7x Wash Coupling Wash

In case of special AAs all microwave methods and commands can be performed manually and adjusted as needed.

6.5.2 Synthesis preparation – Reagents – CarboMax™ Approach

Syntheses were performed in 0.05 mmol and 0.1 mmol scale utilizing the CarboMax™ approach.¹⁸⁷ This approach was designed to improve reaction efficiency, crude purities and reduce the chance of certain AAs to epimerize during the prolonged heat treatment under otherwise standard SPPS conditions. This is achieved by the addition of 0.1 eq. DIPEA to the “activator base” solution containing OxymaPure, and increasing the “activator”-concentration to 10 eq. per addition increasing reaction speed and thus reducing chances of epimerization. The addition of DIPEA improves synthesis efficiency when using acid-labile resins like Cl-MPA ProTide™ due to the overall reduced acidity and thereby reducing premature product cleavage of the resin and minimizing possible side products.

AA solutions for the synthesis are prepared at a concentration of 0.2M unless stated otherwise. Activation was performed using DIC (activator) and OxymaPure® (activator base), their concentration being dependent on the reaction scale (**Table 15**). When using

Cl-MPA ProTide™ resin, dry loading was performed as the first Coupling cycle (DCA chloride loading) facilitated by a potassium iodide and DIPEA solution. Fmoc-protected hydrazine resins were loaded manually prior to the synthesis. Unlike Cl-MPA resins these were swollen in DMF for 30 minutes prior to the MW-assisted synthesis.

Fluorinated AA solutions were prepared at a maximum of 3 eq. per coupling and couple utilizing the “Single coupling extra wash” cycle, unless stated otherwise.

Fmoc-deprotection was performed using a 10-w% piperazine solution in NMP:EtOH 9:1 adding 0.1M HOBt or OxymaPure® respectively. **Table 15** summarizes all reagents the respective concentrations used during synthesis.

Table 15: Reagent solutions as prepared for 0.05 mM and 0.1 mM scale synthesis. All reagents dissolved in DMF.

	Total concentration [M]	Amount/coupling [mL]
DCA (chloride) loading		
KI + DIPEA		
0.05 mmol	0.125M + 1M	2
0.1 mmol	0.125M + 1M	4
“Activator” DIC		
0.05 mmol	0.5	1
0.1 mmol	1.0	1
“Activator base”		
OxymaPure® + 0.1 eq. DIPEA		
0.05 mmol	0.5	0.5
0.1 mmol	1	0.5
Fmoc-AAs		
0.05 mmol	0.2 M	1.25
0.01 mmol	0.2 M	2.5
Fluorinated Fmoc-AAs	2 eq.	1.25
Deprotection - Piperazine	10-w% in NMP/EtOH 9:1	
	+ 0.1M HOBt	3

6.6 Analytics

6.6.1 General procedure for test-cleavages

Reaction control was performed by cleaving minimal amounts of the peptides of the resin. Therefore, a tip of the spatula of air-dried resin was transferred into a 2 mL fritted syringe reactor. To this was added 200-400 μL of TFA cleavage cocktail (**Table 16**). Depending on the primary sequence cleavage was performed between 1 to 4 hours at room temperature. Afterwards the cocktail was transferred into an Eppendorf tube where the TFA-cocktail was removed under gentle nitrogen flow. The peptides were then precipitated with ice-cold diethylether. After centrifugation the ether was decanted and the remaining crude peptide was redissolved a 1:1 mixture of MeCN and water 0.1% (v/v) TFA respectively. The solution was then filtered through a 13 mm filter with a 0.2 μm PTFE membrane (VWR International GmbH, Darmstadt, Germany).

Table 16: TFA base cleavage cocktails used for test- and full cleavages.

	Composition	Ratio [%]
A)	TFA/Water/TIS	95/2.5/2.5
B)	TFA/Water/TIS/EDT	94/2.5/1/2.5

6.6.2 General procedure for full cleavage

Properly dried resin was distributed equally into 25 mL fritted syringe reaction vessels. To each TFA cleavage cocktail (**B, Table 16**) was added at 3 mL per 200 mg or dry resin. Under constant agitation reactions were performed for four to five hours. Afterwards the reaction solution was combined in a 100 mL round bottom flask. The resin remaining in the reactors was washed with 3mL DCM three times. The combined organic phase was removed under reduced pressure. The remaining crude was taken up in copious amounts of ice-cold diethylether precipitating the peptidic product. The suspension was transferred into 50 mL tubes and subjected to centrifugation (4°C, 4.4 rpm, five minutes). The sedimented product was transferred back into the 100 mL flask and combined washed with diethyl ether. It was then dried *in vacuo*. Purification of peptide fragments was conducted using preparative HPLC methods if not stated otherwise.

6.7 Purification and Analysis

Analytical HPLCs for characterization of synthesized proteins were performed on Hitachi Chromaster HPLC system, LaChrom *Elite* HPLC system and Primaide HPLC system.

6.7.1 Chromaster HPLC system

The VWR-Hitachi Chromaster HPLC system (VWR International GmbH, Darmstadt, Germany) with a pressure limit of 600 bar consists of a 5160 pump unit with a 6-channel solvent degasser, a 5260 autosampler with a 100 μ L sample loop, a 5310 column oven and a 430 diode array detector (DAD) with 10mm flow cell. Connected to this system was a Kinetex[®] C18 column (5 μ m, 100 Å , 250 x 4.6 mm, Phenomenex[®], Torrance, CA, USA) with a SecurityGuard[™] cartridge kit containing a C18 cartridge (4 x 3.0 mm, Phenomenex[®], Torrance, CA, USA) as precolumn. HPLC eluents were MilliQ-Water (A) and MeCN (B) with 0.01% TFA (v/v) additive. Measurements were performed at 24°C if not stated otherwise. Detection was carried out at 220 nm or 280 nm. Data was collected and evaluated using EZChrome *Elite* 3.3.2.a software (Agilent Technologies, Santa Clara, CA, USA). The device was operated at a flowrate of 1mL/min.

6.7.2 LaChrom Elite HPLC system

The LaChrom *Elite* HPLC system (Hitachi - VWR International GmbH, Darmstadt, Germany) consists of an organizer module, two L-2130 HPLC-pumps with solvent degasser, an L2200 autosampler with 100 μ L sample loop, a L-2455 diode array and a high-pressure mixing chamber. The system was used with a Kinetex[®] C18 column (5 μ m, 100 Å , 250 x 4.6 mm, Phenomenex[®], Torrance, CA, USA) featuring a SecurityGuard[™] cartridge kit, containing a C18 cartridge (4 x 3.0 mm, Phenomenex[®], Torrance, CA, USA) as pre-colum, or a Jupiter[®] C18 column (5 μ m, 300 Å , 250 x 4.6 mm, Phenomenex[®], Torrance, CA, USA) utilizing the aforementioned pre-column. HPLC eluents were analogue to Hitachi Chromaster HPLC system. Data was collected and evaluated using EZChrome *Elite* 3.3.2.a software (Agilent Technologies, Santa Clara, CA, USA). The device was operated at a flowrate of 1mL/min.

6.7.3 Primaid HPLC system

The Primaide™ DAD system (VWR/Hitachi, Germany) operates on a low-pressure gradient. It consists of an organizer, a pump module (1110) with a 6- channel degasser, an autosampler (1210) featuring a 100 µL sample loop, a column oven (1310) and a diode array detector (DAD) (1430). Connected to this system was either a Kinetex® C18 column (5 µm, 100 Å, 250 x 4.6 mm, Phenomenex®, Torrance, CA, USA) with a SecurityGuard™ cartridge kit containing a C18 cartridge (4 x 3.0 mm, Phenomenex®, Torrance, CA, USA) as pre-column, or a Jupiter® C18 column (5 µm, 300 Å, 250 x 4.6 mm, Phenomenex®, Torrance, CA, USA) utilizing the aforementioned pre-column. Data was collected and evaluated using EZChrome *Elite* 3.3.2.a software (Agilent Technologies, Santa Clara, CA, USA).

The device was operated at a flowrate of 1mL/min. Gradients used for all analytical HPLCs are collected in **Table 17**.

Table 17: Gradients used for analysis of crude and purified peptides. Eluents: A = water 0.1% TFA (v/v), B = MeCN + 0.1% TFA (v/v).

Name: 10-80 18 min				Name: 10-80 18 min 5min prerun			
Time [min]	A [%]	B [%]	Flow [mL/min]	Time [min]	A [%]	B [%]	Flow [mL/min]
0	90	10	1.0	0	90	10	1.0
18	20	80	1.0	5	90	10	1.0
19	0	100	1.0	23	20	80	1.0
22	0	100	1.0	25	0	100	1.0
23	10	10	1.0	26	0	100	1.0
26	10	10	1.0	28	90	10	1.0
				30	90	10	1.0

6.7.4 Preparative HPLC LaPrepΣ

Synthesized peptide fragments were purified using a LaPrepΣ HPLC system (VWR International GmbH, Darmstadt, Germany), consisting of LaPrepΣ LP 1200 preparative pump with 100 mL titanium pump head, a low-pressure gradient, a dynamic Knauer xx mixing chamber, a 6-port-3-channel injection valve with a preparative 10 mL sample loop. Connected to it was a LaPrepΣ 3101 1-channel UV-detector, a LaPrepΣ semi-preparative flow cell with 0.5 mm path length and a LaPrepSigma LP 2016 17-port/1-channel fractionation valve. The system was using a Kinetex® C18 preparative HPLC Column (5 µm, 100 Å, 250 x 21.2 mm, Phenomenex®, Torrance, CA, USA) featuring a SecuritaGuard™ Cartridge Kit with a C18 cartridge, or a Jupiter® C18 preparative HPLC Column (5 µm, 300 Å, 250 x 21.2 mm, Phenomenex®, Torrance, CA, USA). Samples were purified running linear gradients collected in table 15 with UV detection occurring at 220 nm. Data was collected and analyzed using EZChrome *Elite* 3.3.2 SP2 software (Agilent Technologies, Santa Clara, CA, USA)

Table 18: Gradients used for purification. Eluents: A = water 0.1% TFA (v/v), B = MeCN + 0.1% TFA (v/v).

Name: 10-80 18 min				Name: 10-80 18 min 5min prerun			
Time [min]	A [%]	B [%]	Flow [mL/min]	Time [min]	A [%]	B [%]	Flow [mL/min]
0	90	10	15.0	0	90	10	15.0
18	20	80	15.0	5	90	10	15.0
19	0	100	15.0	23	20	80	15.0
22	0	100	15.0	25	0	100	15.0
23	10	10	15.0	26	0	100	15.0
26	10	10	15.0	28	90	10	15.0
				30	90	10	15.0

6.8 Purification of Barnase variants – Dialysis and Size Exclusion Chromatography (SEC)

All synthesized crude full-length barnase variants were subjected to purification using a combination of dialysis prior to size exclusion chromatography followed by additional HPLC purification. To facilitate this method the simple and reversible folding mechanism of barnase was exploited. Crude protein was dissolved in minimal amounts 6 M GnHCl containing buffer (10 mM phosphate 50 mM Na₂SO₄, pH 6.4). The solution was then prepared for dialysis overnight in 10 mM phosphate buffer + 50 mM Na₂SO₄, to steadily remove GnHCl facilitating controlled refolding. Precipitate was removed and the solution was then loaded on to a Superdex column. SEC was carried out in the group of Christian Roth (Max-Planck-Institute of Colloids and Interfaces, Biomolecular Systems, Berlin), on an ÄKTA pure (Cytiva Europe GmbH) equipped with a HiLoad™ 16/600 Superdex™ 75 µg column. The system was used with a 10 mM phosphate buffer containing 50 mM Na₂SO₄ at pH 6.4. Isolated product was further purified using analytical HPLC methods. Purity was assessed by ESI-MS spectroscopy.

Eluent A (buffer)	Eluent B (wash)
10 mM phosphate buffer 50 mM Na ₂ SO ₄ pH 6.4	0.1 M NaOH

6.9 Lyophilization

HPLC purified peptides and proteins were freeze dried using a laboratory freeze dryer ALPHA 1-2 LD (Christ, Gefriertrocknungsanlagen GmbH, Osterode am Harz, Germany). Connected was a hybrid pump RV 6 (Vacuubrand GmbH + Co. KG., Wertheim, Germany).

6.10 Determination of protein concentration

UV-measurements to determine protein concentration, based on absorbance at 280 nm, were performed on an Eppendorf *Biophotometer plus* utilizing one-time-use cuvettes

UVette® (Eppendorf SE, Hamburg, German). Proteins received after purification were stored in 50 µL aliquots buffer solution (10 mM phosphate buffer, 50 mM Na₂SO₄, pH 6.4). Their concentration was determined following Lambert-Beer-Law, allowing calculation based on UV absorbance at specific wavelengths.

$$E_{\lambda} = \varepsilon_{\lambda} \cdot c \cdot d$$
$$\frac{E_{\lambda}}{\varepsilon_{\lambda} \cdot d} = c$$

6.11 Hydrazide-based native chemical ligation

Following a ligation procedure described by Mong et al.¹⁶⁵ NCL was performed in two steps, opposed to generally suggested one-pot reactions. Therefore a peptide-hydrazide fragment was transformed into the corresponding thioester and isolated using standard preparative HPLC methods. The pure thioester was then ligated to the thiol-bearing C-terminal fragment. After reduction the ligation product can be isolated using standard LC methods.

6.11.1 General procedure to the synthesis of MPAA thioester

1 eq. of corresponding hydrazide peptide was dissolved in 1 mL ligation buffer (6 M GnHCl, 0.2 M Na₂HPO₄, pH 6.4). Prior to the reaction the pH was adjusted to 3 using 1 M HCl. The solution was cooled to -17°C and 0.03 eq. NaNO₂ (oxidative solution) were added and the solution was incubated at -17°C for 20 minutes. Afterwards 22 eq. 0.2 M MPAA dissolved in 1 mL ligation buffer at pH 6.4 were added and the solution was allowed to warm to room temperature where it was left for 20 minutes. The reaction was quenched using 1 mL 1 M DTT_{aq}-solution. After additional 10 minutes the crude product can be isolated using standard HPLC methods.

6.11.2 General procedure to native chemical ligation

All necessary steps to ligation were conducted under inert atmosphere. 1 eq. of thioester fragment was dissolved in minimal amounts of ligation buffer (6 M GnHCl, 10 mM phosphate buffer, pH 6.8). To the solution 10 eq. MPAA was added and the pH was adjusted to 6.5. 1.1 eq. of peptide-thiol fragment was dissolved in ligation buffer and added to the reaction mixture. The reaction vessel was kept for 42 h in inert atmosphere, control samples were taken after 24 h and 42 h and checked using standard HPLC methods. After 42 h the reaction was quenched using a solution of 1 M DTT and 6 M GnHCl. The ligation product can be isolated using standard HPLC methods. The isolated product can be desulfurized following the procedure published by Mong et al.¹⁶⁵

6.12 CD Spectroscopy

CD spectra were taken on a JASCO-810 spectropolarimeter (JASCO Deutschland GmbH, Pfungstadt, Germany), connected to as JASCO PTC-423S Peltier element and a HAAKE WKL water recirculator (Thermo Electron GmbH, Karlsruhe, Germany) for temperature control. Measurements were performed at a constant N₂ flow of 3.0 l/min in the UV range of 190 nm to 250 nm. Spectra were taken at 3 scans and baseline corrected utilizing corresponding blank buffers. Data was collected using the software JWS-510-J-800 Spectra Manager version 2. (JASCO Deutschland GmbH, Pfungstadt, Germany). Data analysis was performed using software OriginPro 2019b version 9.6.5.169 (OriginLab Corporation, Northampton, MA, USA). Data normalization towards mean residue molar ellipticity was performed according to the following equation

$$[\theta] = \frac{\theta_{obs}}{c * n * l * 10} 10^3 deg dmol^{-1} cm^2 residue^{-1}$$

θ_{obs} = ellipticity measured, c = concentration in mol*L⁻¹, n = number of amide bonds, l = path length in cm.

Table 19: Internal device settings & parameters.

PARAMETER	SETTING
WAVELENGTH (START – END)	250 nm – 190 nm
SENSITIVITY	100 mdeg
DATA PITCH	0.5 nm
SCANNING MODE	Continuous
SCANNING SPEED	100 nm/min
RESPONSE TIME	4 sec
ACCUMULATION	3
BANDWIDTH	2 nm

6.13 RNase activity Assay

Enzyme activity was determined utilizing RNaseAlert™ Substrate Nuclease Detection System (IDT Integrated DNA Technologies, BVBA, Leuven, Belgium). RNaseAlert™ Substrate contains a synthetic oligonucleotide fitted with a fluorescence label (fluoresceine) and a quencher. In the presence of RNase, the substrate is cleaved (**Figure 62, Chapter 4.5**) showing green fluorescence detectable using a fluorimeter (490 nm excitation, 520 nm emission). Assays were screened in black 96-well plates (BrandPlates® pureGrade™, BRAND GMBH + CO KG, Wertheim, Germany) using a TECAN plate reader (Tecan Group Ltd., Männedorf, Switzerland).

Sample preparation:

10 nM enzyme aliquots of 300 µL were prepared in 10 mM phosphate buffer 50 mM Na₂SO₄ at pH 6.4, stored flash frozen at -20°C, thawed as needed. Concentration was determined at 280 nm UV absorbance. (see **Section 6.10**). Ordered substrate is designed to give a 2 µM solution when rehydrated using RNase free water. In order to evaluate Michaelis Menten kinetics RNaseAlert™ substrate was rehydrated to a concentration of 8 µM. A dilution series was prepared to achieve substrate concentrations of 6 µM, 4 µM, 2 µM, 1 µM and 0.5 µM. 10 µL of prepared substrate solution was added to each well

adding 10 μ L of 10X RNaseAlert buffer (IDT Integrated DNA Technologies, BVBA, Leuven, Belgium). To the resulting solution 80 μ L of the prepared 10 nM enzyme solution was added resulting in a final concentration of 8 nM enzyme. To each sample a negative and positive control well was prepared, validating the assay using 1 μ L of stock RNase A (IDT Integrated DNA Technologies, BVBA, Leuven, Belgium). The 96-well plate was covered using sealing film (Carl Roth GmbH + Co. KG (Karlsruhe, Germany)). Measurements were performed over 10 hours at 37°C. Data was collected using Tecan i-control 2.0 (Tecan Group Ltd., Männedorf, Switzerland) and analyzed using OriginPro 2019b version 9.6.5.169 (OriginLab Corporation, Northampton, MA, USA).

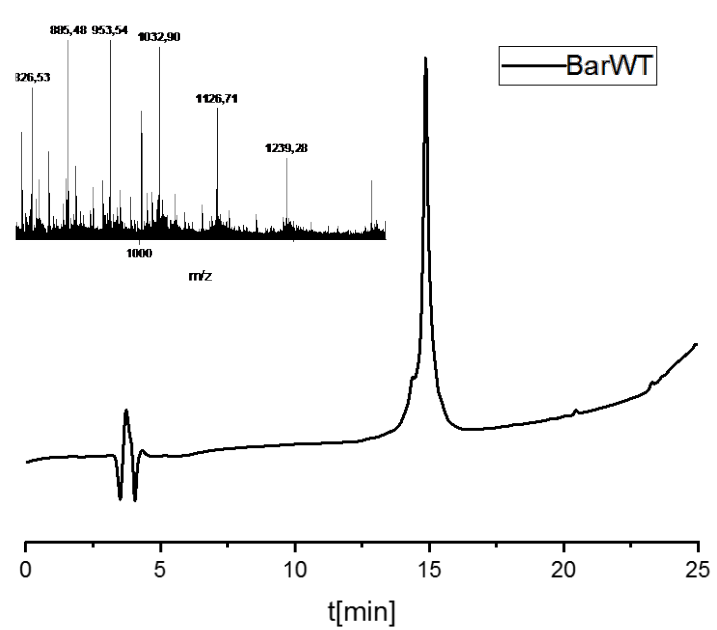
6.14 Synthesized Barnase variants and fragments

All relevant barnase variants were synthesized on Liberty Blue microwave assisted peptide synthesizer. The following tables summarize coupling conditions, methods of purification and analytical data of all purified proteins. If not stated otherwise all proteins were synthesized on Cl-MPA ProTide resin (0.14 mmol/g). Resin loading was carried out as the first step to each synthesis, loading success was not individually assessed, as these methods were pre-developed and showed quantitative yields in the past. Successful protein synthesis validates this decision. Test- and full cleavages were conducted using cleavage cocktail B (**Table 16**) if not specifically stated otherwise. Analysis and purification was carried out using HPLC and SEC methods. If not specifically mentioned, gradient of choice was “10-80 18min, 5min pre run”. Purity was assessed using analytical HPLC and high-resolution ESI-MS. Respective chromatograms and MS data of final products is given in **tables 20-30**.

6.14.1 Synthesis of wild-type barnase

Wild-type barnase was synthesized in two steps. During the first step the segment Bar⁵¹Ile-¹¹⁰Arg was synthesized. Reaction success was confirmed with test cleavage followed by analytical HPLC and ESI-MS. In the second step the remaining fragment Bar¹Ala-⁵⁰Ser was added.

Table 20: Summary of synthesis parameters for BarWT.

Name	Sequence	
BarWT	H ₂ N-AQVINTFDGV ADYLQTYHKL PDNYITKSEA QALGWVASKG NLADVAPGKS IGGDIFSNRE GKLPGKSGRT WREADINYTS GFRNSDRILY SSDWLIYKTT DHYQTFKIR-COOH	
Scale [mmol]	Resin	Resin amount [mg]
0.05	CI-MPA ProTide® 0.18 mmol/g	280
Synthesis conditions		
MW SPPS	Arg (1) – Chloride Loading 2-20 – 4 min single coupling 21-110 – 4 min double coupling Fmoc-His(Boc)-OH – Single 10 min 50°C	Fmoc deprotection – piperazine solution
Cleavage	Purification	Purity [%]
TFA/TIS/H ₂ O/EDT 4-5h	Refolding > Dialysis > SEC	>90
		
DAD: 220 nm		Retention time 14.9 min
[M+12H ⁺] ¹²⁺ _{calc} : 1032.90; [M+12H ⁺] ¹²⁺ _{exp} : 1032.90		

6.14.2 Synthesis of BarAbu27

BarnaseL27Abu (BarAbu27) was synthesized in a manner analogous to wild-type barnase.

Table 21: Summary of synthesis parameter for BarAbu27.

Name	Sequence	
BarAbu27	H ₂ N-AQVINTFDGV ADYLQTYHKL PDNYIT Abu SEA QALGWVASKG NLADVAPGKS IGGDIFSNRE GKLPKGSGRT WREADINYTS GFRNSDRILY SSDWLIYKTT DHYQTFTKIR-COOH	
Scale [mmol]	Resin	Resin amount [mg]
0.05	Cl-MPA ProTide® 0.18 mmol/g	280
Synthesis conditions		
MW SPPS	Arg (1) – Chloride Loading 2-20 – 4 min single coupling 21-110 – 4 min double coupling Fmoc-His(Boc)-OH – Single 10 min 50°C	Fmoc deprotection – piperazine solution
Cleavage	Purification	Purity [%]
TFA/TIS/H ₂ O/EDT 4-5h	Refolding > Dialysis > SEC	>90
DAD: 220 nm		Retention time: 15.1
[M+10H ⁺] ¹⁰⁺ calc: 1234,96; [M+10H ⁺] ¹⁰⁺ exp: 1234.96		

6.14.3 Synthesis of BarTfeGly27

BarnaseL27TfeGly (BarTfeGly27) was synthesized in four steps. Analogous to wild-type barnase, during the first step fragment Bar⁵¹Ile-¹¹⁰Arg was synthesized. In the second step the segment Bar²⁹Glu-⁵⁰Ser. Next two AAs ²⁸Ser and ²⁷TfeGly were added. TfeGly was incorporated at 5 eq. Synthesis success was assessed by analytical HPLC and ESI-MS. In the final step missing segment Bar¹Ala-²⁶Thr was added.

Table 22: Summary of synthesis parameter for BarTfeGly27.

Name	Sequence	
BarTfeGly27	H ₂ N-AQVINTFDGV ADYLQTYHKL PDNYIT TfeGly SEA QALGWVASKG NLADVAPGKS IGGDIFSNRE GKLPKSGRT WREADINYTS GFRNSDRILY SSDWLIYKTT DHYQTFTKIR-COOH	
Scale [mmol]	Resin	Resin amount [mg]
0.05	Cl-MPA ProTide® 0.18 mmol/g	280
Synthesis conditions		
MW SPPS	Arg (1) – Chloride Loading 2-20 – 4 min single coupling 21-110 – 4 min double coupling Fmoc-His(Boc)-OH – Single coupling 10 min 50°C Fmoc-TfeGly-OH – 10min Single Coupling, extra washes	Fmoc deprotection – piperazine solution
Cleavage	Purification	Purity [%]
TFA/TIS/H ₂ O/EDT 4-5h	Refolding > Dialysis > SEC	>90
DAD: 220 nm		Retention time: 14.9 min
[M+12H ⁺] ¹²⁺ _{calc} : 1033.26; [M+12H ⁺] ¹²⁺ _{exp} : 1033.82		

6.14.4 Synthesis of BarDfeGly27

BarnaseL27DfeGly (BarDfeGly27) was synthesized analogously to BarTfeGly27. The fAA was incorporated at 3 eq.

Table 23: Summary of synthesis parameter for BarDfeGly27.

Name	Sequence	
BarDfeGly27	H ₂ N-AQVINTFDGV ADYLQTYHKL PDNYITDfeGlySEA QALGWVASKG NLADVAPGKS IGGDIFSNRE GKLPKSGRT WREADINYTS GFRNSDRILY SSDWLIYKTT DHYQTFKIR-COOH	
Scale [mmol]	Resin	Resin amount [mg]
0.05	Cl-MPA ProTide® 0.16 mmol/g	315
Synthesis conditions		
MW SPPS	Arg (1) – Chloride Loading 2-20 – 4 min single coupling 21-110 – 4 min double coupling Fmoc-His(Boc)-OH – Single coupling 10 min 50°C Fmoc-DfeGly-OH – 10min Single Coupling, extra washes	Fmoc deprotection – piperazine solution
Cleavage	Purification	Purity [%]
TFA/TIS/H ₂ O/EDT 4-5h	Refolding > Dialysis > SEC > analyt. HPLC (Jupiter® C18 column)	>95
DAD: 280 nm		Retention time: 16.0 min
[M+14H ⁺] ¹⁴⁺ _{calc} : 884.4462; [M+14H ⁺] ¹⁴⁺ _{exp} : 884.8257		

6.14.5 Synthesis of BarMfeGly27

BarnaseL27MfeGly (BarMfeGly27) was synthesized analogous to BarTfeGly27. The fAA was incorporated at 3 eq.

Table 24: Summary of synthesis parameter for BarMfeGly27.

Name	Sequence	
BarMfeGly27	H ₂ N-AQVINTFDGV ADYLQTYHKL PDNYITMfeGlySEA QALGWVASKG NLADVAPGKS IGGDIFSNRE GKLPKSGRT WREADINYTS GFRNSDRILY SSDWLIYKTT DHYQTFTKIR-COOH	
Scale [mmol]	Resin	Resin amount [mg]
0.05	Cl-MPA ProTide® 0.16 mmol/g	315
Synthesis conditions		
MW SPPS	Arg (1) – Chloride Loading 2-20 – 4 min single coupling 21-110 – 4 min double coupling Fmoc-His(Boc)-OH – Single coupling 10 min 50°C Fmoc-MfeGly-OH – 10min Single Coupling, extra washes	Fmoc deprotection – piperazine solution
Cleavage	Purification	Purity [%]
TFA/TIS/H ₂ O/EDT 4-5h	Refolding > Dialysis > SEC > analyt. HPLC (Jupiter® C18 column)	>95
DAD: 220 nm		Retention time 16.3 min
[M+14H ⁺] ¹⁴⁺ _{calc} : 883.6925; [M+14H ⁺] ¹⁴⁺ _{exp} : 883.4755		

6.14.6 Synthesis of BarPfpGly27

BarnaseL27PfpGly (BarPfpGly27) was synthesized analogues to BarTfeGly27. The fAA was incorporated at 3 eq.

Table 25: Summary of synthesis parameter for BarPfpGly27.

Name	Sequence	
BarPfpGly27	H ₂ N-AQVINTFDGV ADYLQTYHKL PDNYIT PfpGly SEA QALGWWASKG NLADVAPGKS IGGDIFSNRE GKLPGKSGRT WREADINYTS GFRNSDRILY SSDWLIYKTT DHYQTFTKIR-COOH	
Scale [mmol]	Resin	Resin amount [mg]
0.05	Cl-MPA ProTide® 0.16 mmol/g	315
Synthesis conditions		
MW SPPS	Arg (1) – Chloride Loading 2-20 – 4 min single coupling 21-110 – 4 min double coupling Fmoc-His(Boc)-OH – Single coupling 10 min 50°C Fmoc-PfpGly-OH – 10min Single Coupling, extra washes	Fmoc deprotection – piperazine solution
Cleavage	Purification	Purity [%]
TFA/TIS/H ₂ O/EDT 4-5h	Refolding > Dialysis > SEC > analyt. HPLC (Jupiter® C18 column)	>95%
DAD: 220 nm		Retention time 16.1

6.14.7 Synthesis of BarDfpGly27

BarnaseL27DfpGly (BarDfpGly27) was synthesized analogues to BarTfeGly27. The fAA was incorporated at 3 eq. Purification of this variant was not possible using established methods of SEC and HPLC.

Table 26: Summary of synthesis parameter for BarDfpGly27.

Name	Sequence	
BarDfpGly27	H ₂ N-AQVINTFDGV ADYLQTYHKL PDNYIT DfpGly SEA QALGWVASKG NLADVAPGKS IGGDIFSNRE GKLPKGSGRT WREADINYTS GFRNSDRILY SSDWLIYKTT DHYQTFTKIR-COOH	
Scale [mmol]	Resin	Resin amount [mg]
0.05	Cl-MPA ProTide® 0.16 mmol/g	315
Synthesis conditions		
MW SPPS	Arg (1) – Chloride Loading 2-20 – 4 min single coupling 21-110 – 4 min double coupling Fmoc-His(Boc)-OH – Single coupling 10 min 50°C Fmoc-DfpGly-OH – 10min Single Coupling, extra washes	Fmoc deprotection – piperazine solution
Cleavage	Purification	Purity [%]
TFA/TIS/H ₂ O/EDT 4-5h	-	-

6.14.8 Synthesis of Bar1-36-NHNH₂

Barnase¹Ala-³⁶Val-NHNH₂ was synthesized on a Fmoc-Val-NHN=Pyv Resin which had been previously prepared. Loading was determined to be 0.41 mmol/g.

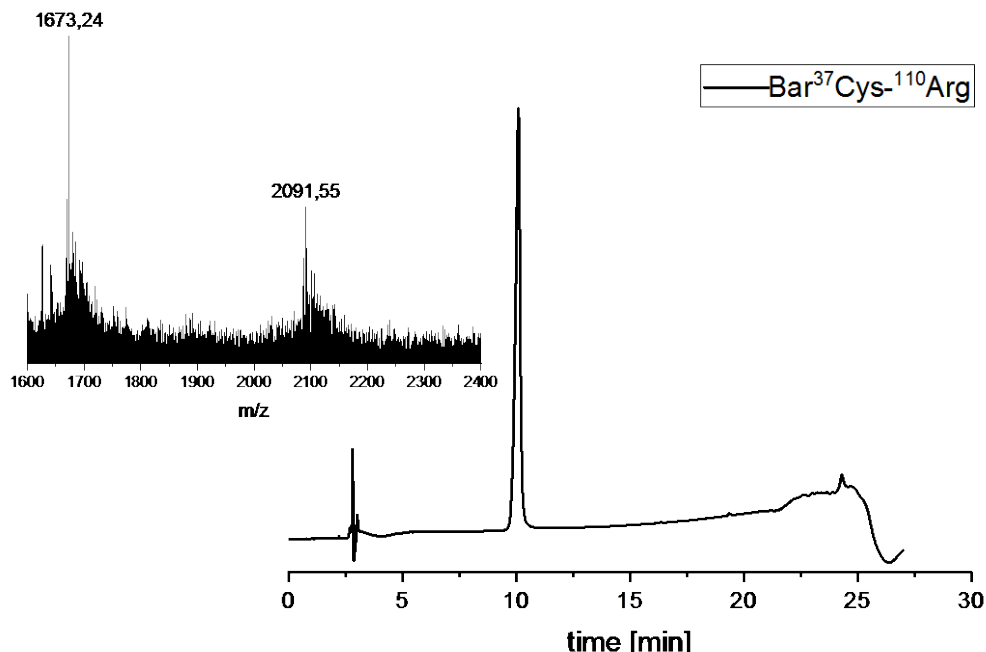
Table 27: Summary of synthesis parameter for Bar1-36-NHNH₂.

Name	Sequence	
Bar ¹ Ala- ³⁶ Val-NHNH ₂	H2N-AQVINTFDGV ADYLQTYHKL PDNYITKSEA QALGWV-NHNH ₂	
Scale [mmol]	Resin	Resin amount [mg]
0.05	Fmoc-Val-NHN=Pyv 0.41 mmol/g	120
Synthesis conditions		
MW SPPS	Trp (1) – double deprotection, 2min double coupling 2-20 – 2 min single coupling 21-36 – 2 min double coupling Fmoc-His(Boc)-OH – Single coupling 10 min 50°C	Fmoc deprotection – piperazine solution
Cleavage	Purification	Purity [%]
TFA/TIS/H ₂ O/EDT 3h	HPLC (10-80 18 min)	>95
DAD: 220		Retention time: 11.7 min
[M+3H ⁺] ³⁺ _{calc} : 1362.51.47; [M+3H ⁺] ³⁺ _{exp} : 1362.33		

6.14.9 Synthesis of Bar³⁷Cys-¹¹⁰Arg

Barnase fragment Bar³⁷Cys-¹¹⁰Arg was synthesized analogues to BarWT.

Table 28: Summary of synthesis parameter for Bar³⁷Cys-¹¹⁰Arg.

Name	Sequence	
Bar ³⁷ Cys- ¹¹⁰ Arg-COOH ₂	H ₂ N- C SKG NLADVAPGKS IGGDIFSNRE GKLPGKSGRT WREADINYTS GFRNSDRILY SSDWLIYKTT DHYQTFTKIR-COOH	
Scale [mmol]	Resin	Resin amount [mg]
0.1	Cl-MPA ProTide® 0.18 mmol/g	560
Synthesis conditions		
MW SPPS	Arg(1) – Chloride loading 2-20 – 4 min single coupling 21-82 – 4 min double coupling Fmoc-His(Boc)-OH – Single coupling 10 min 50°C	Fmoc deprotection – piperazine solution
Cleavage	Purification	Purity [%]
TFA/TIS/H ₂ O/EDT 3h	HPLC (10-80 18 min)	>95
		
DAD: 220 nm		Retention time: 10.1
[M+5H ⁺] ⁵⁺ _{calc} : 1673.47; [M+5H ⁺] ⁵⁺ _{exp} : 1673.24		

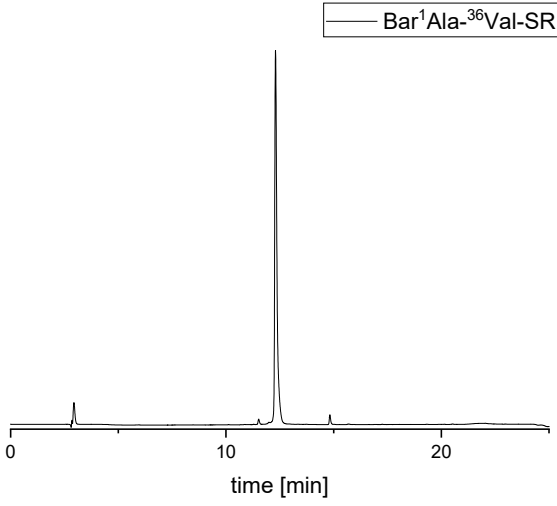
6.15 Native Chemical Ligation Approach to barnase

6.15.1 Synthesis of Bar¹Ala-³⁶Val-SR.

5.05 mg (1 eq., 923 μmol) of Bar(1-36)NHNH₂ was dissolved in 1 mL ligation buffer (6 M GnHCl, 0.2 M Na₂HPO₄, pH 6.4) and the pH was adjusted to 3 using 1 M HCl. The solution was cooled to -17°C and NaNO₂ (150 μL , 0.03 eq., 30 μmol) were added. After 20 minutes 1 mL MPAA (22 mol, 22 eq. 0.2 M) added. The solution was allowed to warm to room temperature for another 20 minutes. The reaction was quenched using 1 mL DTT_{aq}⁻ solution (1 M, 1 mmol, 1.2 eq.). After additional 10 minutes the crude product was isolated using standard HPLC methods.

Table 29: Summary of synthesis parameter for Bar¹Ala-³⁶Val-SR.

Name	Sequence
Bar ¹ Ala- ³⁶ Val-SR	H2N-AQVINTFDGV ADYLQTYHKL PDNYITKSEA QALGWV-SR
Scale [μmol]	923
Synthesis approach	Oxidative thioesterification
Purification	HPLC (10-80 18 min 5 min prerun)
Purity	>95%



— Bar¹Ala-³⁶Val-SR

DAD: 280 nm	Retention time: 12.3 min
[M+4H ⁺] ⁴⁺ _{calc} : 1198.4; [M+4H ⁺] ⁴⁺ _{exp} : 1198.8	

6.15.2 Synthesis of BarA37C variant by native chemical ligation

All necessary steps to ligation were conducted under inert atmosphere. 2 mg (1 eq., 0.26 μmol) of thioester fragment was dissolved in 100 μL ligation buffer (6M GnHCl, 10 mM Phosphate, pH 6.8). To the solution MPAA (10 eq., 2.6 μmol , 10 eq.) was added and the pH was adjusted to 6.5. 25 μL of peptide-thiol fragment (0.29 μmol , 1.1 eq.) was added to the reaction mixture. The reaction vessel was kept for 42 h in inert atmosphere at room temperature, control samples were taken after 24 h and 42 h and checked using standard HPLC methods. After 42 h the reaction was quenched adding 300 μL 1 M DTT and 6 M GnHCl. The crude product was isolated and purified using standard analytical HPLC methods, yielding 650 μg BarnaseCys37 variant (15% yield).

Table 30: Summary of synthesis parameter for BarCys37 by means of native chemical ligation.

Name	Sequence
Bar ¹ Ala- ¹¹⁰ Arg-COOH	H ₂ N- AQVINTFDGV ADYLQTYHKL PDNYITKSEA QALGWV CSKG NLADVAPGKS IGGDIFSNRE GKLPKSGRT WREADINYTS GFRNSDRILY SSDWLIYKTT DHYQTFKIR-COOH
Scale [μmol]	0.26
Synthesis approach	Native Chemical Ligation
Purification	HPLC (10-80 18 min 5 min prerun)
Purity	>95%

The figure displays an HPLC chromatogram for BarA37C. The x-axis represents time in minutes, ranging from 0 to 30. A single, sharp peak is observed at a retention time of 20.9 minutes. An inset mass spectrum is provided, showing relative intensity versus m/z. The x-axis of the inset ranges from 1000 to 1500 m/z. Three prominent peaks are labeled with their m/z values: 1035.7, 1128.4, and 1602.4. The peak at 1035.7 m/z is the most intense, corresponding to the calculated mass of the [M+12H]¹²⁺ ion.

DAD: 220 nm	Retention time: 20.9 min
[M+12H] ¹²⁺ _{calc} : 1035.5; [M+12H] ¹²⁺ _{exp} : 1035,7	

7 References

1. Brändén, C.-I.; Tooze, J., *Introduction to protein structure*. 2nd ed.; Garland Pub.: New York, 1999; p xiv, 410 p.
2. Lehninger, A. L.; Nelson, D. L.; Cox, M. M., *Lehninger principles of biochemistry*. 6th ed.; W.H. Freeman: New York, 2013.
3. Joël, J.; Shoshanna, W.; Michael, L.; Bernard, M., Conformation of amino acid side-chains in proteins. *Journal of Molecular Biology* **1978**, *125* (3), 357-386.
4. Muñoz, V.; Serrano, L., Intrinsic secondary structure propensities of the amino acids, using statistical ϕ - ψ matrices: Comparison with experimental scales. **1994**, *20* (4), 301-311.
5. Fujiwara, K.; Toda, H.; Ikeguchi, M., Dependence of α -helical and β -sheet amino acid propensities on the overall protein fold type. *BMC Structural Biology* **2012**, *12* (1), 18.
6. Barlow, D. J.; Thornton, J. M., Helix geometry in proteins. *Journal of Molecular Biology* **1988**, *201* (3), 601-619.
7. Rehman, I.; Farooq, M.; Botelho, S., Biochemistry, Secondary Protein Structure. In *StatPearls*, StatPearls Publishing Copyright © 2023, StatPearls Publishing LLC.: Treasure Island (FL), 2023.
8. Pauling, L.; Corey, R. B.; Branson, H. R., The structure of proteins; two hydrogen-bonded helical configurations of the polypeptide chain. *Proc Natl Acad Sci U S A* **1951**, *37* (4), 205-11.
9. Boyle, A. L., 3 - Applications of de novo designed peptides. In *Peptide Applications in Biomedicine, Biotechnology and Bioengineering*, Koutsopoulos, S., Ed. Woodhead Publishing: 2018; pp 51-86.
10. Schlick, T., Protein Structure Hierarchy. In *Molecular Modeling and Simulation: An Interdisciplinary Guide: An Interdisciplinary Guide*, Schlick, T., Ed. Springer New York: New York, NY, 2010; pp 105-128.
11. Eisenberg, D., The discovery of the α -helix and β -sheet, the principal structural features of proteins. **2003**, *100* (20), 11207-11210.
12. Hughes, R. M.; Waters, M. L., Model systems for β -hairpins and β -sheets. *Current Opinion in Structural Biology* **2006**, *16* (4), 514-524.
13. Crichton, R. R., Chapter 3 - Structural and Molecular Biology for Chemists. In *Biological Inorganic Chemistry (Second Edition)*, Crichton, R. R., Ed. Elsevier: Oxford, 2012; pp 35-68.
14. Anfinsen, C. B., Principles that Govern the Folding of Protein Chains. **1973**, *181* (4096), 223-230.
15. Anfinsen, C. B.; Haber, E.; Sela, M.; White, F. H., THE KINETICS OF FORMATION OF NATIVE RIBONUCLEASE DURING OXIDATION OF THE REDUCED POLYPEPTIDE CHAIN. **1961**, *47* (9), 1309-1314.
16. Levinthal, C. J. J. C. P., Are there pathways for protein folding? **1968**, *65*, 44-45.
17. Heidarsson, P. O.; Naqvi, M. M.; Sonar, P.; Valpapuram, I.; Cecconi, C., Chapter Three - Conformational Dynamics of Single Protein Molecules Studied by Direct Mechanical Manipulation. In *Advances in Protein Chemistry and Structural Biology*, Karabencheva-Christova, T., Ed. Academic Press: 2013; Vol. 92, pp 93-133.

18. Leopold, P. E.; Montal, M.; Onuchic, J. N., Protein folding funnels: a kinetic approach to the sequence-structure relationship. *Proc Natl Acad Sci U S A* **1992**, *89* (18), 8721-5.
19. Mogk, A.; Mayer, M. P.; Deuerling, E., Mechanisms of Protein Folding: Molecular Chaperones and Their Application in Biotechnology. **2002**, *3* (9), 807-814.
20. Dobson, C. M.; Šali, A.; Karplus, M., Protein Folding: A Perspective from Theory and Experiment. **1998**, *37* (7), 868-893.
21. Camilloni, C.; Bonetti, D.; Morrone, A.; Giri, R.; Dobson, C. M.; Brunori, M.; Gianni, S.; Vendruscolo, M., Towards a structural biology of the hydrophobic effect in protein folding. *Scientific Reports* **2016**, *6* (1), 28285.
22. Li, J.; Hou, C.; Ma, X.; Guo, S.; Zhang, H.; Shi, L.; Liao, C.; Zheng, B.; Ye, L.; Yang, L.; He, X., Entropy-Enthalpy Compensations Fold Proteins in Precise Ways. **2021**, *22* (17), 9653.
23. Wittung-Stafshede, P., Role of Cofactors in Protein Folding. *Accounts of Chemical Research* **2002**, *35* (4), 201-208.
24. Beissinger, M.; Buchner, J., How chaperones fold proteins. *Biological chemistry* **1998**, *379* (3), 245-59.
25. Ahmed, M. H.; Ghatge, M. S.; Safo, M. K., Hemoglobin: Structure, Function and Allostery. *Sub-cellular biochemistry* **2020**, *94*, 345-382.
26. Yang, F.; Moss, L. G.; Phillips, G. N., The molecular structure of green fluorescent protein. *Nature Biotechnology* **1996**, *14* (10), 1246-1251.
27. Kissinger, C. R.; Sieker, L. C.; Adman, E. T.; Jensen, L. H., Refined crystal structure of ferredoxin II from *Desulfovibrio gigas* at 1.7 Å. *Journal of Molecular Biology* **1991**, *219* (4), 693-715.
28. Czapinska, H.; Otlewski, J.; Krzywda, S.; Sheldrick, G. M.; Jaskólski, M., High-resolution structure of bovine pancreatic trypsin inhibitor with altered binding loop sequence. *J Mol Biol* **2000**, *295* (5), 1237-49.
29. Bycroft, M.; Ludvigsen, S.; Fersht, A. R.; Poulsen, F. M., Determination of the three-dimensional solution structure of barnase using nuclear magnetic resonance spectroscopy. *Biochemistry* **1991**, *30* (35), 8697-701.
30. Levitt, M.; Chothia, C., Structural patterns in globular proteins. *Nature* **1976**, *261* (5561), 552-558.
31. Andreeva, A.; Howorth, D.; Chothia, C.; Kulesha, E.; Murzin, A. G., SCOP2 prototype: a new approach to protein structure mining. *Nucleic acids research* **2014**, *42* (Database issue), D310-4.
32. Andreeva, A.; Kulesha, E.; Gough, J.; Murzin, A. G., The SCOP database in 2020: expanded classification of representative family and superfamily domains of known protein structures. *Nucleic acids research* **2019**, *48* (D1), D376-D382.
33. Ouellette, R. J.; Rawn, J. D., 14 - Amino Acids, Peptides, and Proteins. In *Principles of Organic Chemistry*, Ouellette, R. J.; Rawn, J. D., Eds. Elsevier: Boston, 2015; pp 371-396.
34. Morris, R.; Black, Katrina A.; Stollar, Elliott J., Uncovering protein function: from classification to complexes. *Essays in Biochemistry* **2022**, *66* (3), 255-285.
35. McDonald, A. G.; Tipton, K. F., Enzyme nomenclature and classification: the state of the art. *n/a* (n/a).
36. Ring, B.; Wrighton, S. A.; Mohutsky, M., Reversible Mechanisms of Enzyme Inhibition and Resulting Clinical Significance. In *Enzyme Kinetics in Drug*

- Metabolism: Fundamentals and Applications*, Nagar, S.; Argikar, U. A.; Tweedie, D., Eds. Springer US: New York, NY, 2021; pp 29-50.
37. Kovach, I. M., Competitive irreversible inhibition of enzymes in the presence of a substrate: scope and limitations. *Journal of enzyme inhibition* **1991**, *4* (3), 201-12.
 38. Ochs, R., Understanding Enzyme Inhibition. *Journal of Chemical Education - J CHEM EDUC* **2000**, *79*.
 39. Mauguen, Y.; Hartley, R. W.; Dodson, E. J.; Dodson, G. G.; Bricogne, G.; Chothia, C.; Jack, A., Molecular structure of a new family of ribonucleases. *Nature* **1982**, *297* (5862), 162-164.
 40. Hartley, R. W., Homology between prokaryotic and eukaryotic ribonucleases. *Journal of Molecular Evolution* **1980**, *15* (4), 355-358.
 41. Hill, C.; Dodson, G.; Heinemann, U.; Saenger, W.; Mitsui, Y.; Nakamura, K.; Borisov, S.; Tischenko, G.; Polyakov, K.; Pavlovsky, S., The structural and sequence homology of a family of microbial ribonucleases. *Trends in Biochemical Sciences* **1983**, *8* (10), 364-369.
 42. Priest, F. G.; Goodfellow, M.; Shute, L. A.; Berkeley, R. C. W., *Bacillus amyloliquefaciens* sp. nov., nom. rev. **1987**, *37* (1), 69-71.
 43. Susumu, N.; Masayasu, N., Ribonuclease of *Bacillus subtilis*. *Biochimica et Biophysica Acta* **1958**, *30* (2), 430-431.
 44. Hartley, R. W., A reversible thermal transition of the extracellular ribonuclease of *Bacillus amyloliquefaciens*. *Biochemistry* **1968**, *7* (6), 2401-2408.
 45. Serrano, L.; Matouschek, A.; Fersht, A. R., The folding of an enzyme: VI. The folding pathway of barnase: Comparison with theoretical models. *Journal of Molecular Biology* **1992**, *224* (3), 847-859.
 46. Hartley, R. W., Barnase and barstar: two small proteins to fold and fit together. *Trends in Biochemical Sciences* **1989**, *14* (11), 450-454.
 47. Hartley, R. W., 2 - Barnase and Barstar. In *Ribonucleases*, D'Alessio, G.; Riordan, J. F., Eds. Academic Press: New York, 1997; pp 51-100.
 48. Mossakowska, D. E.; Nyberg, K.; Fersht, A. R., Kinetic characterization of the recombinant ribonuclease from *Bacillus amyloliquefaciens* (barnase) and investigation of key residues in catalysis by site-directed mutagenesis. *Biochemistry* **1989**, *28* (9), 3843-3850.
 49. Meiering, E. M.; Serrano, L.; Fersht, A. R., Effect of active site residues in barnase on activity and stability. *Journal of Molecular Biology* **1992**, *225* (3), 585-589.
 50. Meiering, E. M.; Bycroft, M.; Fersht, A. R., Characterization of phosphate binding in the active site of barnase by site-directed mutagenesis and NMR. *Biochemistry* **1991**, *30* (47), 11348-56.
 51. Day, A. G.; Parsonage, D.; Ebel, S.; Brown, T.; Fersht, A. R., Barnase has subsites that give rise to large rate enhancements. *Biochemistry* **1992**, *31* (28), 6390-5.
 52. Giuseppe D' Alessio, J. F. R., *Ribonucleases: Structures and functions*. Academic Press: New York; 1997; p 670 pp.
 53. Lau, P. C.; Rowsome, R. W.; Zuker, M.; Visentin, L. P., Comparative nucleotide sequences encoding the immunity proteins and the carboxyl-terminal peptides of colicins E2 and E3. *Nucleic acids research* **1984**, *12* (22), 8733-45.
 54. Guillet, V.; Laphorn, A.; Hartley, R. W.; Mauguen, Y., Recognition between a bacterial ribonuclease, barnase, and its natural inhibitor, barstar. *Structure* **1993**, *1* (3), 165-176.

55. Buckle, A. M.; Schreiber, G.; Fersht, A. R., Protein-protein recognition: Crystal structural analysis of a barnase-barstar complex at 2.0-Å resolution. *Biochemistry* **1994**, *33* (30), 8878-8889.
56. Hartley, R. W., Directed mutagenesis and barnase-barstar recognition. *Biochemistry* **1993**, *32* (23), 5978-84.
57. Schreiber, G.; Fersht, A. R., Interaction of barnase with its polypeptide inhibitor barstar studied by protein engineering. *Biochemistry* **1993**, *32* (19), 5145-5150.
58. Schreiber, G.; Buckle, A. M.; Fersht, A. R., Stability and function: two constraints in the evolution of barstar and other proteins. *Structure* **1994**, *2* (10), 945-951.
59. Schreiber, G.; Fersht, A. R., Energetics of protein-protein interactions: Analysis of the Barnase-Barstar interface by single mutations and double mutant cycles. *Journal of Molecular Biology* **1995**, *248* (2), 478-486.
60. Haupt, A., *Organic and Inorganic Fluorine Chemistry: Methods and Applications*. De Gruyter: 2021.
61. Budisa, N.; Kubyskin, V.; Schulze-Makuch, D., Fluorine-Rich Planetary Environments as Possible Habitats for Life. **2014**, *4* (3), 374-385.
62. Harper, D. B.; O'Hagan, D., The fluorinated natural products. *Natural Product Reports* **1994**, *11* (0), 123-133.
63. Koga, K. T.; Rose-Koga, E. F., Fluorine in the Earth and the solar system, where does it come from and can it be found? *Comptes Rendus Chimie* **2018**, *21* (8), 749-756.
64. O'Hagan, D.; Deng, H., Enzymatic Fluorination and Biotechnological Developments of the Fluorinase. *Chemical Reviews* **2015**, *115* (2), 634-649.
65. Gregson, R. P.; Baldo, B. A.; Thomas, P. G.; Quinn, R. J.; Bergquist, P. R.; Stephens, J. F.; Horne, A. R., Fluorine Is a Major Constituent of the Marine Sponge *Halichondria moorei*. *Science* **1979**, *206* (4422), 1108-9.
66. Cooke, J. A.; Johnson, M. S.; Davidson, A. W.; Bradshaw, A. D., Fluoride in plants colonising fluorspar mine waste in the peak district and wardale. *Environmental Pollution (1970)* **1976**, *11* (1), 9-23.
67. Schmedt auf der Günne, J.; Mangstl, M.; Kraus, F., Occurrence of Difluorine F₂ in Nature—In Situ Proof and Quantification by NMR Spectroscopy. **2012**, *51* (31), 7847-7849.
68. O'Hagan, D.; Harper, D., Fluorine-containing natural products. *Journal of Fluorine Chemistry* **1999**, *100* (1), 127-133.
69. Gribble, G. W., The diversity of naturally produced organohalogens. *Chemosphere* **2003**, *52* (2), 289-297.
70. Cheng, X.; Ma, L., Enzymatic synthesis of fluorinated compounds. *Applied Microbiology and Biotechnology* **2021**, *105* (21), 8033-8058.
71. Dehnen, S.; Schafer, L. L.; Lectka, T.; Togni, A., Fluorine: A Very Special Element and Its Very Special Impacts on Chemistry. *Inorganic Chemistry* **2021**, *60* (23), 17419-17425.
72. Agricola, G., *De Re Metallica Libri XII - zwölf Bücher vom Berg- und Hüttenwesen*. Marix Verlag: 2006.
73. Bondi, A., van der Waals Volumes and Radii. *The Journal of Physical Chemistry* **1964**, *68* (3), 441-451.

74. Smart, B. E., Characteristics of C-F Systems. In *Organofluorine Chemistry: Principles and Commercial Applications*, Banks, R. E.; Smart, B. E.; Tatlow, J. C., Eds. Springer US: Boston, MA, 1994; pp 57-88.
75. Meanwell, N. A., Fluorine and Fluorinated Motifs in the Design and Application of Bioisosteres for Drug Design. *Journal of Medicinal Chemistry* **2018**, *61* (14), 5822-5880.
76. Tang, Y.; Ghirlanda, G.; Petka, W. A.; Nakajima, T.; DeGrado, W. F.; Tirrell, D. A., Fluorinated Coiled-Coil Proteins Prepared In Vivo Display Enhanced Thermal and Chemical Stability. **2001**, *40* (8), 1494-1496.
77. Molteni, M.; Pesenti, C.; Sani, M.; Volonterio, A.; Zanda, M., Fluorinated peptidomimetics: synthesis, conformational and biological features. *Journal of Fluorine Chemistry* **2004**, *125* (11), 1735-1743.
78. Nagai, T.; Nishioka, G.; Koyama, M.; Ando, A.; Miki, T.; Kumadaki, I., Reactions of trifluoromethyl ketones. IX. Investigation of the steric effect of a trifluoromethyl group based on the stereochemistry on the dehydration of trifluoromethyl homoallyl alcohols. *Journal of Fluorine Chemistry* **1992**, *57* (1), 229-237.
79. Jäckel, C.; Kocsch, B., Fluorine in Peptide Design and Protein Engineering. **2005**, *2005* (21), 4483-4503.
80. O'Hagan, D.; S. Rzepa, H., Some influences of fluorine in bioorganic chemistry. *Chemical Communications* **1997**, (7), 645-652.
81. O'Hagan, D., Understanding organofluorine chemistry. An introduction to the C-F bond. *Chemical Society Reviews* **2008**, *37* (2), 308-319.
82. Wiberg, N., De Gruyter: Berlin, Boston, 2008.
83. Dunitz, J. D., Organic Fluorine: Odd Man Out. **2004**, *5* (5), 614-621.
84. Hunter, L., The C-F bond as a conformational tool in organic and biological chemistry. *Beilstein J Org Chem* **2010**, *6*.
85. Howard, J. A. K.; Hoy, V. J.; O'Hagan, D.; Smith, G. T., How good is fluorine as a hydrogen bond acceptor? *Tetrahedron* **1996**, *52* (38), 12613-12622.
86. Taylor, R., The hydrogen bond between N-H or O-H and organic fluorine: favourable yes, competitive no. *Acta Crystallographica Section B* **2017**, *73* (3), 474-488.
87. Pietruś, W.; Kafel, R.; Bojarski, A. J.; Kurczab, R., Hydrogen Bonds with Fluorine in Ligand-Protein Complexes-the PDB Analysis and Energy Calculations. **2022**, *27* (3), 1005.
88. Purser, S.; Moore, P. R.; Swallow, S.; Gouverneur, V., Fluorine in medicinal chemistry. *Chemical Society Reviews* **2008**, *37* (2), 320-330.
89. Inoue, M.; Sumii, Y.; Shibata, N., Contribution of Organofluorine Compounds to Pharmaceuticals. *ACS Omega* **2020**, *5* (19), 10633-10640.
90. Fish, D. N.; Chow, A. T., The Clinical Pharmacokinetics of Levofloxacin. *Clinical Pharmacokinetics* **1997**, *32* (2), 101-119.
91. Zarganes-Tzitzikas, T.; Neochoritis, C. G.; Dömling, A., Atorvastatin (Lipitor) by MCR. *ACS Medicinal Chemistry Letters* **2019**, *10* (3), 389-392.
92. Ogawa, Y.; Tokunaga, E.; Kobayashi, O.; Hirai, K.; Shibata, N., Current Contributions of Organofluorine Compounds to the Agrochemical Industry. *iScience* **2020**, *23* (9), 101467.

93. Alexandrino, D. A. M.; Almeida, C. M. R.; Mucha, A. P.; Carvalho, M. F., Revisiting pesticide pollution: The case of fluorinated pesticides. *Environmental Pollution* **2022**, *292*, 118315.
94. Lasee, S.; McDermett, K.; Kumar, N.; Guelfo, J.; Payton, P.; Yang, Z.; Anderson, T. A., Targeted analysis and Total Oxidizable Precursor assay of several insecticides for PFAS. *Journal of Hazardous Materials Letters* **2022**, *3*, 100067.
95. Cordner, A.; De La Rosa, V. Y.; Schaidler, L. A.; Rudel, R. A.; Richter, L.; Brown, P., Guideline levels for PFOA and PFOS in drinking water: the role of scientific uncertainty, risk assessment decisions, and social factors. *Journal of Exposure Science & Environmental Epidemiology* **2019**, *29* (2), 157-171.
96. Alauddin, M. M., Positron emission tomography (PET) imaging with (18)F-based radiotracers. *American journal of nuclear medicine and molecular imaging* **2012**, *2* (1), 55-76.
97. Partridge, S.; Timothy, A.; O'Doherty, M. J.; Hain, S. F.; Rankin, S.; Mikhaeel, G., 2-Fluorine-18-fluoro-2-deoxy-D glucose positron emission tomography in the pretreatment staging of Hodgkin's disease: influence on patient management in a single institution. *Annals of oncology : official journal of the European Society for Medical Oncology* **2000**, *11* (10), 1273-9.
98. Duhaylongsod, F. G.; Lowe, V. J.; Patz, E. F., Jr.; Vaughn, A. L.; Coleman, R. E.; Wolfe, W. G., Detection of primary and recurrent lung cancer by means of F-18 fluorodeoxyglucose positron emission tomography (FDG PET). *The Journal of thoracic and cardiovascular surgery* **1995**, *110* (1), 130-9; discussion 139-40.
99. Tirota, I.; Dichiarante, V.; Pigliacelli, C.; Cavallo, G.; Terraneo, G.; Bombelli, F. B.; Metrangolo, P.; Resnati, G., 19F Magnetic Resonance Imaging (MRI): From Design of Materials to Clinical Applications. *Chemical Reviews* **2015**, *115* (2), 1106-1129.
100. Knight, J. C.; Edwards, P. G.; Paisey, S. J., Fluorinated contrast agents for magnetic resonance imaging; a review of recent developments. *RSC Advances* **2011**, *1* (8), 1415-1425.
101. Berger, A. A.; Völler, J.-S.; Budisa, N.; Kokschi, B., Deciphering the Fluorine Code—The Many Hats Fluorine Wears in a Protein Environment. *Accounts of Chemical Research* **2017**, *50* (9), 2093-2103.
102. Monkovic, J. M.; Gibson, H.; Sun, J. W.; Montclare, J. K., Fluorinated Protein and Peptide Materials for Biomedical Applications. **2022**, *15* (10), 1201.
103. Moschner, J.; Stulberg, V.; Fernandes, R.; Huhmann, S.; Leppkes, J.; Kokschi, B., Approaches to Obtaining Fluorinated α -Amino Acids. *Chemical Reviews* **2019**, *119* (18), 10718-10801.
104. Romoff, T. T.; Palmer, A. B.; Mansour, N.; Creighton, C. J.; Miwa, T.; Ejima, Y.; Moriwaki, H.; Soloshonok, V. A., Scale-up Synthesis of (R)- and (S)-N-(2-Benzoyl-4-chlorophenyl)-1-(3,4-dichlorobenzyl)pyrrolidine-2-carboxamide Hydrochloride, A Versatile Reagent for the Preparation of Tailor-Made α - and β -Amino Acids in an Enantiomerically Pure Form. *Org Process Res Dev* **2017**, *21* (5), 732-739.
105. Romoff, T. T.; Ignacio, B. G.; Mansour, N.; Palmer, A. B.; Creighton, C. J.; Abe, H.; Moriwaki, H.; Han, J.; Konno, H.; Soloshonok, V. A., Large-Scale Synthesis of the Glycine Schiff Base Ni(II) Complex Derived from (S)- and (R)-N-(2-Benzoyl-4-chlorophenyl)-1-[(3,4-dichlorophenyl)methyl]-2-pyrrolidinecarboxamide. *Org Process Res Dev* **2020**, *24* (2), 294-300.

106. Mei, H.; Hiramatsu, T.; Takeda, R.; Moriwaki, H.; Abe, H.; Han, J.; Soloshonok, V. A., Expedient Asymmetric Synthesis of (S)-2-Amino-4,4,4-trifluorobutanoic Acid via Alkylation of Chiral Nucleophilic Glycine Equivalent. *Org Process Res Dev* **2019**, *23* (4), 629-634.
107. Belokon, Y. N.; Bulychev, A. G.; Vitt, S. V.; Struchkov, Y. T.; Batsanov, A. S.; Timofeeva, T. V.; Tsiryapkin, V. A.; Ryzhov, M. G.; Lysova, L. A., General method of diastereo- and enantioselective synthesis of β -hydroxy- α -amino acids by condensation of aldehydes and ketones with glycine. *Journal of the American Chemical Society* **1985**, *107* (14), 4252-4259.
108. Han, J.; Takeda, R.; Liu, X.; Konno, H.; Abe, H.; Hiramatsu, T.; Moriwaki, H.; Soloshonok, V. A., Preparative Method for Asymmetric Synthesis of (S)-2-Amino-4,4,4-trifluorobutanoic Acid. **2019**, *24* (24), 4521.
109. Zou, Y.; Han, J.; Saghyan, A. S.; Mkrtchyan, A. F.; Konno, H.; Moriwaki, H.; Izawa, K.; Soloshonok, V. A., Asymmetric Synthesis of Tailor-Made Amino Acids Using Chiral Ni(II) Complexes of Schiff Bases. An Update of the Recent Literature. **2020**, *25* (12), 2739.
110. Wang, J.; Lin, D.; Zhou, S.; Ding, X.; Soloshonok, V. A.; Liu, H., Asymmetric Synthesis of Sterically and Electronically Demanding Linear ω -Trifluoromethyl Containing Amino Acids via Alkylation of Chiral Equivalents of Nucleophilic Glycine and Alanine. *The Journal of Organic Chemistry* **2011**, *76* (2), 684-687.
111. Hohmann, T.; Dyrks, M.; Chowdhary, S.; Weber, M.; Nguyen, D.; Moschner, J.; Kokschi, B., Gram-Scale Asymmetric Synthesis of Fluorinated Amino Acids Using a Chiral Nickel(II) Complex. *The Journal of Organic Chemistry* **2022**, *87* (16), 10592-10604.
112. Ni, C.; Hu, J., The unique fluorine effects in organic reactions: recent facts and insights into fluoroalkylations. *Chemical Society Reviews* **2016**, *45* (20), 5441-5454.
113. Chaume, G.; Lensen, N.; Caupène, C.; Brigaud, T., Convenient Synthesis of N-Terminal Tfm-Dipeptides from Unprotected Enantiopure α -Tfm-Proline and α -Tfm-Alanine. **2009**, *2009* (33), 5717-5724.
114. Devillers, E.; Pytkowicz, J.; Chelain, E.; Brigaud, T., Synthesis of protected enantiopure (R) and (S)- α -trifluoromethylalanine containing dipeptide building blocks ready to use for solid phase peptide synthesis. *Amino acids* **2016**, *48* (6), 1457-68.
115. Kokschi, B.; Sewald, N.; Hofmann, H.-J.; Burger, K.; Jakubke, H.-D., Proteolytically stable peptides by incorporation of α -Tfm amino acids. **1997**, *3* (3), 157-167.
116. Hoffmann, W.; Langenhan, J.; Huhmann, S.; Moschner, J.; Chang, R.; Accorsi, M.; Seo, J.; Rademann, J.; Meijer, G.; Kokschi, B.; Bowers, M. T.; von Helden, G.; Pagel, K., An Intrinsic Hydrophobicity Scale for Amino Acids and Its Application to Fluorinated Compounds. *Angewandte Chemie (International ed. in English)* **2019**, *58* (24), 8216-8220.
117. Mant, C. T.; Hodges, R. S., Reversed-phase liquid chromatography as a tool in the determination of the hydrophilicity/hydrophobicity of amino acid side-chains at a ligand-receptor interface in the presence of different aqueous environments. I. Effect of varying receptor hydrophobicity. *Journal of chromatography. A* **2002**, *972* (1), 45-60.

118. Pliška, V.; Schmidt, M.; Fauchère, J.-L., Partition coefficients of amino acids and hydrophobic parameters π of their side-chains as measured by thin-layer chromatography. *Journal of Chromatography A* **1981**, *216*, 79-92.
119. Samsonov, S. A.; Salwiczek, M.; Anders, G.; Koksich, B.; Pisabarro, M. T., Fluorine in Protein Environments: A QM and MD Study. *The Journal of Physical Chemistry B* **2009**, *113* (51), 16400-16408.
120. Erdbrink, H.; Nyakatura, E. K.; Huhmann, S.; Gerling, U. I. M.; Lentz, D.; Koksich, B.; Czekelius, C., Synthesis of enantiomerically pure (2S,3S)-5,5,5-trifluoroisoleucine and (2R,3S)-5,5,5-trifluoro-*allo*-isoleucine. *Beilstein J Org Chem* **2013**, *9*, 2009-2014.
121. Gerling, U. I. M.; Salwiczek, M.; Cadicamo, C. D.; Erdbrink, H.; Czekelius, C.; Grage, S. L.; Wadhwani, P.; Ulrich, A. S.; Behrends, M.; Haufe, G.; Koksich, B., Fluorinated amino acids in amyloid formation: a symphony of size, hydrophobicity and α -helix propensity. *Chemical Science* **2014**, *5* (2), 819-830.
122. Robalo, J. R.; Huhmann, S.; Koksich, B.; Vila Verde, A., The Multiple Origins of the Hydrophobicity of Fluorinated Apolar Amino Acids. *Chem* **2017**, *3* (5), 881-897.
123. Kraml, J.; Kamenik, A. S.; Waibl, F.; Schauerl, M.; Liedl, K. R., Solvation Free Energy as a Measure of Hydrophobicity: Application to Serine Protease Binding Interfaces. *Journal of Chemical Theory and Computation* **2019**, *15* (11), 5872-5882.
124. Robalo, J. R.; Vila Verde, A., Unexpected trends in the hydrophobicity of fluorinated amino acids reflect competing changes in polarity and conformation. *Physical Chemistry Chemical Physics* **2019**, *21* (4), 2029-2038.
125. Chiu, H.-P.; Suzuki, Y.; Gullickson, D.; Ahmad, R.; Kokona, B.; Fairman, R.; Cheng, R. P., Helix Propensity of Highly Fluorinated Amino Acids. *Journal of the American Chemical Society* **2006**, *128* (49), 15556-15557.
126. Erdbrink, H.; Peuser, I.; Gerling, U. I. M.; Lentz, D.; Koksich, B.; Czekelius, C., Conjugate hydrotrifluoromethylation of α,β -unsaturated acyl-oxazolidinones: synthesis of chiral fluorinated amino acids. *Organic & Biomolecular Chemistry* **2012**, *10* (43), 8583-8586.
127. Chakrabarty, A.; Kortemme, T.; Baldwin, R. L., Helix propensities of the amino acids measured in alanine-based peptides without helix-stabilizing side-chain interactions. **1994**, *3* (5), 843-852.
128. Son, S.; Tanrikulu, I. C.; Tirrell, D. A., Stabilization of bzip Peptides through Incorporation of Fluorinated Aliphatic Residues. **2006**, *7* (8), 1251-1257.
129. Gottler, L. M.; Lee, H. Y.; Shelburne, C. E.; Ramamoorthy, A.; Marsh, E. N., Using fluorous amino acids to modulate the biological activity of an antimicrobial peptide. *ChemBiochem* **2008**, *9* (3), 370-3.
130. Porcelli, F.; Buck-Koehntop, B. A.; Thennarasu, S.; Ramamoorthy, A.; Veglia, G., Structures of the Dimeric and Monomeric Variants of Magainin Antimicrobial Peptides (MSI-78 and MSI-594) in Micelles and Bilayers, Determined by NMR Spectroscopy. *Biochemistry* **2006**, *45* (18), 5793-5799.
131. Hallock, K. J.; Lee, D.-K.; Ramamoorthy, A., MSI-78, an Analogue of the Magainin Antimicrobial Peptides, Disrupts Lipid Bilayer Structure via Positive Curvature Strain. *Biophysical Journal* **2003**, *84* (5), 3052-3060.
132. Chin, J. W.; Cropp, T. A.; Anderson, J. C.; Mukherji, M.; Zhang, Z.; Schultz, P. G., An expanded eukaryotic genetic code. *Science* **2003**, *301* (5635), 964-7.

133. Link, A. J.; Mock, M. L.; Tirrell, D. A., Non-canonical amino acids in protein engineering. *Current Opinion in Biotechnology* **2003**, *14* (6), 603-609.
134. Buer, B. C.; Meagher, J. L.; Stuckey, J. A.; Marsh, E. N. G., Structural basis for the enhanced stability of highly fluorinated proteins. **2012**, *109* (13), 4810-4815.
135. More, H. T.; Zhang, K. S.; Srivastava, N.; Frezzo, J. A.; Montclare, J. K., Influence of Fluorination on Protein-Engineered Coiled-Coil Fibers. *Biomacromolecules* **2015**, *16* (4), 1210-1217.
136. Bilgiçer, B.; Fichera, A.; Kumar, K., A Coiled Coil with a Fluorous Core. *Journal of the American Chemical Society* **2001**, *123* (19), 4393-4399.
137. Alexeev, D.; Barlow, P. N.; Bury, S. M.; Charrier, J.-D.; Cooper, A.; Hadfield, D.; Jamieson, C.; Kelly, S. M.; Layfield, R.; Mayer, R. J.; McSparron, H.; Price, N. C.; Ramage, R.; Sawyer, L.; Starkmann, B. A.; Uhrin, D.; Wilken, J.; Young, D. W., Synthesis, Structural and Biological Studies of Ubiquitin Mutants Containing (2S, 4S)-5-Fluoroleucine Residues Strategically Placed in the Hydrophobic Core. **2003**, *4* (9), 894-896.
138. Horng, J.-C.; Raleigh, D. P., Φ -Values beyond the Ribosomally Encoded Amino Acids: Kinetic and Thermodynamic Consequences of Incorporating Trifluoromethyl Amino Acids in a Globular Protein. *Journal of the American Chemical Society* **2003**, *125* (31), 9286-9287.
139. Kuhlman, B.; Luisi, D. L.; Evans, P. A.; Raleigh, D. P., Global analysis of the effects of temperature and denaturant on the folding and unfolding kinetics of the N-terminal domain of the protein L911 Edited by P. E. Wright. *Journal of Molecular Biology* **1998**, *284* (5), 1661-1670.
140. Ventura, S.; Vega, M. C.; Lacroix, E.; Angrand, I.; Spagnolo, L.; Serrano, L., Conformational strain in the hydrophobic core and its implications for protein folding and design. *Nature structural biology* **2002**, *9* (6), 485-93.
141. Mousa, R.; Lansky, S.; Shoham, G.; Metanis, N., BPTI folding revisited: switching a disulfide into methylene thioacetal reveals a previously hidden path. *Chemical Science* **2018**, *9* (21), 4814-4820.
142. Deisenhofer, J.; Steigemann, W., Crystallographic refinement of the structure of bovine pancreatic trypsin inhibitor at 1.5 Å resolution. *Acta Crystallographica Section B* **1975**, *31* (1), 238-250.
143. McCammon, J. A.; Gelin, B. R.; Karplus, M., Dynamics of folded proteins. *Nature* **1977**, *267* (5612), 585-590.
144. Donovan, A. J.; Dowle, J.; Yang, Y.; Weiss, M. A.; Kent, S. B. H., Total synthesis of bovine pancreatic trypsin inhibitor and the protein diastereomer [Gly37D-Ala]BPTI using Boc chemistry solid phase peptide synthesis. **2020**, *112* (4), e24166.
145. Ascenzi, P.; Bocedi, A.; Bolognesi, M.; Spallarossa, A.; Coletta, M.; De Cristofaro, R.; Menegatti, E., The bovine basic pancreatic trypsin inhibitor (Kunitz inhibitor): a milestone protein. *Curr Protein Pept Sci* **2003**, *4* (3), 231-51.
146. Capasso, C.; Rizzi, M.; Menegatti, E.; Ascenzi, P.; Bolognesi, M., Crystal structure of the bovine α -chymotrypsin:kunitz inhibitor complex. An example of multiple protein:protein recognition sites. **1997**, *10* (1), 26-35.
147. BECKMANN, J.; MEHLICH, A.; SCHRÖDER, W.; WENZEL, H. R.; TSCHESCHE, H., Preparation of chemically 'mutated' aprotinin homologues by semisynthesis. **1988**, *176* (3), 675-682.

148. Ye, S.; Loll, B.; Berger, A. A.; Mülrow, U.; Alings, C.; Wahl, M. C.; Kokschi, B., Fluorine teams up with water to restore inhibitor activity to mutant BPTI. *Chemical Science* **2015**, *6* (9), 5246-5254.
149. Krowarsch, D.; Otlewski, J., Amino-acid substitutions at the fully exposed P1 site of bovine pancreatic trypsin inhibitor affect its stability. **2001**, *10* (4), 715-724.
150. Leppkes, J.; Dimos, N.; Loll, B.; Hohmann, T.; Dyrks, M.; Wieseke, A.; Keller, B. G.; Kokschi, B., Fluorine-induced polarity increases inhibitory activity of BPTI towards chymotrypsin. *RSC Chemical Biology* **2022**, *3* (6), 773-782.
151. Wehrhan, L.; Leppkes, J.; Dimos, N.; Loll, B.; Kokschi, B.; Keller, B. G., Water Network in the Binding Pocket of Fluorinated BPTI–Trypsin Complexes—Insights from Simulation and Experiment. *The Journal of Physical Chemistry B* **2022**, *126* (48), 9985-9999.
152. Fan, C.; Deng, Q.; Zhu, T. F., Bioorthogonal information storage in l-DNA with a high-fidelity mirror-image Pfu DNA polymerase. *Nature Biotechnology* **2021**, *39* (12), 1548-1555.
153. S.K. Singh, J. M. C., K.A. Porter, M.J. Karney. Large Scale Stepwise Synthesis of Ubiquitin.
154. Hartrampf, N.; Saebi, A.; Poskus, M.; Gates, Z. P.; Callahan, A. J.; Cowfer, A. E.; Hanna, S.; Antilla, S.; Schissel, C. K.; Quartararo, A. J.; Ye, X.; Mijalis, A. J.; Simon, M. D.; Loas, A.; Liu, S.; Jessen, C.; Nielsen, T. E.; Pentelute, B. L., Synthesis of proteins by automated flow chemistry. **2020**, *368* (6494), 980-987.
155. Dumy, P.; Keller, M.; Ryan, D. E.; Rohwedder, B.; Wöhr, T.; Mutter, M., Pseudo-Prolines as a Molecular Hinge: Reversible Induction of cis Amide Bonds into Peptide Backbones. *Journal of the American Chemical Society* **1997**, *119* (5), 918-925.
156. Palasek, S. A.; Cox, Z. J.; Collins, J. M., Limiting racemization and aspartimide formation in microwave-enhanced Fmoc solid phase peptide synthesis. **2007**, *13* (3), 143-148.
157. Bacsa, B.; Horváti, K.; Bösze, S.; Andreae, F.; Kappe, C. O., Solid-phase synthesis of difficult peptide sequences at elevated temperatures: a critical comparison of microwave and conventional heating technologies. *J Org Chem* **2008**, *73* (19), 7532-42.
158. PUGH, K. C.; YORK, E. J.; STEWART, J. M., Effects of resin swelling and substitution on solid phase synthesis. **1992**, *40* (3-4), 208-213.
159. Sandhya, K.; Ravindranath, B., A protocol for racemization-free loading of Fmoc-amino acids to Wang resin. *Tetrahedron Letters* **2008**, *49* (15), 2435-2437.
160. JONES, J. H.; RAMAGE, W. I.; WITTY, M. J., MECHANISM OF RACEMISATION OF HISTIDINE DERIVATIVES IN PEPTIDE SYNTHESIS. **1980**, *15* (3), 301-303.
161. Fletcher, A. R.; Jones, J. H.; Ramage, W. I.; Stachulski, A. V., The use of the N(π)-phenacyl group for the protection of the histidine side chain in peptide synthesis. *Journal of the Chemical Society, Perkin Transactions 1* **1979**, (0), 2261-2267.
162. Neumann, K.; Farnung, J.; Baldauf, S.; Bode, J. W., Prevention of aspartimide formation during peptide synthesis using cyanosulfurylides as carboxylic acid-protecting groups. *Nature Communications* **2020**, *11* (1), 982.
163. Mergler, M.; Dick, F.; Sax, B.; Weiler, P.; Vorherr, T., The aspartimide problem in Fmoc-based SPPS. Part I. **2003**, *9* (1), 36-46.

164. Luna, O. F.; Gomez, J.; Cárdenas, C.; Albericio, F.; Marshall, S. H.; Guzmán, F., Deprotection Reagents in Fmoc Solid Phase Peptide Synthesis: Moving Away from Piperidine? **2016**, *21* (11), 1542.
165. Mong, S. K.; Vinogradov, A. A.; Simon, M. D.; Pentelute, B. L., Rapid Total Synthesis of DARPin pE59 and Barnase. **2014**, *15* (5), 721-733.
166. Thapa, P.; Zhang, R.-Y.; Menon, V.; Bingham, J.-P., Native Chemical Ligation: A Boon to Peptide Chemistry. **2014**, *19* (9), 14461-14483.
167. Conibear, A. C.; Watson, E. E.; Payne, R. J.; Becker, C. F. W., Native chemical ligation in protein synthesis and semi-synthesis. *Chemical Society Reviews* **2018**, *47* (24), 9046-9068.
168. Guan, I.; Williams, K.; Liu, J. S. T.; Liu, X., Synthetic Thiol and Selenol Derived Amino Acids for Expanding the Scope of Chemical Protein Synthesis. **2022**, *9*.
169. Malins, L. R.; Payne, R. J., Synthetic Amino Acids for Applications in Peptide Ligation–Desulfurization Chemistry %J Australian Journal of Chemistry. **2015**, *68* (4), 521-537.
170. Blanco-Canosa, J. B.; Dawson, P. E., An efficient Fmoc-SPPS approach for the generation of thioester peptide precursors for use in native chemical ligation. *Angewandte Chemie (International ed. in English)* **2008**, *47* (36), 6851-5.
171. Zheng, J.-S.; Tang, S.; Qi, Y.-K.; Wang, Z.-P.; Liu, L., Chemical synthesis of proteins using peptide hydrazides as thioester surrogates. *Nature Protocols* **2013**, *8* (12), 2483-2495.
172. Fang, G.-M.; Li, Y.-M.; Shen, F.; Huang, Y.-C.; Li, J.-B.; Lin, Y.; Cui, H.-K.; Liu, L., Protein Chemical Synthesis by Ligation of Peptide Hydrazides. **2011**, *50* (33), 7645-7649.
173. Melnyk, O.; Simonneau, C.; Vicogne, J., Protein Chemical Synthesis by SEA Ligation. In *Chemical Ligation*, 2017; pp 89-123.
174. Bode, J. W.; Fox, R. M.; Baucom, K. D., Chemoselective Amide Ligations by Decarboxylative Condensations of N-Alkylhydroxylamines and α -Ketoacids. **2006**, *45* (8), 1248-1252.
175. Zhang, Y.; Xu, C.; Lam, H. Y.; Lee, C. L.; Li, X., Protein chemical synthesis by serine and threonine ligation. *Proc Natl Acad Sci U S A* **2013**, *110* (17), 6657-62.
176. Agouridas, V.; El Mahdi, O.; Diemer, V.; Cargoët, M.; Monbaliu, J.-C. M.; Melnyk, O., Native Chemical Ligation and Extended Methods: Mechanisms, Catalysis, Scope, and Limitations. *Chemical Reviews* **2019**, *119* (12), 7328-7443.
177. Gude, M.; Ryf, J.; White, P. D., An accurate method for the quantitation of Fmoc-derivatized solid phase supports. *Letters in Peptide Science* **2002**, *9* (4), 203-206.
178. Johnson, E. C. B.; Kent, S. B. H., Insights into the Mechanism and Catalysis of the Native Chemical Ligation Reaction. *Journal of the American Chemical Society* **2006**, *128* (20), 6640-6646.
179. Sakamoto, K.; Tsuda, S.; Mochizuki, M.; Nohara, Y.; Nishio, H.; Yoshiya, T., Imidazole-Aided Native Chemical Ligation: Imidazole as a One-Pot Desulfurization-Amenable Non-Thiol-Type Alternative to 4-Mercaptophenylacetic Acid. **2016**, *22* (50), 17940-17944.
180. Jin, K.; Li, X., Advances in Native Chemical Ligation–Desulfurization: A Powerful Strategy for Peptide and Protein Synthesis. **2018**, *24* (66), 17397-17404.

181. Loewenthal, R.; Sancho, J.; Fersht, A. R., Fluorescence spectrum of barnase: contributions of three tryptophan residues and a histidine-related pH dependence. *Biochemistry* **1991**, *30* (27), 6775-6779.
182. Greenfield, N. J., Using circular dichroism spectra to estimate protein secondary structure. *Nature Protocols* **2006**, *1* (6), 2876-2890.
183. Joseph Alan Walder, M. A. B., Eric Jeffrey Devor, Lingyan Huang Compositions and methods for visual ribonuclease detection assays. 2003.
184. Okorokov, A. L.; Hartley, R. W.; Panov, K. I., An Improved System for Ribonuclease Ba Expression. *Protein Expression and Purification* **1994**, *5* (6), 547-552.
185. Schulga, A.; Kurbanov, F.; Kirpichnikov, M.; Protasevich, I.; Lobachov, V.; Ranjbar, B.; Chekhov, V.; Polyakov, K.; Engelborghs, Y.; Makarov, A., Comparative study of binase and barnase: experience in chimeric ribonucleases. *Protein Engineering, Design and Selection* **1998**, *11* (9), 775-782.
186. Chelushkin, P. S.; Polyanichko, K. V.; Leko, M. V.; Dorosh, M. Y.; Bruckdorfer, T.; Burov, S. V., Convenient method of peptide hydrazide synthesis using a new hydrazone resin. *Tetrahedron Letters* **2015**, *56* (4), 619-622.
187. CEM, CarboMax™ - Enhance Peptide Coupling at Elevated Temperature. CEM: <https://cem.com/en/carbomax-enhanced-peptide-coupling-at-elevated-temperatures>, 2018; p 5.